Surface silanization of carbon nanofibers and nanotubes for altering the properties of epoxy composites

Dissertation

zur Erlangung des akademischen Grades
Doktor rerum naturalium
- Dr. rer. nat. –

eingereicht an der
Fakultät für Mathematik und Naturwissenschaften
der Technischen Universität Ilmenau
von

Yaru Nie

Gutachter: apl. Prof. Dr. Uwe Ritter
Dr. Thomas Hübert
Prof. Dr. Peter Scharff

Tag der Einreichung: 02.02.2012
Tag der wissenschaftlichen Aussprache: 30.03.2012

urn:nbn:de:gbv:ilm1-2012000133

The work presented here was carried out from April 1, 2009 to January 30, 2012 in BAM Bundesanstalt für Materialforschung und -prüfung, Berlin in the Department 6 - Materials Protection and Surface Technologies.

List of Abbreviations

General abbreviations

AC	alternating current
CVD	chemical vapor deposition
DC	direct current
DMA	dynamical mechanical analysis
EDX	energy-dispersive X-ray spectroscopy
FTIR	Fourier transform infrared spectroscopy
IEP	isoelectric point
IR	infrared spectroscopy
RT	room temperature
SEM	scanning electron microscopy
TEM	transmission electron microscopy
TGA	thermogravimetric analysis
XPS	X-ray photoelectron spectroscopy
XRD	X-ray diffraction spectroscopy

Abbreviations of samples

CNF	carbon nanofiber
CNF-AS	oxidized carbon nanofiber by the acid mixture of H_2SO_4/HNO_3 under bath sonication
CNF-AH	oxidized carbon nanofiber by the acid mixture of H_2SO_4/HNO_3 under heating treatment
CNF-GS	silanized carbon nanofiber with 3-glycidoxypropyltrimethoxysilane
CNF-I	carbon nanofiber first silanized with 3-isocyanatopropyltriethoxysilane
CNF-I-AP	CNF-I further silanized with 3-aminopropyltrimethoxysilane

CNF-N	reduced carbon nanofiber terminated with alcoholic hydroxyl group
CNF-N-AP	carbon nanofiber silanized with 3-aminopropyltrimethoxysilane
CNF-O	original carbon nanofiber
CNF-PMH	oxidized carbon nanofiber by the mixture of $KMnO_4/H_2SO_4$ under heating treatment
CNF-PMS	oxidized carbon nanofiber by the mixture of $KMnO_4/H_2SO_4$ under bath sonication
CNT	carbon nanotube
MWCNT	multi-walled carbon nanotube
MWCNT-AS	oxidized multi-walled carbon nanotube by the acid mixture of H_2SO_4/HNO_3 under bath sonication
MWCNT-PMH	oxidized multi-walled carbon nanotube by the mixture of $KMnO_4/H_2SO_4$ under heating treatment
MWCNT-PMH-N	reduced multi-walled carbon nanotube terminated with alcoholic hydroxyl group
MWCNT-PMH-N-AP	multi-walled carbon nanotube silanized with 3-aminopropyltrimethoxysilane
SWCNT	single-walled carbon nanotube
VGCF	vapor grown carbon fiber
VGCNF	vapor grown carbon nanofiber

Abbreviations of chemicals

APTES	3-aminopropyltriethoxysilane
APTMS	3-aminopropyltrimethoxysilane
CTAB	cetyltrimethyl ammonium bromide
DGEBA	diglycidyl ether of bisphenol A
DMF	N, N-dimethylformamide
EtOH	ethanol
GPTMS	3-glycidoxypropyltrimethoxysilane

IPTES	3-isocyanatopropyltriethoxysilane
MPS	3-methacryloxypropyltrimethoxysilane
TEA	triethylamine
TFAA	trifluoroacetic anhydride
TFBA	4-(trifluoromethyl) benzaldehyde
THF	tetrahydrofuran
VTS	vinyltriethoxysilane

Acknowledgements

First and foremost, I would like to thank my supervisor Dr. Thomas Hübert for providing me the opportunity to work on this topic. His excellent guidance, enlightening discussions and great patience gave me valuable support throughout my work. Without his kind help and encouragements, I would not have been able to complete this thesis.

At the same time, I would like to thank Prof. Dr. Uwe Ritter to accept me as a Ph.D student in Ilmenau University of Technology. Without his academic advices and valuable discussions of my results, I would not have survived my Ph.D journey.

This work was supported by European funds for regional development (EFRE) (ProFit No. 10140631). I am very grateful for our project partner Polymerics GmbH for DMA tests (Mr. Andre Leistner) and tensile shear strength measurements (Ms. Elke Brockhausen).

Sincere thanks to my colleagues Mr. Andreas Lippitz, Mr. René Illgen, Dr. Oskar Haase, Dr. Asmus Meyer-Plath, Mr. Stefan Zirker, Mr. Lothar Buchta, Mr. Mario Sahre, Dr. Guillermo Orts Gil, Dr. Andreas Subaric-Leitis, Dr. Gabriele Steinborn, Ms. Margrit Krull, Ms. Sigrid Benemann and Ms. Birgid Strauß for their technical measurements of my samples and fruitful suggestions for my experiments.

Great thanks to Ms. Büttner for her help in the management of office documents.

I express my sincere gratitude to Ms. Heidi Lorenz, Dr. Ulrich Banach, Dr. Carlo Tiebe, Dr. Cindy Lang, Ms. Silvana Puhlmann, Mr. Muhammad Shabir Mahr and Mr. Fabian Kelling in working group 6.44 for giving me so much support and providing me a very friendly work environment.

Many thanks to all my friends in China and Germany for giving me the courage to move forwards.

Finally I would like to thank my parents and sister in China. I would not have accomplished this work without their encouragement and support.

Abstract

Surface silanization of carbon nanofibers (CNFs) and multi-walled nanotubes (MWCNTs) was carried out to investigate its effect on properties of epoxy composites.

Unlike previous researches which worked mainly on the silanization of carbon nanotubes (CNTs), the focus of this thesis was the silanization of oxygenated CNFs with alkoxysilanes. However, oxygenated MWCNTs were also silanized as a comparison.

In the first part, different oxidations were applied on CNFs and MWCNTs to find the optimal condition to introduce carboxyl groups on the surface. Three silanization procedures were performed on oxidized CNFs:

1) direct silanization with 3-glycidoxypropyltrimethoxysilane
2) first reduction of carboxyl groups on oxidized CNFs into alcoholic hydroxyl groups and then silanization with 3-aminopropyltrimethoxysilane
3) initially silanization with 3-isocyanatopropyltriethoxysilane and then a further silanization with 3-aminopropyltrimethoxysilane

The procedure 2) was also performed on oxidized MWCNTs. The oxidation as well as the silanization of CNFs and MWCNTs was characterized systematically and explicitly by various analytical methods.

In the second part, epoxy nanocomposites with CNFs or MWCNTs were prepared. Silanized CNFs improved the mechanical properties of composites. The electrical conductivity of composites was increased with the addition of fillers, but silanized CNFs/epoxy composites demonstrated smaller increments than original CNFs/epoxy composites due to the insulating silane coating on the CNF surface. Silanization has a greater effect on changing the electrical conductivity of MWCNTs/epoxy composites than CNFs/epoxy composites. The thermal conductivity of epoxy composites was also improved by the infusion of CNFs. Depending on the amount of silanes on CNFs, the thermal conductivity of epoxy composites with silanized CNFs could be higher or lower than that of composites with original CNFs. Epoxy composites with aligned MWCNTs could be prepared under alternating current electric field, which was confirmed by the anisotropy in the electrical conductivity of composites.

The silanization of carbon nanofillers provides a facile way to adjust the properties of polymer composites by strengthening the interfacial interaction between fillers and polymer matrices as well as improving the dispersion of fillers in the matrix.

Zusammenfassung

Diese Arbeit beschreibt die Oberflächenmodifizierung von Kohlenstoffnanofasern (CNFs) und mehrwandigen Kohlenstoffnanoröhren (MWCNTs) sowie die Eigenschaften von damit hergestellten Epoxid-Kompositen. Es wurden Korrelationen zwischen chemischen Oberflächenmodifizierungen und Kompositeigenschaften untersucht.

Im ersten Teil wurden nach einer Oxidation zur Erzeugung von Carboxygruppen daran anknüpfend drei unterschiedliche Reaktionswege zur Silanisierung der oxidierten Oberflächen der nanoskaligen Kohlenstoffmaterialien untersucht:

1) direkte Silanisierung mit 3-Glycidoxypropyltrimethoxysilan
2) Reduktion der Carboxygruppen zu den alkoholischen Hydroxygruppen und Silanisierung mit 3-Aminopropyltrimethoxysilan
3) Silanisierung mit 3-Isocyanatopropyltriethoxysilan und weitere Silanisierung mit 3-Aminopropyltrimethoxysilan

Die Oxidation sowie die Silanisierung der CNFs und MWCNTs wurden systematisch und detailliert anhand verschiedener analytisch-chemischer Methoden charakterisiert.

Im zweiten Teil wurden CNFs oder MWCNTs in Epoxidharzen dispergiert und die physikalischen Eigenschaften der daraus hergestellten Nanokomposite beschrieben. So zeigten Epoxid-Komposite, die mit silanisierten CNFs versetzt wurden, verbesserte mechanische Eigenschaften. Auch die elektrische Leitfähigkeit der Epoxid-Komposite stieg mit zunehmendem Gehalt der Nanofüllstoffe, wobei die elektrische Leitfähigkeit von Epoxid-Kompositen mit silanisierten CNFs aufgrund der isolierenden Silanschicht niedriger war als die der Epoxid-Komposite mit unmodifizierten CNFs. Bei MWCNTs-Epoxid-Kompositen bewirkte die Silanisierung eine größere Änderung der elektrischen Leitfähigkeit im Vergleich zu den CNFs-Epoxid-Kompositen. Das Einbringen von CNFs in das Epoxidharz erhöhte die thermische Leitfähigkeit. Die Wärmeleitfähigkeit der Epoxid-Komposite konnte in Abhängigkeit von der Silanmenge auf den CNFs höher oder niedriger sein als die der Epoxid-Komposite mit unmodifizierten CNFs. Die MWCNTs in den Epoxid-Kompositen konnten durch Anlegen eines elektrischen Wechselstromfeldes parallel zu den Feldlinien ausgerichtet werden, was Messungen einer anisotropen elektrischen Leitfähigkeit an den Kompositen belegten.

Die nasschemische Silanisierung der nanoskaligen Kohlenstoffmaterialien stellt eine vielseitige und einfache Methode dar, die Eigenschaften von Polymerkompositen gezielt zu modifizieren. Diese Änderungen der Materialeigenschaften wurden dann vor allem durch stärkere Wechselwirkungen an den Grenzflächen zwischen Füllstoffen und Polymer sowie durch eine bessere Verteilung der Füllstoffe in der Polymermatrix erreicht.

Table of Contents

List of Abbreviations ..... **II**

Acknowledgements ..... **V**

Abstract ..... **VI**

Zusammenfassung ..... **VII**

Table of Contents **1**

1 Introduction **4**

1.1 Background *4*

1.2 Organization of the thesis *5*

1.3 State of the art *6*

1.3.1 Structures and properties of carbon nanofibers (CNFs) and carbon nanotubes (CNTs) 6

1.3.1.1 Differences between CNFs and CNTs 7

1.3.1.2 Electrical conductivities 8

1.3.1.3 Thermal conductivities 9

1.3.1.4 Mechanical properties 9

1.3.2 Synthesis of CNFs and CNTs 10

1.3.2.1 Preparation of CNFs 10

1.3.2.2 Preparation of CNTs 11

1.3.3 Epoxy polymers 12

1.3.4 CNFs and CNTs/polymer composites 13

1.3.4.1 Mechanical properties of composites 13

1.3.4.2 Electrical conductivities of composites 15

1.3.4.3 Thermal conductivities of composites 17

1.3.5 Chemical modification of CNFs and CNTs 19

1.3.5.1 General review 19

1.3.5.2 Silanization 20

1.4 Motivation *24*

1.5 Objectives *25*

2 Chemical modification of CNFs and MWCNTs with silanes **26**

2.1 Materials *26*

2.2 Modification *28*

2.2.1 Oxidation of CNFs and MWCNTs 28

2.2.2 Functionalization of CNFs with glycidoxysilane 29

2.2.3 Functionalization of CNFs with aminosilane 29

2.2.4 Functionalization of CNFs with isocyanatesilane and aminosilane 30
2.2.5 Functionalization of MWCNTs with aminosilane 31
2.2.6 Derivatization of modified MWCNTs 31
2.3 Characterization 32
2.4 Results and discussion 34
2.4.1 Oxidation of CNFs 34
2.4.1.1 IR spectra 34
2.4.1.2 XPS analysis 35
2.4.1.3 Raman spectra 36
2.4.1.4 SEM characterization 37
2.4.2 Silanization of CNFs with glycidoxysilane 38
2.4.2.1 IR spectra 38
2.4.2.2 XPS analysis 40
2.4.2.3 SEM and EDX analysis 42
2.4.2.4 TGA measurements 43
2.4.2.5 Raman spectra 44
2.4.2.6 Behavior of CNF suspension under electric field 45
2.4.3 Silanization of CNFs with aminosilane 46
2.4.3.1 IR spectra 46
2.4.3.2 XPS analysis 48
2.4.3.3 TGA measurements 50
2.4.3.4 Streaming potential measurements 51
2.4.3.5 Raman spectra 52
2.4.4 Silanization of CNFs with isocyanatesilane and aminosilane 53
2.4.4.1 IR spectra 53
2.4.4.2 XPS analysis 54
2.4.4.3 TGA measurements 56
2.4.4.4 Streaming potential measurements 57
2.4.4.5 XRD results 58
2.4.4.6 Raman spectra 59
2.4.5 Oxidation of MWCNTs 60
2.4.5.1 IR spectra 60
2.4.5.2 Raman spectra 61
2.4.6 Silanization of MWCNTs with aminosilane 62
2.4.6.1 IR spectra 62
2.4.6.2 XPS analysis 63
2.4.6.3 Raman spectra 67
2.5 Summary 67
3 CNFs/epoxy and MWCNTs/epoxy composites 70
3.1 Preparation of composites 70

3.1.1 Materials ... 70
3.1.2 CNFs/epoxy composites ... 70
3.1.3 MWCNTs/epoxy composites ... 71
3.2 Characterization ... 72
3.3 Results and discussion ... 73
3.3.1 Morphology of CNFs/epoxy composites ... 73
3.3.1.1 Comparison of CNF-GS/epoxy with CNF-O/epoxy composites ... 73
3.3.1.2 Comparison of CNF-N-AP/epoxy with CNF-O/epoxy composites ... 75
3.3.1.3 Comparison of CNF-I-AP/epoxy with CNF-O/epoxy composites ... 76
3.3.1.4 Summary of the morphology characterization ... 77
3.3.2 Mechanical properties of CNFs/epoxy composites ... 78
3.3.2.1 DMA anylysis of CNF-GS/epoxy and CNF-O/epoxy composites ... 78
3.3.2.2 Mechanical strength of CNF-N-AP/epoxy compared with CNF-O/epoxy composites ... 81
3.3.2.3 Shear strength of CNF-I-AP/epoxy compared with CNF-O/epoxy composites ... 82
3.3.2.4 Summary of the mechanical properties ... 83
3.3.3 Electrical conductivities of CNFs/epoxy composites ... 84
3.3.3.1 Electrical conductivities of CNF-GS/epoxy composites ... 84
3.3.3.2 Electrical conductivities of CNF-N-AP/epoxy composites ... 86
3.3.3.3 Electrical conductivities of CNF-I-AP/epoxy composites ... 89
3.3.3.4 Summary of the electrical conductivities ... 90
3.3.4 Thermal conductivities of CNFs/epoxy composites ... 92
3.3.4.1 Thermal conductivities of CNF-GS/epoxy composites ... 92
3.3.4.2 Thermal conductivities of CNF-N-AP/epoxy composites ... 94
3.3.4.3 Thermal conductivities of CNF-I-AP/epoxy composites ... 95
3.3.4.4 Summary of the thermal conductivities ... 96
3.3.5 Electrical conductivities of MWCNTs/epoxy composites ... 96
3.4 Summary ... 98
4 Conclusion and discussion ... 99
4.1 Conclusion of the experimental results ... 99
4.2 Overall discussion ... 104
5 Outlook ... 111
6 References ... 112
7 List of Figures ... 118
8 List of Tables ... 123
9 List of Publications ... 124

1 Introduction

1.1 Background

Carbon nanofibers (CNFs) and nanotubes (CNTs) have potential applications in the fields like microelectronics, gas storage, catalyst supports, battery electrodes etc. due to their excellent thermal and electrical conductivities and good mechanical behaviors [1-4]. In most cases, they are used as fillers in polymer matrices to alter the physical properties of composites. Due to their size in the nano range, very low surface energy, and low bulk density, they are easy to intertwine and bundle together [5]. Therefore it is difficult to disperse CNFs or CNTs homogeneously in polymer matrices.

Some researchers show mechanical reinforcements of polymer composites by chemically modified CNFs or CNTs [6, 7], while others indicate negative results for mechanical properties [8, 9]. The electrical insulating polymer matrices can be changed into conductive materials by the addition of trace amount of CNFs or CNTs [10], however, the thermal conductivity increases only modestly with a high filler loading [11]. The relationship between physical properties and composite structures is not always explicit. Great efforts have been made to find out the factors affecting properties of polymer composites, such as the surface chemistry of fillers, the interfacial adhesion between fillers and matrices, and the dispersion of fillers in the matrix.

It is discovered that the chemical surface modification of CNFs or CNTs can avoid the aggregation of fillers, disentangle the bundles and construct strong adhesions between fillers and the polymer matrix. Thus it is highly desirable that the surface chemical modification of graphitic carbon nanofibers or nanotubes is carried out to improve the filler dispersion in polymer matrices. Moreover, the covalent bonds between polymer matrices and fillers can optimize the effective stress transfer from matrices to carbon nanofillers and thus improve mechanical properties of polymer-based composites.

The modification of CNFs or CNTs can be divided into two categories: direct attachments of functional groups onto the pristine graphitic surface; the functionalization based on oxygenated groups on fillers. On the sidewalls of CNFs or CNTs, carbon atoms form mostly sp^2 hybrid bonds, which are electrons rich due to the highly delocalized π electrons. Therefore they are easy to take part in electrophilic addition reactions to modify the sidewalls of CNFs or CNTs. The direct sidewall functionalization normally needs very active addends and strict

conditions. Furthermore, the chemical derivatives on sidewalls always result in the loss of surface graphitic structures, and consequently decrease the mechanical property and thermal conductivity of carbon nanofillers [2, 12, 13]. In contrast, the chemical modification of carbon nanofillers based on oxygen containing groups from the sidewall defects or the ends of fillers preserves the sidewall electronic structures in a large extent and thus the superior physical properties of CNFs or CNTs.

The introduction of oxygenated functional groups can be realized by the treatment with H_2SO_4, HNO_3, $KMnO_4$, OsO_4, plasma [14], etc.. Due to the high cost and small yield, plasma treatment is unsuitable for large scale applications. Oxidants attack the sp^2 bonding at the sidewall defects easily and the sp^2 hybridization is converted into sp^3 hybridization. As a result, CNFs or CNTs may be cut from the defect sites, lowering their aspect ratio and accordingly some of their physical properties. In order to realize their maximal potential as fillers for improving the properties of polymer composites, it is crucial to find a balance between keeping the surface graphitic structures as well as the aspect ratio of CNFs or CNTs and introducing chemical moieties with good affinities to polymer matrices.

Silane coupling agents are known to be a good choice for joining both inorganic fillers and polymer matrices due to their bifunctionality. As mentioned before, for CNFs or CNTs, the maintenance of surface graphitic structures is critical for their excellent physical properties. The silane coating on CNFs or CNTs can induce further reaction with the polymer matrices without disruption of the CNF or CNT structures [15]. The available rich silane chemistry also provides various possibilities of the surface modification of CNFs or CNTs to form covalent bonds between carbon nanofillers and many polymer matrices. Moreover, the silane coating on the surface of CNFs or CNTs introduces insulating moieties into the system, which may affect the intrinsic conductivity of fillers [16]. Therefore it is worthwhile to investigate the silanization process of CNFs or CNTs in a detailed way.

1.2 Organization of the thesis

The work in this thesis consists of two parts:

1) chemical modification of CNFs and MWCNTs
2) preparation and property investigation of composites containing CNFs or MWCNTs

In chapter 1, the background and state of the art are reviewed. In chapter 2, three silanizations of CNFs are fully characterized by IR, XPS, Raman, TGA, XRD, EDX, SEM and streaming potential measurements. One of the silanization procedures - aminosilanization is also

transferred to MWCNTs. In chapter 3, the mechanical property, the electrical conductivity and the thermal conductivity of composites containing CNFs or MWCNTs are discussed and compared. Part of the work concerning the silanization of CNFs with aminosilane is based on the publication in [17] © 2011 Society of Chemical Industry, first published by John Wiley & Sons Ltd.. The work of the silanization with glycidoxysilane has been submitted to Composites Part A: Applied Science and Manufacturing.

1.3 State of the art

1.3.1 Structures and properties of carbon nanofibers (CNFs) and carbon nanotubes (CNTs)

The basic units comprising of CNFs or CNTs are hexagonal carbon crystalline planes, which resemble the structure of graphite (Figure 1.1). Each carbon is connected with four other carbons, three of which are sp^2 hybridizations (bond length is 1.415 Å), while the other one is based on loose interlamellar stacking (inter layer spacing is 3.35 Å). The sp^2 carbon bonding in the hexagonal rings has aromaticity - the electrons on carbons are highly delocalized and easy to transport between different hexagons, which render the graphitic cylindrical CNFs or CNTs very good electrical conductivity. The thermal conductivity of CNFs and CNTs is also extraordinary and comparable to metals such as copper (390 $W \cdot m^{-1} \cdot K^{-1}$). Because of their small size and high aspect ratio, they possess extremely high surface area to volume ratio, which enables their maximal interaction with the polymer matrix. Therefore CNFs and CNTs are promising filler candidates for improving the properties of polymer materials.

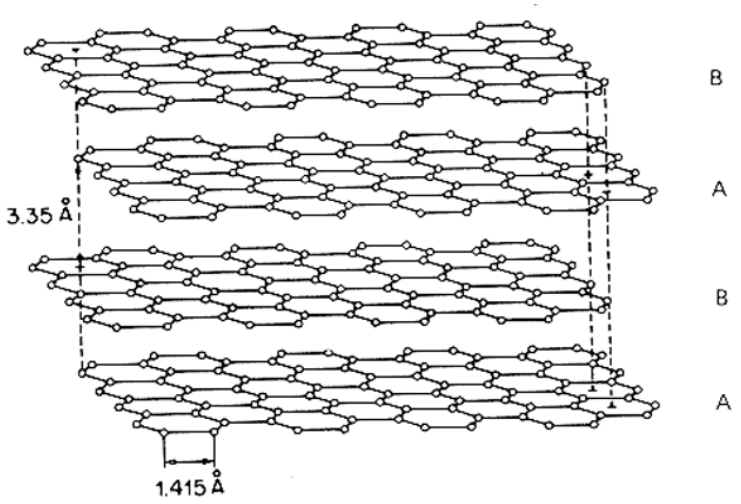

Figure 1.1 Graphite crystallite structures (the balls represent carbon atoms and the sticks represent the bonding) [18].

CNTs can be either single or multi-walled. The diameter range is between 0.6 - 50 nm. CNFs are nanofibers with a larger diameter in the range of 50 - 200 nm. Depending on the size and structures, the property of these carbon nanostructures varies drastically. According to the rolling direction of the graphene planes relative to the tube axis, different morphologies of single-walled carbon nanotubes (SWCNTs) is defined as armchair, zigzag（Figure 1.2）or chiral respectively.

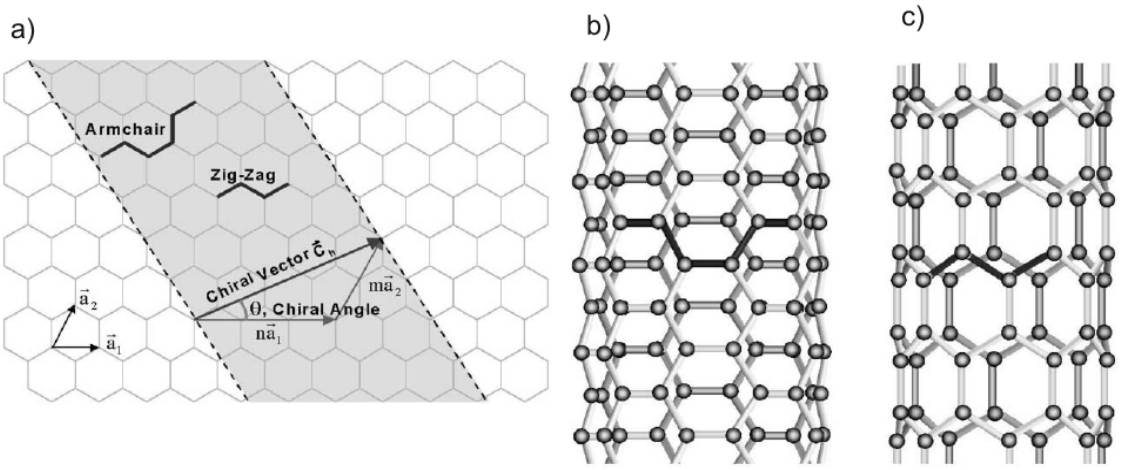

Figure 1.2 a) Schematic diagram of how the graphene sheet rolling up into SWCNT b) armchair SWCNT c) zig-zag SWCNT [19].

1.3.1.1 Differences between CNFs and CNTs

Due to the much smaller diameter of CNTs (0.6 – 50 nm) than CNFs (50 – 200 nm), CNTs possess extremely large aspect ratio (typically 300 - 1×10^5), which renders them a unique combination of mechanical, electrical, and thermal properties. Besides their varied diameters, they also have different microstructures on the surface: in CNFs, the rolled graphene layers are canted with the fiber axis, which gives them more active open edges for chemical reactions; in CNTs, the graphene planes are rolled in a concentric way, so that they are parallel with the tube axis. This concentric structure makes the CNT surface rather chemically inert, but on the other hand, avoids defects on the surface, which ensures better physical properties for CNTs than CNFs. Figure 1.3 shows the main difference between CNFs and MWCNTs.

CNFs distinguish from CNTs in physical properties due to their structure and size differences. CNFs are entitled to have a tensile strength of 2.9 GPa, tensile modulus of 240 GPa, thermal conductivity of 1950 $W\cdot m^{-1}\cdot K^{-1}$, and electrical conductivity of 1×10^6 $S\cdot m^{-1}$ [1, 20-22], while CNTs have even superior properties: thermal conductivity of 3000 - 6000 $W\cdot m^{-1}\cdot K^{-1}$, electrical conductivity of 5×10^4 – 1×10^6 $S\cdot m^{-1}$, tensile strength and tensile modulus of

10 - 500 GPa and 1000 - 1500 GPa respectively [23-25]. However, the price of CNTs is the biggest problem which hinders their potential applications in industry. According to the report in 2007 [26], the prices of CNFs, MWCNTs and SWCNTs were $125/lb, $350/lb and $30000/lb respectively. Due to the greater van der Waals attraction of smaller CNTs, they tend to form agglomerates or bundles, which weaken their performance as reinforcement agents. On the other hand, CNFs have a greater diameter, which makes them disperse more easily than CNTs and the relatively active surface structure of CNFs enables facile surface chemical functionalization, which is also helpful for their dispersion in the polymer matrix.

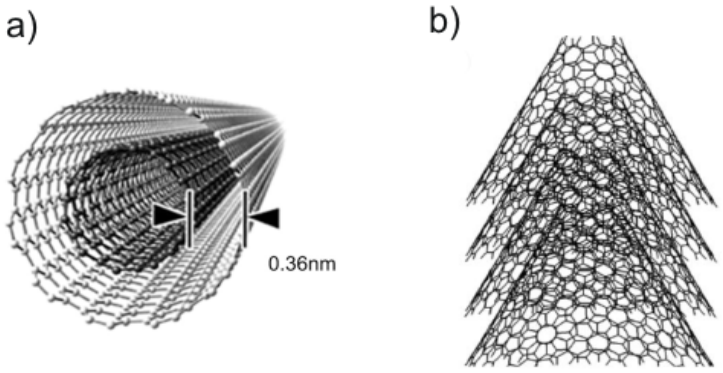

Figure 1.3 Comparison of structures between a) MWCNTs [27] and b) CNFs [28].

1.3.1.2 Electrical conductivities

Unlike graphite, which is always electrically conductive, the electrical behavior of SWCNTs is controlled by their diameter and their cylindrical symmetry. According to the tight binding theory, SWCNTs with a vector (n, m), which satisfies the condition of (2n+m)/3 to be an integer, are conductive; while the other CNTs are semi-conductive [29-32]. So armchair SWCNTs with a vector of (n, n) are always conductive, while zigzag and chiral SWCNTs are either metallic or semi-conductive depending on their helicity. During the synthesis, about two thirds of SWCNTs is semi-conductive, while the other one third is metallic. CNFs and MWCNTs have the electrical conductivity as turbostratic graphite due to their greater diameters and negligible confinement effects [33]. In addition, the interlayer interaction of MWCNTs or CNFs will also facilitate the electron transport.

A single SWCNT has the conductivity in the range of $10 - 1\times10^{6}$ $S\cdot m^{-1}$ depending on the helicity and the diameter. The electrical conductivity of SWCNT bundles varies between 1×10^{4} and 3×10^{6} $S\cdot m^{-1}$, which is comparable to the in-plane conductivity of graphite (2.5×10^{6} $S\cdot m^{-1}$) [34-37]. The conductivity of individual MWCNTs is between 20 and 2×10^{7} $S\cdot m^{-1}$, relying on the extent of surface defects or the helicity of the outmost graphene layer

[38-41]. The electrical conductivity of individual CNFs is estimated to be about 2×10^5 $S\cdot m^{-1}$ [42]. When the structures of CNFs or CNTs are perfect graphitic crystallites, they are ballistic electron transporters. Resistance occurs only when electrons collide with some defects in the crystalline structures. Those defects or amorphous impurities hinder the electron transport, reduce the mean free path of electrons and lower the electrical conductivity. In 3D conductors, electrons are free to scatter in any angle, and each scattering leads to electrical resistance; while in 1D conductors like CNFs or CNTs, electrons can only travel back and forward along the fiber axis, which significantly decreases the chance of collision with defects [43]. Thus CNFs or CNTs, especially those with high aspect ratio, have very high electrical conductivity.

1.3.1.3 Thermal conductivities

Theoretical thermal conductivity of CNTs is estimated to be 6600 $W\cdot m^{-1}\cdot K^{-1}$, which is twice higher than that of diamond, and CNFs are estimated to have a thermal conductivity of 1950 $W\cdot m^{-1}\cdot K^{-1}$. The thermal conductivity of carbon nanofillers obeys equation 1 [44]:

$$K = \sum C v_z^2 \tau \qquad (1)$$

where K is the thermal conductivity; C is the specific heat, from the contribution of both electrons (C_{el}) and phonons (C_{ph}) ($C = C_{ph} + C_{el}$); v_z is the group velocity of phonons; and τ is the phonon relaxation time. Based on the assumption from Benedict and Hone, C_{el} is 100 times smaller than C_{ph}, which suggests that the phonon excitations dominate the thermal properties of CNFs or CNTs [44-46]. The relaxation time is influenced by the scattering of impurities and defects. The fewer defects are in fillers, the longer is the relaxation time of phonons. Reduced amounts of structure defects also lead to longer phonon mean free path. As a result, the group velocity of phonons will increase under this condition.

1.3.1.4 Mechanical properties

The carbon bonds in CNFs and CNTs comprise mostly of sp^2 hybridization, which is much stronger than sp^3 hybridization found in aliphatic alkanes. The tensile modulus of graphite is known to be 1.06 TPa [47], and the strength is estimated to be 130 GPa based on the properties of sp^2 carbon bonds [48]. Thus CNTs should also have a very high mechanical strength based on the similar bonding as graphite. However, MWCNTs or SWCNTs prefer to form bundles due to van der Waals attraction arising from their small diameter. The intertube slippage in bundles greatly reduces the mechanical strength of CNTs [49, 50]. Small diameter SWCNTs have been measured to possess tensile modulus and tensile strength of 1 TPa and tens of GPa respectively [51], comparable to the properties of graphite. MWCNTs tend to

have lower stiffness: tensile modulus and tensile strength in the range of 0.27 - 0.95 TPa and 11 - 63 GPa respectively. In addition, the surface defects on carbon nanofillers will reduce their mechanical strength significantly. For CNTs produced in large quantity by chemical vapor deposition (CVD) methods, it was found that the tensile modulus and tensile strength were only 0.45 TPa and 4 GPa respectively [52]. Because the surface of CNFs consists of truncated cones rather than the parallel graphitic crystalline planes, which deteriorate the effective mechanical load transfer in the direction along the fiber axis, the tensile properties of CNFs are much lower compared to CNTs. It is claimed that CNFs had a tensile modulus of 240 GPa and a tensile strength of 2.92 GPa [53].

1.3.2 Synthesis of CNFs and CNTs

1.3.2.1 Preparation of CNFs

Since 1970s and 1980s, it is found out that carbon fibers are able to enhance the properties of polymer matrices as fillers. Many efforts have been done to reduce the production cost. Vapor grown carbon fibers (VGCFs) were developed by Hyperion Catalysis in the early 1980s and then commercialized in a large production capacity. Later in 1991, Applied Sciences, Inc. produced vapor grown carbon nanofibers (VGCNFs) with a relatively lower cost (about $200/kg) and in a large quantity. These nanofibers had stacked-cup surface structures and possessed good physical properties. They were used by many researchers and a lot of publications were based on this kind of nanofibers. Scientists in Japan had done plenty of work to understand the structure of stacked-cup or herringbone structures of CNFs. Based on their theoretical researches, Japanese companies Sumitomo, Showa, Mitsui, and etc. tried various ways to control the size of CNFs and these nanofibers had been applied in battery industry [20].

CNFs are mainly produced by CVD method. A hydrocarbon precursor such as natural gas, propane, benzene, or carbon monoxide is fed into a reactor containing catalysts at a temperature between 500 and 1500 °C. The carbon source decomposes over the catalyst and grows into nanofibers [26]. Pyrograf III CNFs are the most widely used CNFs in either scientific researches or practical applications. Scheme for an apparatus of the preparation is shown in Figure 1.4. Natural gas is used as the carbon source, NH_3 and H_2S as the activator of the catalyst $Fe(CO)_5$, and the reaction is maintained at 1100 °C. The residence of carbon source in the reactor lasts only milliseconds, and then it accumulates to form CNFs in the collection chamber. These nanofibers are with diameters in the range of 70 - 200 nm, lengths of 30-100 μm and possess an electrical conductivity of 1.8×10^6 $S\cdot m^{-1}$. The morphology and

properties of CNFs vary with the carbon feedstock, the catalyst and the operation conditions. CNFs synthesized from propane on nickel-copper catalyst had linear morphology; those prepared from ethylene with the same catalyst consisted mostly of twisted conformation; CNFs produced by acetylene on pure nickel catalyst had coiled and helical conformation [54]. Depending on different demands, these CNFs have potential applications in many areas.

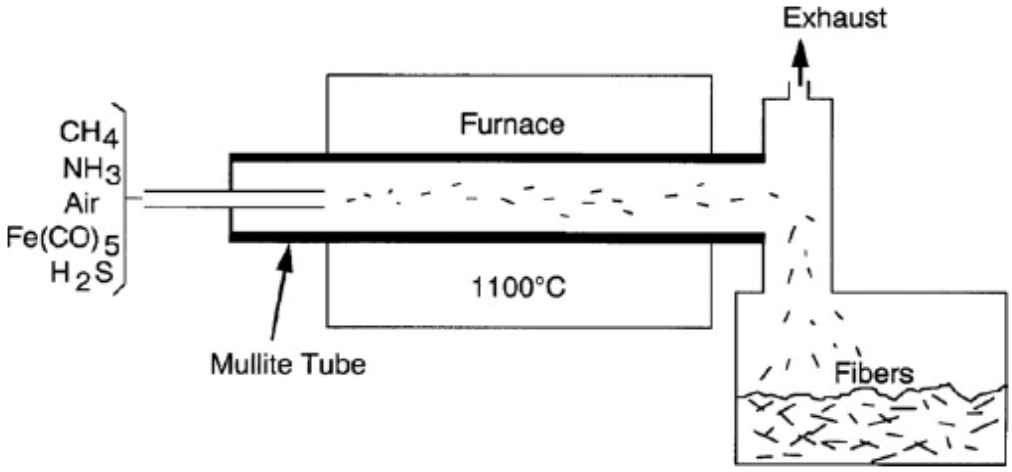

Figure 1.4 Scheme of an apparatus for the preparation of Pyrograf III CNFs [20].

1.3.2.2 Preparation of CNTs

In 1991, Iijima discovered MWCNTs by electric arc discharge method [55]. After that, abundant literatures sprung out to prepare CNTs with variable diameters, lengths and properties. Typically, a DC voltage of 20 - 25 volts and a high temperature of 2000 - 3000 °C were utilized to prepare CNTs in the arc discharge method. DC plasma was produced between two graphite electrodes in an inert gas. Transitional metals like Fe, Co or Ni as catalysts were embedded onto one of the electrodes to generate very fine carbon sources for forming SWCNTs. Depending on the reaction condition such as temperature, catalyst, time etc., the best yield of SWCNTs for large scale production was around 75 % [56].

Another method to prepare high quality and purity nanotubes is by laser ablation. In 1996, SWCNTs with a yield higher than 70 % was prepared by laser vaporization of a composite rod of graphite and transitional metal at 1200 °C [57]. Due to the lower temperature, the growth condition is easier to control and the vaporization of carbon is more uniform than that in the arc discharge method.

In electric discharge and laser ablation, high temperature facilitates the annealing of surface defects on nanotubes. However, CNTs generated in both ways are always entangled in bundles and hard to disperse, which causes a great problem for potential applications;

moreover, both methods rely on the vaporization of graphite source, which is quite expensive for large scale production.

In contrast, CVD method is a versatile way for large quantity preparation of CNTs with relatively low cost. A gaseous hydrocarbon source or precursor passes through the reaction chamber at a temperature of 700 - 1500 °C under the protection of an inert gas, and it is then decomposed to form CNTs under the catalyzation of transitional metal [58, 59]. Catalysts can be either deposited onto a solid substrate, such as Si, polymer or metals, or directly injected into the system in the form of a solution of an organometallic compound. Pre-deposited catalysts induce aligned CNTs growing on substrates [59, 60], while liquid catalysts can prepare free standing CNTs. Therefore CVD method not only has the advantage to deposit nanotubes on solid substrates, but also can produce CNTs continuously in large amount, which significantly widens the application field of CNTs.

1.3.3 Epoxy polymers

Epoxy polymers represent an important segment in the polymer industry. Despite single component epoxy precursor exists, generally epoxy polymer kit consists of two parts, epoxy resin and hardener. Epoxy resins can be monomers or short chain polymers, which have two epoxy rings at each end of the molecule. Those oxirane rings homopolymerize or react with the active hydrogen from amines, phenols and acids to form long chain epoxy polymers [61]. Most epoxy resins (more than 90 %) are synthesized by the reaction of bisphenol A with epichlorohydrin, although the former can be exchanged into bisphenol F or other monomers. The chemical formula of bisphenol A based epoxy resin is shown in Figure 1.5. Depending on the value of n, epoxy resin can be either liquid or solid. When n is close to zero, the resin is liquid; solid resins generally have a n value in the range of 3 - 30. For room temperature curing applications like coatings or paints, liquid resin is preferred. High molecular weight resin is used for moldings, encapsulations or other applications which require stronger adhesion and mechanical strengths [62].

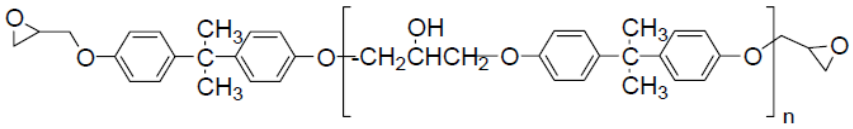

Figure 1.5 Chemical formula of the epoxy resin based on diglycidyl ether of bisphenol A (DGEBA) [62].

By curing treatment with a hardener, a 3D crosslinking network is formed in the epoxy polymer, which renders epoxy a very good thermal stability and much better mechanical strength compared with the thermoplastic materials like polypropylene or polyurethane. In addition, epoxy polymers have excellent chemical and water resistance, electrical insulation and superior adhesion on polar surfaces. They have wide applications as coatings, adhesives, varnishes, encapsulations, moldings, etc. in automotive, aerospace and civil construction industries.

1.3.4 CNFs and CNTs/polymer composites

Due to their intrinsic good mechanical strength, excellent heat and electron transportability, CNFs or CNTs have been incorporated into epoxy polymer to improve their mechanical properties and conductive properties. The infusion of trace amount of these high performance fillers can significantly enhance the polymer property because of their unique high ratios of length over radius and surface area over volume.

1.3.4.1 Mechanical properties of composites

Mechanical reinforcement of epoxy composites is generally the first expectation from these strong nanofillers for the preparation of composites containing CNFs or CNTs. Composites with either pristine or chemically modified carbon nanofillers are investigated in the last two decades.

CNFs/epoxy composites with epoxy resin Epon 862 and oxidized CNFs as the polymer matrix and fillers respectively showed a maximal modulus increase of three-fold than pure epoxy [63]. Tan et al. prepared composites with the same matrix but with the amine modified CNFs and observed improved tensile modulus and strength compared to pristine CNFs/epoxy composites [64]. Amine functionalized CNFs were imbedded into epoxy resin by twin screw extruder and the tensile strength increased 16 % than the as-prepared CNFs/epoxy. The tensile strength and elongation-to-break were also improved by surface aminosilanized CNFs/epoxy composites [16]. Prolongo and coworkers studied the thermal - physical properties of amine functionalized CNFs/epoxy composites and found out that the increased storage modulus was

because of surface modification [65]. Choi et al. observed similar improvement of the dynamic mechanical properties in their research [66]. The interlaminar shear strength and flexural strength of glass fiber/epoxy composites were enhanced due to the introduction of CNFs in the system [67]. Zhou and coworkers also demonstrated flexural strength enhancement by the infusion of CNFs into epoxy matrices [68]. Patton et al. achieved increased stiffness and large improvement of flexural strength due to the addition of CNFs into epoxy [69]. Thermal treatment of CNFs until 1800 ^{o}C also improved the mechanical strength of epoxy composites due to the better graphitized structure of fillers [70]. Due to the good dispersion of CNFs in the epoxy matrix, the composite showed an improvement of the tensile strength at 1 wt% CNF loading and the theoretical fitting of the tensile and storage modulus matched well with the experimental data [71].

The first work of CNTs/epoxy composites appeared in 1994 [72]. Although the nanotubes were aligned in the matrix, which might result in anisotropic properties in the direction parallel and vertical with the alignment, the mechanical measurement was not carried out on these composites. After that, the research of mechanical reinforcements of CNTs in epoxy matrices was tremendous. Since Young's modulus (Y) depends greatly on the volume fraction of CNTs (V_f), the rate of the increase of Young´s modulus with the volume fraction of CNTs (dY/dV_f) is used as a scale to evaluate the efficiency of reinforcement. Based on the work from Coleman et al., the median value of dY/dV_f for CNT reinforced epoxy polymer is 18 GPa, and in the following only reinforcements higher than that value are quoted here [51]. The first mechanical measurement, which demonstrated the stress-strain properties of MWCNTs/epoxy composites, was done by Schadler and coworkers [73]. Better reinforcement was found in compression (dY/dV_f = 26 GPa) than in tension (dY/dV_f = 18 GPa). It was assumed that the load transfer in compression was attributed to the hydrostatic pressure effect, while that in tension was due to interfacial bonding between fillers and matrices. The introduction of oxidized CNTs into epoxy matrices led to a reinforcement of dY/dV_f = 45 GPa due to the surface bonding between those oxygen containing functional groups on CNTs and the matrix [7]. SWCNTs/epoxy composites prepared by Li and coworkers gave a reinforcement of dY/dV_f = 94 GPa [74]. The excellent mechanical property came from the surface chemical functionalization of CNTs, which strengthened the interfacial force between fillers and matrices. Bai incorporated 1 wt% MWCNTs into epoxy and achieved a double modulus compared to pure polymer, and the reinforcement of dY/dV_f = 330 GPa is the highest for CNTs/epoxy system characterized through tensile measurements [6]. The significant

improvement of mechanical properties was attributed to the superior CNTs/epoxy adhesion or interaction, which was also confirmed by the direct observation of CNT breakage on the fracture surface of composites from SEM.

Based on the above review of previous efforts on mechanical improvement, it is concluded that mechanical properties of composites strongly depends on the dispersion of fillers and the adhesion between fillers and matrices. Good dispersion of fillers can fully develop their role as reinforcement agent on the composite property due to the strong sp^2 carbon bonds in the graphene structure; the interaction at the matrix/filler interface enables the effective mechanical load transfer from matrices to fillers, which enhances the stiffness and strength of composites accordingly.

1.3.4.2 Electrical conductivities of composites

In order to transfer an insulating polymer like epoxy into a conductive material, the concentration of conductive fillers in the matrix must reach a critical value, which is defined as the electrical percolation threshold. At that point the conductivity of composites increases drastically several orders of magnitude than the pure polymer due to the formation of conductive network in the matrix. Afterwards the conductivity keeps at a stable platform. Typical percolation behavior is plotted in Figure 1.6. According to the percolation theory, the electrical conductivity after the percolation threshold obeys equation 2 [75]:

$$\sigma_c = \sigma_o(\phi_f - \phi_{crit})^t \qquad (2)$$

where σ_c is the conductivity of composite; σ_o is the conductivity of the filler; ϕ_f is the volume fraction of fillers; ϕ_{crit} is the percolation threshold; t is the critical exponent. The exponent t is dependent on the dimension of fillers. For 1D spherical fillers, t is about 1.3; for 2D spherical fillers, t is between 1.6 and 2.0. Nanofibers or nanotubes have t value of about 3, arising from their high aspect ratio [76, 77]. This equation can be combined with experimental data for predicting the percolation threshold.

When CNTs or CNFs are uniformly dispersed into the matrix, the effective electrical conductivity of fillers achieves as high as several thousands or millions of $S \cdot m^{-1}$. A percolation threshold as low as 0.001 wt% is theoretically possible for CNTs with extremely large aspect ratio of 1×10^4. However, this ideal presumption can never be realized due to entanglements and agglomerations of nanofillers. The experimental electrical percolation of CNTs and CNFs is in the range of 0.002 - 8 wt% and 0.5 - 18 wt% respectively [10, 26], depending on the filler alignment, the aspect ratio and the dispersion status of fillers.

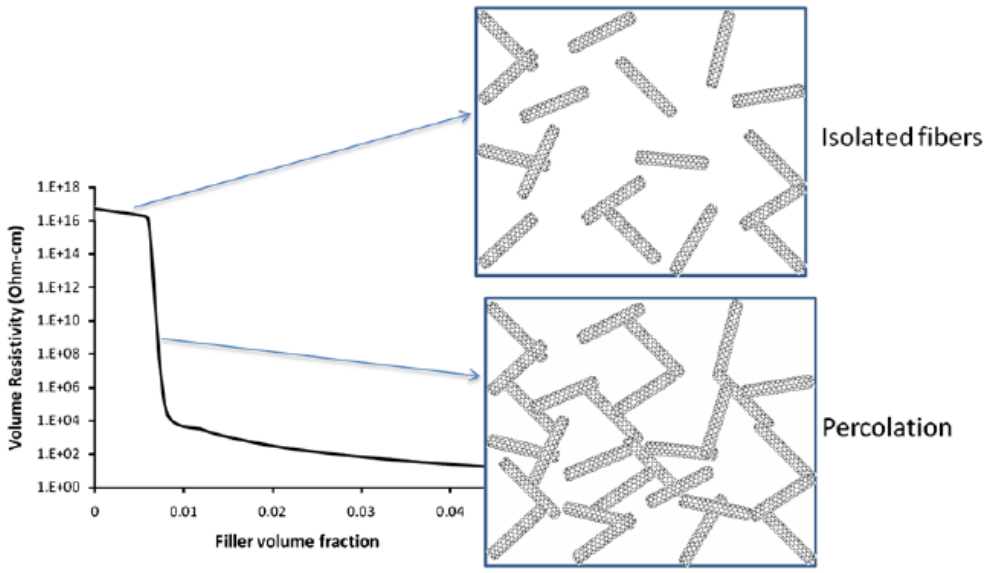

Figure 1.6 The sketch of the percolation behavior of CNFs [26].

It is also found that in order to form percolation network, the uniform distribution of carbon nanofillers in the matrix is not always necessary. On the contrary, the agglomeration of single nanotubes or fibers facilitates the formation of conducting networks. As shown in Figure 1.7, there are four combinations of dispersion and distribution status for nanofibers in the matrix. Conductive paths are not able to generate in these three scenarios - bad distribution and dispersion, good distribution but bad dispersion, good distribution and dispersion. Only when the nanofibers are well dispersed but badly distributed, develops the conductive network. Therefore in the practical work, efforts should focus on dispersing the bundles of CNFs or CNTs into single filaments more than on distributing fillers homogeneously in the matrix in order to get good electrical conductivity.

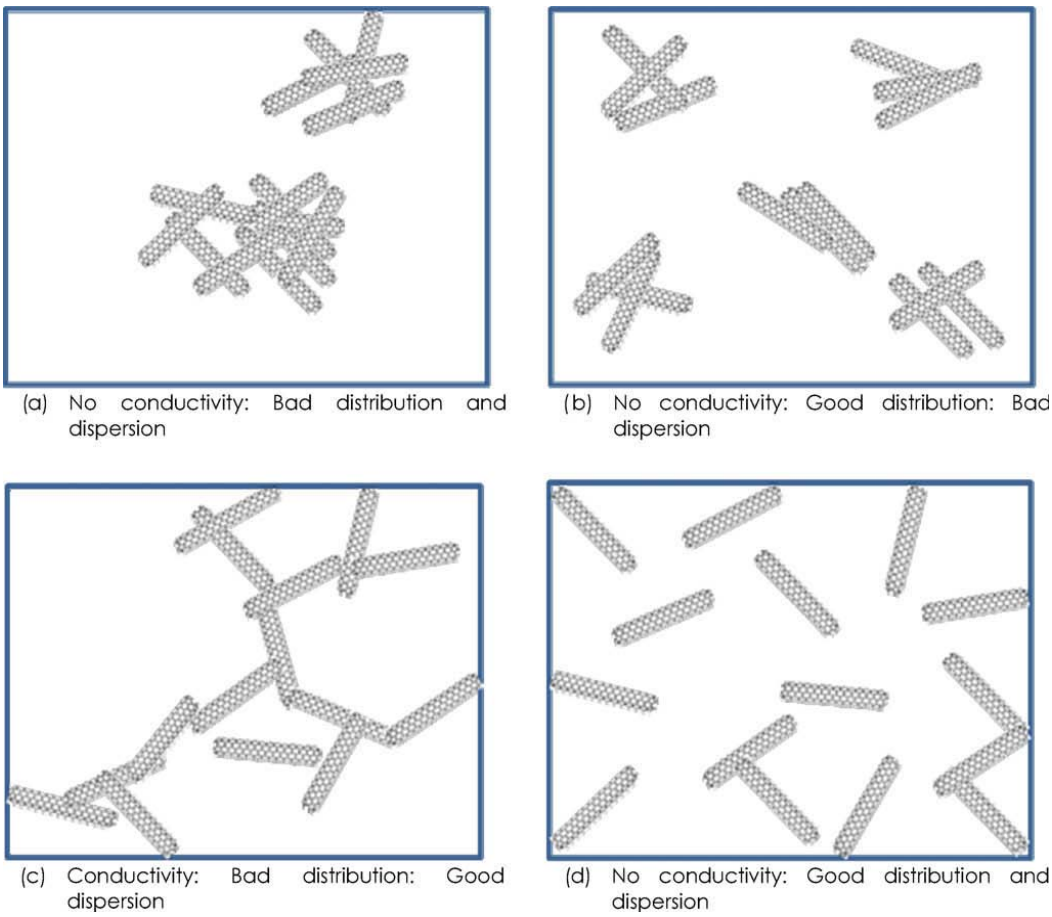

Figure 1.7 Scheme for the distribution and dispersion of CNFs in polymer matrices [26].

1.3.4.3 Thermal conductivities of composites

It was expected that due to their excellent thermal transport, addition of CNFs or CNTs would make a breakthrough of the composite thermal conductivity when a filler network was constructed in the matrix, similar as the percolation behavior of the electrical conductivity. However, according to previous reports, the improvement of thermal properties by infusion of CNFs or CNTs into polymer matrices is disappointing. Some demonstrated remarkable or moderate improvements of thermal conductivities of polymer composites [69, 78], while others showed negative results [79].

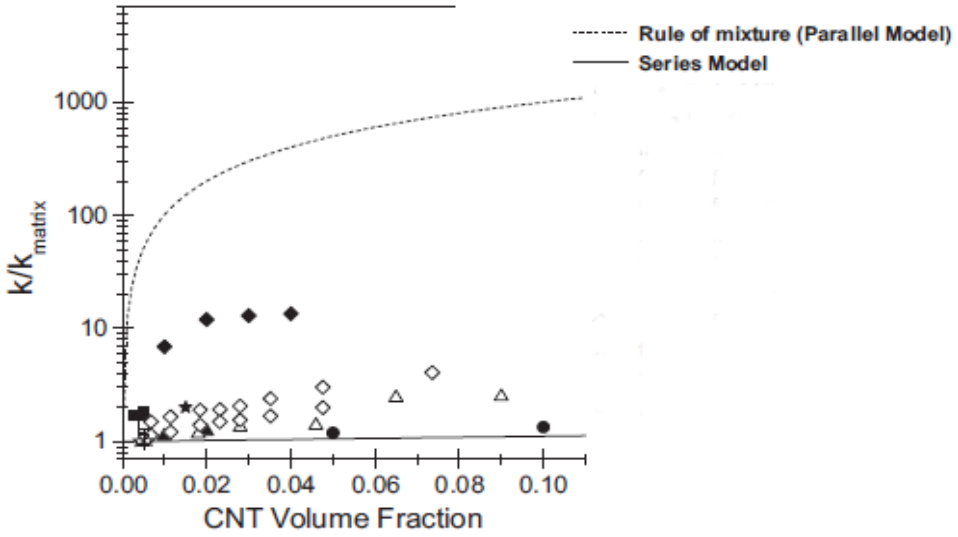

Figure 1.8 The enhancement of thermal conductivity of composites compared to that of pure polymer as a function of CNT volume fraction [80].

An overview of the thermal conductivity of polymer composites containing CNTs was done by Han and Fina (as shown in Figure 1.8). The experimental results lay between the two basic models - rule of mixture and series model. In the rule of mixture (equation 3), it is assumed that the fillers have the perfect thermal contact with each other, i.e. they form conductive networks; on the contrary, the series model (equation 4) presumes that there is no conductive contact between fillers, and fillers are confined in the matrix where they are embedded [80].

$$\text{Rule of mixture:} \qquad K_c = K_f \Phi_f + K_m \Phi_m \qquad (3)$$

$$\text{Series model:} \qquad K_c = \frac{1}{(\Phi_m / K_m + \Phi_f / K_f)} \qquad (4)$$

where K_c, K_f, and K_m are the thermal conductivity of the composite, the filler, and the matrix respectively; Φ_f and Φ_m are the volume fraction of the filler and the matrix respectively [80].

Both models are the extreme situation. In reality, the thermal contact as well as the thermal resistance between fillers should be simultaneously considered.

The contact resistance from filler to filler can compromise the effect of CNFs or CNTs on improving the thermal conductivity of composites. When fillers are dispersed in the matrix randomly, the point contact between fillers produces a much greater resistance than the linear contact of aligned fillers in the matrix. Chen et al. was able to prepare electrical insulating epoxy composites with aligned CNFs to achieve a thermal conductivity of 695 $W \cdot m^{-1} \cdot K^{-1}$, significantly exceeding that of copper (390 $W \cdot m^{-1} \cdot K^{-1}$) and aluminum (190 $W \cdot m^{-1} \cdot K^{-1}$) [81].

Besides the aforementioned two factors, the interfacial thermal resistance between fillers and the polymer matrix affects the thermal conductivity tremendously. Since the heat transport in CNFs or CNTs is carried mainly by phonons, the thermal conductivity of composites containing CNFs or CNTs is also influenced by the phonon vibration mechanism. One origin of the interfacial thermal resistance is the mismatch of phonons between rigid carbon nanofillers and soft polymers. In carbon nanofillers, heat is transported by high frequency phonons, while in polymers the low frequency lattice waves carry the heat. Therefore the high frequency phonons from fillers must be converted into their low frequency counterparts through the phonon coupling in order to go through the interface [82, 83]. Phonon scattering from the surface defects or amorphous materials is another origin of the thermal resistance. Theoretical modeling by Nan et al. indicated that the interfacial thermal resistance between CNTs and polymer matrices hindered the effective heat transport in composites [84]. The phenomenon that composites had a lower conductivity than pure polymer matrix was also attributed to the great thermal resistance at the interface between fillers and the matrix.

A conductive network of fillers in the matrix is beneficial for the heat transport due to the good thermal contact between fillers. However, because of the phonon mismatch and scattering at the interface of filler/polymer, the thermal conductivity of composites increases only modestly in contrast to the bumping electrical conductivity at the percolation threshold.

Based on the above discussion, a decreased interfacial thermal resistance and a conductive network of fillers are essential to prepare composites with a high thermal conductivity. In order to construct a filler network, it is desirable to disperse fillers uniformly in the matrix. Physical blending by the shear force or ultrasonic force, and functionalization of fillers are the mostly used methods to improve the dispersion of fillers. Especially the chemical functionalization of fillers provides the possibility of fillers to further interact with the matrix, which will decrease the interfacial thermal resistance originating from phonon mismatch, and thus improve the thermal conductivity of composites.

1.3.5 Chemical modification of CNFs and CNTs

1.3.5.1 General review

The dispersion state and the interfacial connection between fillers and matrices seem to be the most important factors affecting the properties of composites based on the previous discussion. Despite many techniques, including physical blending, physical functionalization, and chemical modification, have been utilized to improve the dispersion of CNFs/CNTs in

polymer matrices, there is still much room to optimize the dispersion of fillers in matrices. For physical blending, due to the applied high shear force or ultrasonic energy, the aspect ratio of fillers is reduced, which degrades their performance as reinforcing agents. For physical functionalization, usually surfactants were added to increase the repulsion between single CNFs or CNTs. Surfactants or stabilizers are always compromising the mechanical properties of composites because the weak non-covalent interactions are unable to effectively transfer the mechanical load from matrices to fillers. Chemical modification of fillers was the most efficient way to increase the filler/polymer interfacial force due to the formation of covalent bonds at the interface, which is the must for the enhancing properties of polymer composites. In addition, chemical functionalization facilitates the wetting of matrices on fillers for optimizing the dispersion of fillers.

Surface chemical functionalization of CNTs was reviewed by Tasis and coworkers [85]. There are basically two types of chemical modifications for CNFs or CNTs: direct functionalization on non-oxidized fillers and the multi-step modification of fillers with oxygen containing functional groups on the surface (such as COOH or OH). Direct functionalization normally requires strict reaction conditions such as inert gas protection, long reaction time, complicated experimental set-up, etc.. For example, Baek et al. modified CNFs by Friedel-Crafts acylation [86, 87], but high temperature and complicated procedures were required; different polymers were grafted on CNFs and the effect of modification on electrical properties were investigated by Wei and coworkers [88-90]. In all these researches CNFs were wrapped by polymers through either in-situ polymerization or surface grafting with the help of special initiators or catalysts, which raised the cost and increased the complicity. On the contrary, surface modification based on oxidized fillers is a facile method due to the oxidation is easily to be realized with oxidants such as strong acids, $KMnO_4$, etc.. The existence of oxygenated groups enables rich choices for further chemical modification. Therefore chemical functionalization on oxygenated filler surface is a feasible and low cost method for both optimising the dispersion of fillers in the matrix and the interfacial force between carbon fillers and matrices.

1.3.5.2 Silanization

To make a bridge between inorganic fillers and the polymer matrices, a bifunctional molecule which reacts with both the fillers and the polymer is required. Silanization is the process of covering a surface through silane coupling agents with the following structures:

$$R_{(4-n)}\text{-Si-}R'_n$$

where R is a functional group; R' is the releasable organic moiety (alkoxy groups or halogen groups), which can be readily attacked and replaced by hydroxyl groups to form covalent bonds at the interface between the mineral surface and the organic silanes; n is the number of releasable groups (n≤3) [91]. Since there are diverse choices of the functional group R (thiol, amine, epoxy ring, vinyl, aromatic ring etc.), silanization is very attractive as a versatile method to modify the CNF or CNT surface for improving the compatibility and interaction between fillers and polymer matrices. Although silane derivatives containing halogen hydrolyze much faster than their counterparts containing alkoxy groups, they are too sensitive to the moisture, which complicates the experimental procedure. Silanization with alkoxy groups are more controllable. Silanization takes place in four steps: first hydrolysis of silanes into silanols; then condensation of silanols into oligomers; formation of hydrogen bonds between oligomers and surface hydroxyl groups from carbon nanofillers; finally the reaction of Si-OH groups with OH groups on CNFs to build Si-O-C bonds (Figure 1.9).

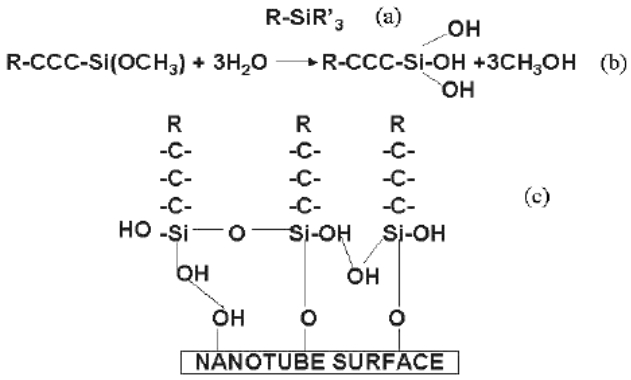

Figure 1.9 Scheme of the silanization process on CNTs [91].

Bag et al. oxidized MWCNTs with the mild oxidant potassium permanganate and then modified the oxidized MWCNTs with 3-methacryloxypropyltrimethoxysilane (MPS) to improve their solubility in organic solvents and possible compatibility with vinyl based monomers [92]. Palencia et al. studied the influence of temperature, reaction time, concentration and types of silanes (3-aminopropyltriethoxy silane, 3-aminopropyltrimetoxysilane, N-(2-aminoethyl)-3-(aminopropyltrimethoxy silane) and 3-glycidoxypropyltrimethoxy silane) on the silanization process of CNFs [93]. CNFs with surface impurities or defects such as COOH and OH groups were silanized with those silanes in one step process. Unlike aminosilanes, 3-glycidoxypropyltrimethoxysilane at high concentration formed multilayers on CNFs, which suggested that it adsorbed easier on the surface than aminosilanes. Ding and coworkers coated the CNT with a porous silica layer by the assistance of a cationic surfactant cetyltrimethyl ammonium bromide (CTAB) [15]. These

porous SiO_2 coated CNTs may find potential applications as mechanical reinforcement agents, elements for electronic devices and nanocarriers, etc.. Modified CNTs or CNFs were then introduced into epoxy polymer to tailor the electrical property and thermal conductivity of composites. Zhou et al. first modified MWCNTs with silica by a sol-gel process, and then with MPS. The functionalized CNTs showed a higher mechanical reinforcement for the propylene polymer than the pristine ones [94]. Vinyltriethoxysilane (VTS) and MPS physically adsorbed onto the surface of CNFs by Nistal and co-workers. It was concluded that VTS adsorbed on CNFs through π-π interaction, while MPS adsorbed on CNFs through silanol-hydroxyl or carbonyl-hydroxyl interaction [95]. This research shows only the possibility to change the solubility of CNFs in different solvents via silane adsorption. However, to form strong covalent bonds, the addition of catalyst or a high temperature treatment is required. Ma et al. first oxidized CNT by UV/O_3 treatment and then CNT further reacted with 3-glycidoxypropyltrimethoxysilane [96]. The silanization improved CNT dispersion and exfoliation in ethanol suspension. Later they imbedded the glycidoxysilanized CNTs into epoxy resin to study their influence on the mechanical properties and electrical conductivities. The modified CNTs showed better dispersion in epoxy matrices, apparent improvement of mechanical strength and thermal properties of composites. The electrical conductivity was lower than the composites with pristine CNTs because of the wrapping of non-conductive silane on CNT surface [97]. Zhu and coworkers silanized CNFs with 3-aminopropyltriethoxysilane (APTES) coupling agent and incorporated these CNFs into epoxy polymers [16]. A significant increase of tensile properties and storage modulus was achieved, but a decrease of electrical conductivity compared to the pristine CNFs/epoxy composites was observed due to the insulating silane layer on the surface (Figure 1.10), which coincided with the results from Ma [97]. Carbon/CNT/epoxy three phase composites were prepared by Lee et al. [98]. CNT silanized with APTES improved the tensile properties and thermal stability of composites. In contrast to results from Ma and Zhu, which showed lower electrical conductivity in composites with silanized fillers, the aminosilanized CNTs improved electrical conductivity of composites due to the low concentration of CNT.

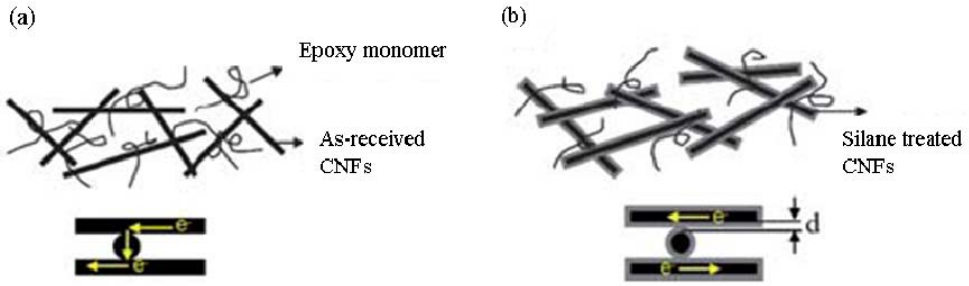

Figure 1.10 Sketch of CNFs in epoxy resin (a) as-received CNFs, (b) silanized CNFs [16].

Based on the above review about state of the art for silanization of CNFs or CNTs, it is found that aminosilane and glycidoxysilane has been used more often to modify the surface of CNFs or CNTs for improving the properties of composites, especially those based on epoxy polymers due to the potential reactions of amino groups in aminosilane with epoxy resin and the epoxy ring in glycidoxysilane with the hardener used in epoxy matrices respectively. Figure 1.11 shows the chemical mechanism of amine and epoxy reaction [99]. The primary amine reacts with the oxirane ring to form a secondary amine (formula 1); the secondary amine reacts further with epoxy ring and a tertiary amine is generated (formula 2). They are the main reactions between epoxy and amine groups. The tertiary amine facilitates the self polymerization of epoxides into polyether (formula 3). However, the homopolymerization is negligible without the existence of Lewis acids or bases. The hydroxyl groups generated during the ring opening process of epoxy ring can react with epoxide to produce ether (formula 4), which is much slower than the epoxy-amine reactions.

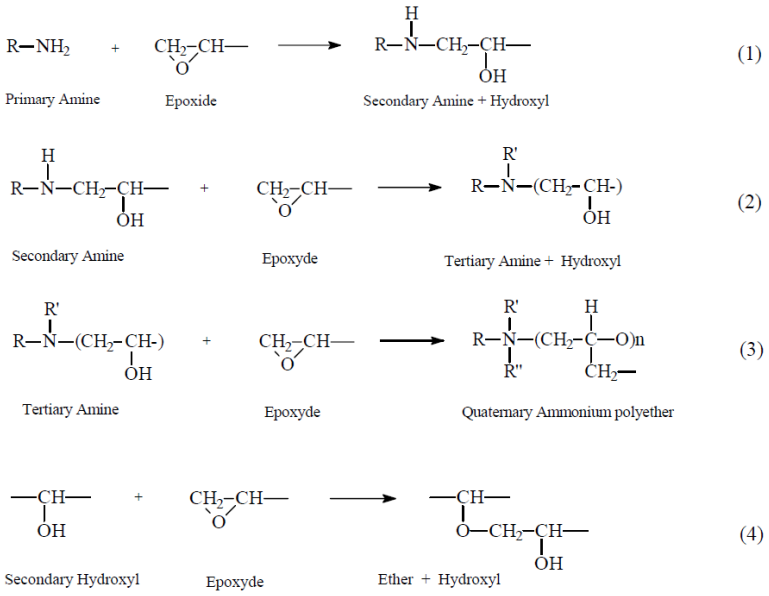

Figure 1.11 Scheme of epoxy-amine reactions (formulas 1-3) and the etherification (formula 4) [99].

1.4 Motivation

Great strides have been stepped out for the preparation of CNFs or CNTs/epoxy composites. However, the poor dispersion and distribution of fillers in matrices, and the lack of interfacial interaction between fillers and matrices still hinder the applications of CNFs or CNTs for improving mechanical, electrical and thermal properties of epoxy polymers.

Silanization is considered to be an effective way to covalently bridge the carbon nanofillers and polymer matrices. But the reaction mechanisms and the effects of different silanizations are not studied explicitly.

The glycidoxysilane and aminosilane are effective to improve the properties of modified carbon nanofillers/epoxy composites by the formation of covalent bonds between fillers and epoxy polymers [97, 98]. It brings us the idea to use these two silanes as models for investigating the reaction mechanism and effects of different silanizations on the properties of CNFs or CNTs/polymer composites. In addition, due to the high chemical activity of isocyanates to react with the carboxyl group on the surface of oxidized CNFs or CNTs, Zhang et al. has modified MWCNTs with octadecylisocyanate, resulting in a good exfoliation of CNTs in the polyimide matrix and enhancing the thermal stability and mechanical property of the polymer composites [100]. It is thus assumed that the introduction of isocyanatesilane on oxidized carbon nanofillers may be another effective way of silanization on carbon nanofillers.

Therefore in this thesis, silanizations were applied on oxidized CNFs or MWCNTs. First the silanization with 3-glycidoxypropyltrimethoxysilane was done on oxidized CNFs. In order to improve the yield of silanization, the carboxyl groups on oxidized CNFs were reduced into alcoholic hydroxyl groups and then reacted with 3-aminopropyltrimethoxysilane. The two-silanization procedure with 3-isocyanatopropyltriethoxysilane and 3-aminopropyltrimethoxysilane was carried out on oxygenated CNFs to further increase the silicon content on CNFs. The silanization procedure with 3-aminopropyltrimethoxysilane followed by reduction was also carried out on MWCNTs for comparison. Various chemical characterizations were performed to confirm the silanization. Both original and modified carbon nanofillers were embedded into epoxy resins to see their influences on the mechanical properties, electrical as well as thermal conductivities of epoxy polymers.

1.5 Objectives

During the research, we try to answer the following questions:

- Is it possible to distinguish the chemical silanization from the physical adsorption of silanes on carbon nanofillers?
- Will the graphitic structure of CNFs or CNTs be damaged due to modification processes?
- What's the effect of silanizations on the properties of carbon nanofillers?
- Is it successful to alter the properties of CNFs/epoxy or CNTs/epoxy composites through silanizations?
- What are the different effects of CNFs and CNTs on the properties of epoxy composites?
- What's the relationship between properties and structures of epoxy composites containing CNFs or CNTs?

2 Chemical modification of CNFs and MWCNTs with silanes

2.1 Materials

CNFs (PR-24-PS) used in this work were obtained from Pyrograf Products Inc., Ohio, USA and were produced via chemical vapor deposition method. The average diameter of CNFs is about 60 - 150 nm, and the length is in the range of 30 - 100 μm, according to the manufacturer's data. The CNFs have a morphology termed "stacked cup" or "herringbone" (Figure 2.1), with exposed edge planes canted with the fiber axis. It is consistent with the schematic structure of CNFs shown in Figure 1.3. These edge sites are highly chemically reactive and allow rapid intercalation and deintercalation of heterogeneous atoms. There is an amorphous layer on the outer wall of the fibers and the crystalline graphenes are parallel with each other but canted with the fiber axis. The interlayer space is 3.38 Å according to the TEM measurement. MWCNTs were produced on oxidized silicon wafers in TU Ilmenau based on spray pyrolysis CVD method. Benzene and acetonitrile with ferrocene were used as the feeding stock. The detailed information for the synthesis was shown in [60]. MWCNTs have a bamboo structure and a diameter in the range of 50 – 100 nm (Figure 2.2).

3-glycidoxypropyltrimethoxysilane (GPTMS, 98 %), 3-aminopropyltrimethoxysilane (APTMS, 97 %) and triethylamine (TEA, 99 %), $KMnO_4$ (99 %) were from Sigma-Aldrich Co., Steinheim, Germany. $NaBH_4$ (98 %) and I_2 (99 %) were from Alfa Aesar Co., Karlsruhe, Germany. H_2SO_4 (98 %), HNO_3 (65 %), tetrahydrofuran (THF, 99 %), N, N-dimethylformamide (DMF, 99 %), ethanol (absolute), acetone (98 %), NaOH (98 %) and HCl (97 %) were from AppliChem GmbH, Darmstadt, Germany. 3-isocyanatopropyltriethoxysilane (IPTES) was from Fluorochem Ltd., Old Glossop, United Kingdom. Trifluoroacetic anhydride (TFAA) and (4-triflurомethyl) benzaldehyde (TFBA) were supplied from Alfa Aesar.

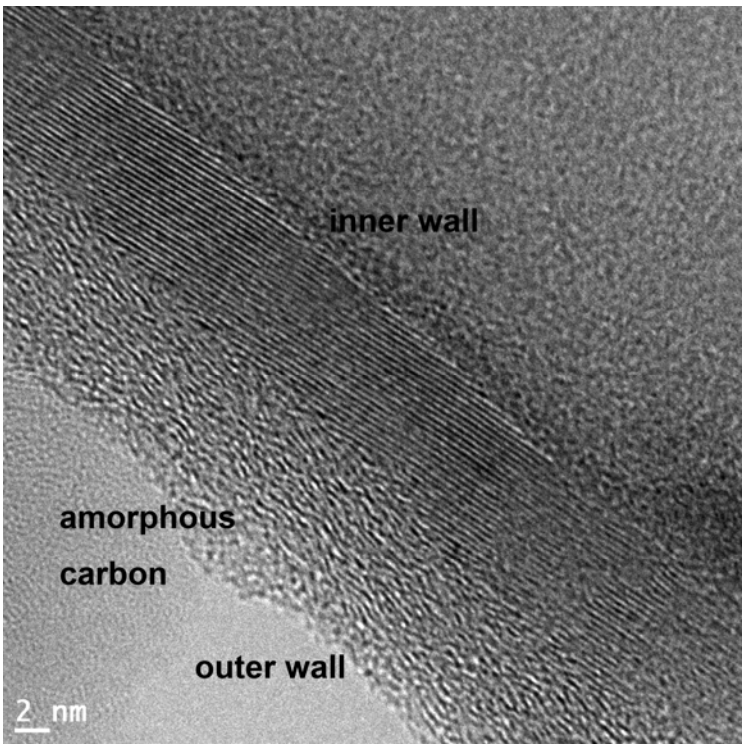

Figure 2.1 TEM picture of original CNFs.

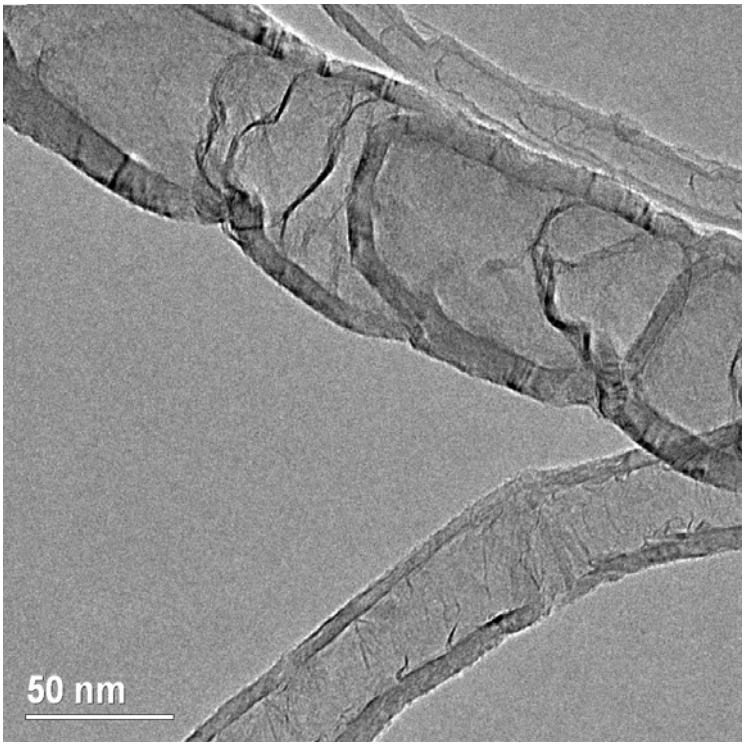

Figure 2.2 TEM picture of pristine MWCNTs.

2.2 Modification

2.2.1 Oxidation of CNFs and MWCNTs

Original, as-received CNFs (CNF-O) were oxidized in different ways (Figure 2.3). The most frequently used two methods for wet-chemical oxidation of graphite based materials are strong acid mixture of concentrated H_2SO_4/HNO_3 or mild $KMnO_4/H_2SO_4$ treatments. In order to find the optimal conditions for oxidation, both methods were tried. In scheme a), 1 g CNFs were suspended into 120 ml mixture of concentrated H_2SO_4/HNO_3 (volume ratio is 3:1), and sonicated in water bath at room temperature (RT) for 3 h (CNF-AS); for scheme b), 1 g CNFs were suspended into 120 ml mixture of H_2SO_4/HNO_3 (volume ratio 3:1), and heated at 70 °C for 3 h (CNF-AH). After the reaction, CNFs were washed repeatedly with a large amount of distilled water and filtered until the pH of filtrate was 7. Scheme c) and d) showed the procedure of $KMnO_4$ oxidation. For scheme c), 50 mg CNF and 262 mg $KMnO_4$ were added into 25 ml 0.5 M H_2SO_4 aqueous solution and sonicated for 3 h at RT. CNFs were then filtered and washed with concentrated HCl to remove MnO_2, followed by rinsing with distilled water until the filtrate was pH neutral (CNF-PMS). For scheme d), typically 120 mg CNFs were dispersed into 20 ml 0.5 M H_2SO_4 aqueous solution by sonication in water bath for 15 min. Then another 20 ml 0.5 M H_2SO_4 containing 1.98 g $KMnO_4$ was added into the CNF suspension dropwisely. The reaction was refluxed at 120 °C for 3 h. The resultant was filtered and washed with concentrated HCl and H_2O respectively until the filtrate was pH neutral (CNF-PMH). Oxidation of MWCNTs was done in the similar way as CNFs. For MWCNTs, only the oxidations with H_2SO_4/HNO_3 under sonication bath and with $KMnO_4/H_2SO_4$ at refluxing condition were carried out for comparison. For acid mixture oxidation process, 100 mg MWCNTs were suspended into 40 ml mixture of concentrated H_2SO_4/HNO_3 (volume ratio 3:1) and sonicated for 3 h. The final product was purified in the same way as in the preparation of CNF-AS, and labeled as MWCNT-AS. For $KMnO_4/H_2SO_4$ heating oxidation, the procedure was exactly the same as that for the preparation of CNF-PMH, and the obtained MWCNT was defined as MWCNT-PMH.

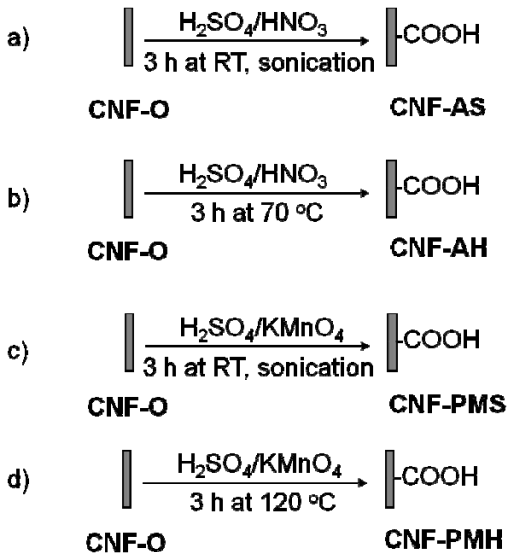

Figure 2.3 Scheme for the different oxidation processes of CNFs.

2.2.2 Functionalization of CNFs with glycidoxysilane

CNFs were oxidized primarily through bath sonication in the mixtures of concentrated sulfuric and nitric acid with volume ratio of 3:1. Afterwards, they were washed repeatedly with distilled water until the pH value of the filtrate was 7. The sample was then rinsed with acetone and further dried at 80 °C overnight (CNF-AS). Then 1 g of CNF-AS was dispersed in 50 ml absolute ethanol by ultrasonic probe (BANDELIN SONOPULS ultrasonic homogenizers GM 2200) for 10 min. 500 μL GPTMS was dissolved in 10 ml ethanol and added dropwisely into the above mentioned ethanol suspention of CNFs and agitated with a magnetic bar at 1100 rpm. The CNF ethanol suspension was kept refluxing for 5 h. Finally the suspention was filtrated, washed with ethanol and acetone three times respectively and dried in a vacuum desiccator for 24 h (CNF-GS). The whole chemical treatment is depicted in Figure 2.4.

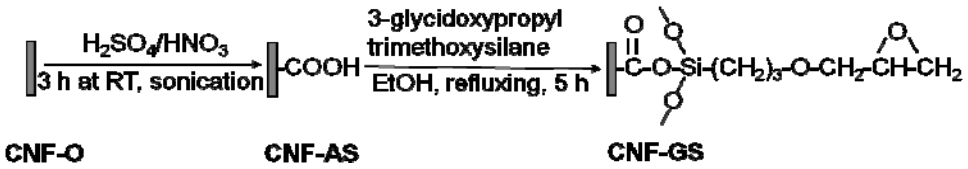

Figure 2.4 Sketch for the silanization process of CNFs with GPTMS.

2.2.3 Functionalization of CNFs with aminosilane

A scheme of the modification process is shown in Figure 2.5. Original CNFs (CNF-O) were first oxidized (CNF-AS). 1.5 g CNF-AS powder was dispersed in 50 ml THF by high power ultrasonic probe for 5 min, then 150 mg $NaBH_4$ was added into the suspension for reduction

of carboxyl groups. The mixture was stirred for 30 min until no bubbles came out. Afterwards, 225 mg I_2 dispersed in 10 ml THF was added into the above suspension and agitated for 24 h with magnetic bar at 900 rpm. The $NaBH_4$ reduced CNFs (CNF-N) were obtained by filtration, sequential washing with 3 M HCl, 3 M NaOH, distilled water, acetone and drying at 80 °C over night. Then 1 g CNF-N powder was dispersed in 50 ml absolute ethanol by ultraprobe sonication for 5 min, and then 10 ml 10 % (volume concentration) ethanol solution of APTMS, 300 µl TEA and 1 ml distilled water were added into the CNF-N suspension dropwisely. TEA was added as a catalyst for enhancing the surface coating efficiency [101, 102]. The mixture was stirred for 3 h at RT. Finally 3-aminopropyltrimethoxysilanized CNFs (CNF-N-AP) were washed with ethanol, acetone repeatedly, and dried overnight in a vacuum desiccator.

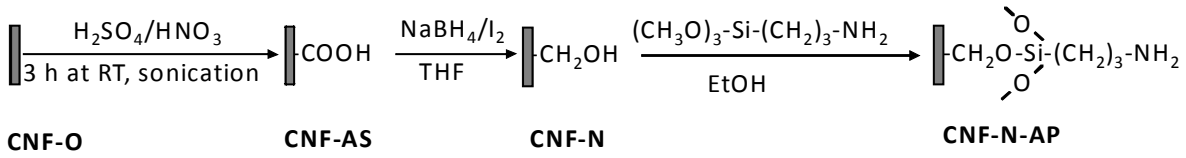

Figure 2.5 Sketch for the silanization process of CNFs with APTMS.

2.2.4 Functionalization of CNFs with isocyanatesilane and aminosilane

CNFs were oxidized by sonication in concentrated acid mixture of H_2SO_4 and HNO_3 (volume ratio 3:1), and purified with distilled water as discribed in section 2.2.1 for the preparation of CNF-AS. Then 1 g CNF-AS was suspended into 50 ml DMF by ultrasonic probe for 10 min, followed by additon of 5 ml DMF solution containing 500 µl IPTES. The reaction mixture was stirred at 900 rpm for 3 h. The product was rinsed with a large amount of DMF and acetone repeatedly, then filtered and dried in the oven at 80 °C overnight. The second silanization with APTMS was done as following: 1g CNF-I was dispersed into 50 ml ethanol by ultraprobe sonication for 10 min; then 1 ml APTMS in 10 ml ethanol was dropped into the suspension under magnetic stirring at 900 rpm. Then 500 µl distilled water and 200 µl TEA was added into the reaction flask. The product was collectd afer 3 h by filtration and repeatedly rinsing with ethanol and acetone (CNF-I-AP). The whole procedure is sketched in Figure 2.6.

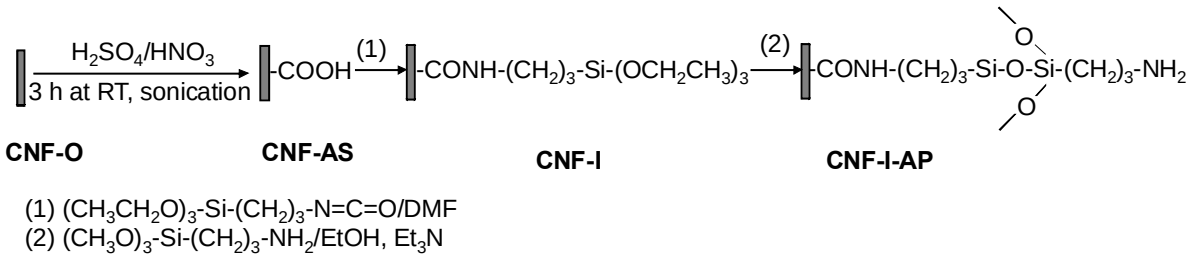

Figure 2.6 Sketch for the silanization process of CNFs with IPTES and APTMS.

2.2.5 Functionalization of MWCNTs with aminosilane

First MWCNTs were oxidized by $H_2SO_4/KMnO_4$ with the same condition used for CNF-PMH described in section 2.2.1 (MWCNT-PMH). Then 100 mg MWCNT-PMH was dispersed in 25 ml THF by ultraprobe sonication for 5 min, followed by addition of 50 mg $NaBH_4$. 75 mg I_2 was dissolved in 5 ml THF and dropwisely added into the aforementioned mixture. The reaction was kept for 24 h, followed by rinsing with 3 M HCl, 3 M NaOH, H_2O and acetone. Then the obtained MWCNT-PMH-N was dried for 12 h at 80 °C. For the silanization, 100 mg MWCNT-PMH-N was dispersed in 25 ml ethanol by ultraprobe for 5 min. Then 300 µL distilled water, 300 µL APTMS dispered in 5 ml ethanol, and 100 µL TEA, was dropped into the suspension sequentially. The mixture was stirred at 900 rpm for 3 h. The final product was washed with ethanol and acetone three times respectively and dried in a vacuum desiccator overnight (MWCNT-PMH-N-AP).

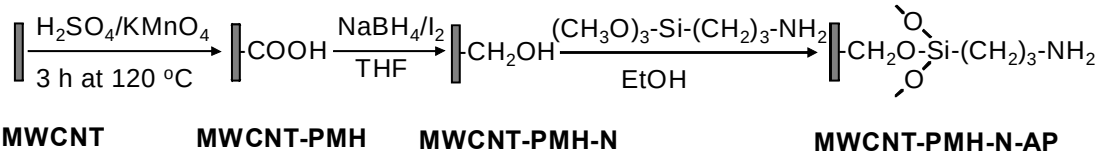

Figure 2.7 Sketch for the silanization process of MWCNTs with APTMS.

2.2.6 Derivatization of modified MWCNTs

The derivatization of modified MWCNT was done in order to quantify functional groups (C-OH or C-NH_2) by XPS analysis. The procedure of the derivatization with TFAA was as below: 100 mg MWCNT-PMH-N was dissolved in 5ml acetonitrile and 5 ml 1,4-dioxane in a 50 ml one-necked round bottomed flask with a magnetic stir bar. Then 50 mg 4-dimethylaminopyridine, 1.0 ml N-ethyldiisopropylamine and 0.5 ml of the TFAA were added and the mixture was refluxed under stirring for 2.5 h. The reaction mixture was cooled down and stirred for another 18 h over night at RT. The derivatized CNTs were filtrated and washed with 1,4-dioxane, acetonitrile and dichloromethane. Finally the derivatized CNTs were dried at 80 °C for 24 h in a vacuum oven.

The derivatization of MWCNT-PMH-N-AP with TFBA was done as gas phase reaction in a 250 ml vacuum chamber at RT. The chamber containing CNTs was vacuumed to a pressure of about 1000 Pa and then filled with N_2. This pumping procedure was repeated for three times. Afterwards the chamber was connected to a container with the liquid TFBA. TFBA vaporized and reacted with CNTs for 4 h. Then the container was isolated from the reaction chamber and the pumping procedure was repeated again for three times before CNTs were taken out.

2.3 Characterization

FTIR spectra were collected on Nicolet 8700. KBr tablets containing 0.01 wt% CNFs were prepared by hydraulic press for IR measurements. XPS measurements were carried out on ESCALAB 200X with non-monochromatic magnesium or aluminum Kα X-ray source. The instrument was calibrated according to ISO 15472 [103]. TGA measurements were done on Setaram TGA 92-16 with a heating rate of 10 $K \cdot min^{-1}$ under the synthetic air. The morphology and surface chemical composition of CNFs was investigated by SEM equipped with an energy dispersive X-ray spectrometer (Hitachi S-4100) and by optical microscope (ZEISS Axiotech 100HD). Detailed surface morphology of CNFs was characterized on a JEOL 2200-FS TEM at high magnification. The morphology of MWCNTs was examined by Philips TECNAI TEM. Raman spectra were obtained on Raman Dilor XY spectrometer with a laser power of 7 mV at constant wave, a laser excitation of 514.5 nm, and a laser spot size of 2 μm. XRD measurements were taken on Seifert XRD 3000 TT, using copper Kα radiation (λ = 0.154178 nm) for 2θ ranging between 10 ° and 90 °.

The surface charge of nanomaterials is an important characteristic because it provides information about their stability. It can be neutral, positive or negative depending on what functional groups on the surface. Determination of the surface charge on CNFs is also interesting to us.

According to the Gouy-Chapman-Stern theory [104, 105], an electric double layer tends to form at the interface when a solid surface contacts with a liquid (Figure 2.8). The first layer is composed of direct adsorption of ions with opposite charges to the surface functional groups, which is called stern layer. The surrounding ions are loosely dispersed in the second layer-diffuse layer. Within a specific distance from the surface, ions attracted by the solid surface travel together with it as an entity, while the ions locating at a position further than that distance stay still. The plane at this specific distance is defined as slipping plane, and the potential on this plane is Zeta potential.

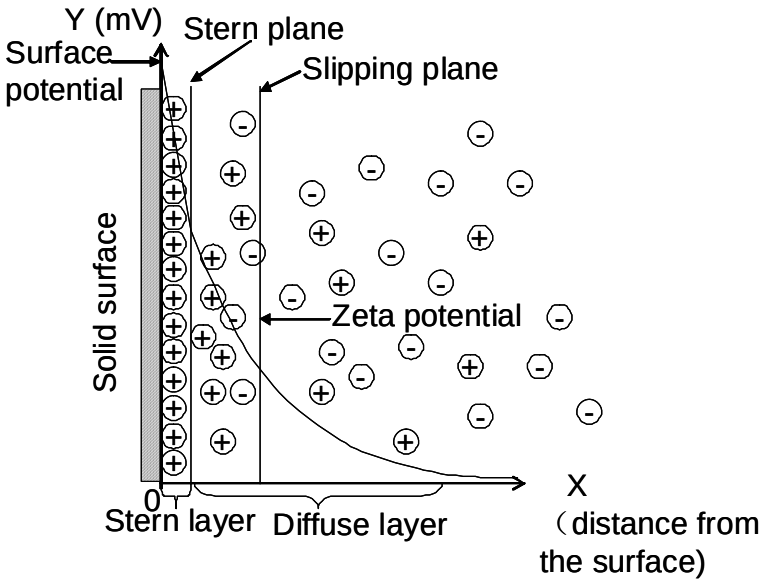

Figure 2.8 Scheme of the electrical double layer and Zeta potential.

Zeta potential highly depends on the pH of the liquid solution. At a certain pH value, the net electric charge of the surface or Zeta potential is zero. It is known as isoelectric point (IEP) and gives additional information about the solid surface. Because of its fast accessibility, streaming potential is measured more often to evaluate Zeta potential or IEP [106]. The relationship between streaming potential and Zeta potential is demonstrated in equation 5 (also referred as Helmholtz-Smoluchowski equation) [107]. Under a fixed temperature and pressure, streaming potential is proportional to the Zeta potential.

$$\frac{E}{\Delta P} = \frac{\varepsilon \xi}{4\pi \mu \kappa} \qquad (5)$$

where E is the streaming potential; ΔP is the pressure ; ε, μ, and κ are the dielectric constant, viscosity and electrical conductivity of the liquid respectively; ξ is the Zeta potential.

The set-up to measure the streaming potential is shown in Figure 2.9. When a liquid suspension of charged particles is moved under pressure in a channel, an electric current is produced in the system and streaming potential is generated to bring the net electricity to zero.

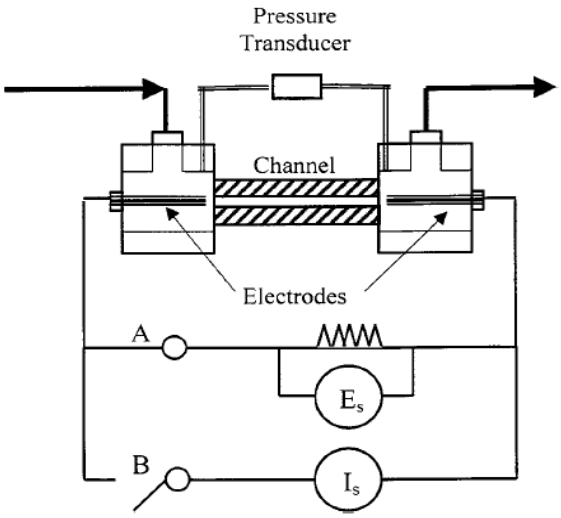

Figure 2.9 Apparatus for the measurement of the streaming potential [108].

In our experiments, streaming potential measurements of water suspension of CNFs were carried out on PCD-03 particle charge detector from Mütek. In order to get information about IEP, water suspension with 1.2 wt% CNFs was titrated with 0.1 M NaOH or 0.1 M HCl water solution. Fixed increment of the titrating solution (0.05 ml) was automatically controlled by the program in the device.

2.4 Results and discussion

2.4.1 Oxidation of CNFs

2.4.1.1 IR spectra

The efficiency of oxidation by different methods was investigated by IR spectroscopy. As shown in Figure 2.10, after oxidation, the presence of characteristic bands of OH stretching (3429 cm^{-1}), C=O stretching (1725 cm^{-1}) are evident in all oxidized samples except for sample CNF-PMS. The reason is that the mixture of $H_2SO_4/KMnO_4$ is a milder oxidative agent than the mixture of H_2SO_4/HNO_3, so the energy provided by bath sonication at RT is not enough to open the C=C graphite bonds for the formation of C=O bonds. There are also other bands at 2920 cm^{-1}, 1583 cm^{-1}, 1460 cm^{-1}, 1623 cm^{-1} [96], 1380 cm^{-1}, 1070 cm^{-1}, and 875 cm^{-1}, which correspond to C-H stretching in CH_2 groups, C=C stretching in the graphitic structure, CH_2 bending, intermediate oxidized products - quinone groups, O-H bending, C-O stretching, and epoxy ring stretching respectively. In sample CNF-AS, besides OH stretching band (3429 cm^{-1}), C-O stretching band (1070 cm^{-1}) also appears, which suggests that the oxidation efficiency is the highest.

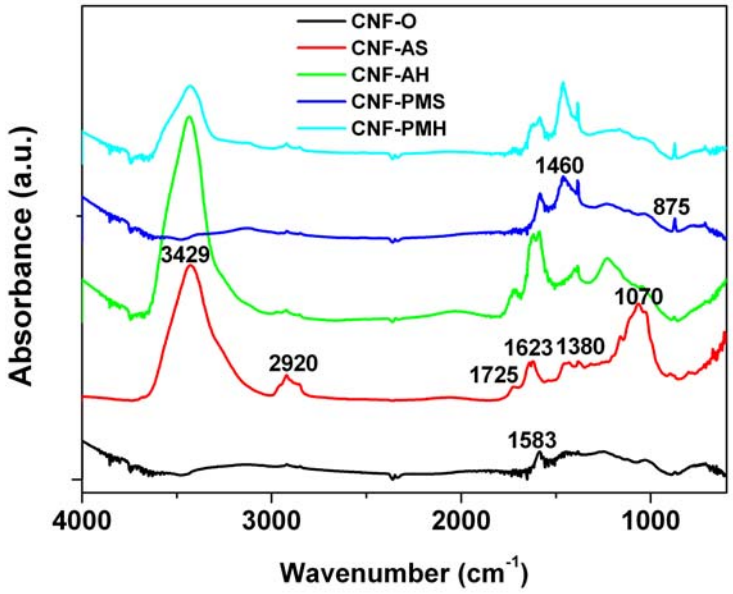

Figure 2.10 IR spectra of original CNFs (CNF-O) and oxidized CNFs (CNF-AS, CNF-AH, CNF-PMS, CNF-PMH).

2.4.1.2 XPS analysis

XPS measurements (Table 2.1 and 2.2) show that the content of oxygen increases a lot after each oxidation treatment. Especially for CNF-AS, the oxygen content is 20.6 %. There is also trace amount of S or Mn detectable, which is attributed to the residue of incomplete rinsing from H_2SO_4 or $KMnO_4$. The origin of detected Si and Al is not identified, perhaps coming from contamination. The relative percentage of functional groups derived from the deconvolution of respective peaks on XPS spectra gives additional confirmation of the successful oxidation processes. The C 1s spectra are deconvoluted by Unifit program into seven subpeaks, which are attributed to different functional groups based on [109, 110]. The peak around 284.6 eV corresponds to the sp^2 hybridized carbon double bond, while the peak at 285 eV is attributed to the carbon sp^3 hybridization in alkyl groups on the surface. CNF-AS keeps the highest ratio of C=C over CH_x structures, indicating that the surface graphitic structure is maintained to the largest extent. It is worth to note that the relative percentage of COOC or COOH groups is quite low compared with the graphitic C=C bonds. This gives us a hint that the surface oxidation probably proceeds in low efficiency, which coincides with results from other researchers [111-113]. Another possible explanation is that XPS measurements usually detect up to a depth of 10nm, which means not only the surface carbon, but also the structure beneath the surface contributes to the C signal. As a result, many more

C=C groups can be detected than COOC or COOH groups regarding to their relative percentage. CNF-PMS and CNF-PMH show a relative higher concentration of C-O-C or C-OH groups but lower amount of COOC or COOH groups compared to the acid mixture treated samples (CNF-AS and CNF-AH). Combined with IR spectra, it is assumed that the intermediate oxidation products in the mild $KMnO_4/H_2SO_4$ method are C-O-C or C-OH groups, and later on they are converted to C=O or COOC, COOH groups.

Table 2.1 XPS measurements of CNF surface composition.

	Content of elements in at%					
Sample	**C**	**O**	**S**	**Si**	**Al**	**Mn**
CNF-O	**96.4**	**3.3**	**0.3**	**-**	**-**	**-**
CNF-AS	**79.1**	**20.6**	**0.1**	**0.2**	**-**	**-**
CNF-AH	**81.1**	**18.3**	**0.2**	**0.1**	**0.3**	**-**
CNF-PMS	**86.0**	**13.1**	**-**	**0.2**	**0.5**	**0.2**
CNF-PMH	**89.1**	**10.4**	**-**	**-**	**-**	**0.5**

Table 2.2 Relative percentage of functional groups from the deconvolution of XPS C 1s peak.

	Relative percentage of functional groups (%)					
Binding energy and assignation	**C=C (284.6 eV)**	**C-C, C-H (285.0 eV)**	**C-O-C, C-OH (286.0 eV)**	**C=O (287.0-287.5eV)**	**COOC, COOH (288.7-289.3 eV)**	**p - p* Shake up (290.2-291.7 eV)**
CNF-O	**84**	**12**	**3**	**-**	**-**	**1**
CNF-AS	**70**	**16**	**6**	**-**	**8**	**-**
CNF-AH	**57**	**25**	**9**	**-**	**9**	**-**
CNF-PMS	**22**	**42**	**25**	**5**	**5**	**1**
CNF-PMH	**39**	**39**	**12**	**4**	**5**	**1**

2.4.1.3 Raman spectra

The information about the graphitic crystalline structure and the amorphous carbon or defects on CNFs was also acquired from Raman spectra [114] (Figure 2.11). The bands at around 1568 cm^{-1} and 1342 cm^{-1} correspond to the high crystalline graphite vibration in the tangential stretching mode (graphitic lattice mode E_{2g}) and the disorder induced phonon mode, which originates from the mode of boundaries in Brillouin zone, respectively [115-117]. The higher is the intensity ratio between G band and D band (I_G/I_D), the more crystalline is the CNF structure. There is also a shoulder peak around 1620 cm^{-1}, which is another indication of the surface defects on CNFs [118, 119]. This shoulder is hardly discernible in CNF-O, but

appears more evidently in the oxidized samples, especially in CNF-AH. Considering the smallest I_G/I_D ratio (1.20), CNF-AH is the oxidized sample with the fewest graphitic crystallite. From CNF-O to CNF-AS and CNF-AH, the G band shifts 5 - 8 cm^{-1} to the high wavenumber region, which is attributed to the vibration of interstitial carbon atom between the aromatic graphitic planes [120-123]. It is an indication that some functional groups are introduced on CNFs [124-126]. It is interesting to note that both permanganate oxidation processes show higher ratio of I_G/I_D compared to that of CNF-O, which is perhaps due to the removal of some amorphous impurity from the surface via the oxidation. Sample CNF-AS shows little change of the I_G/I_D ratio, which suggests that the surface graphitic structure is not damaged in this treatment.

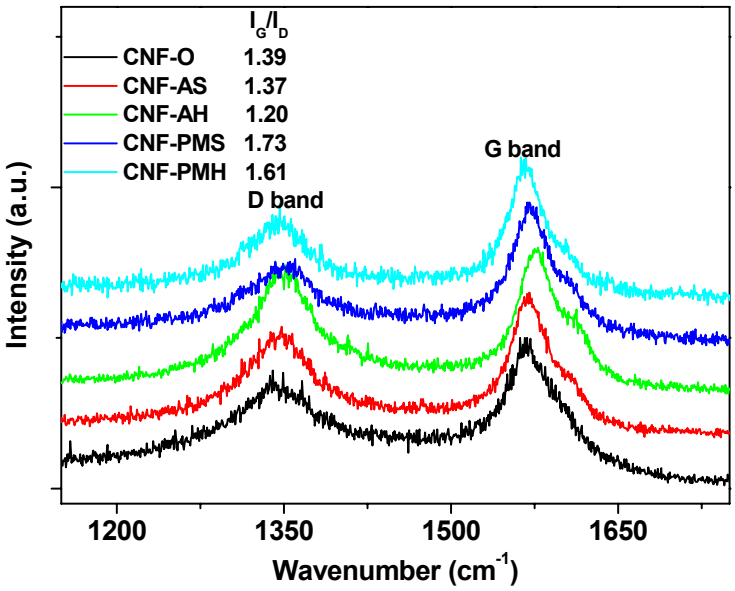

Figure 2.11 Raman spectra of original CNFs (CNF-O) and oxidized CNFs (CNF-AS, CNF-AH, CNF-PMS, CNF-PMH).

2.4.1.4 SEM characterization

Figure 2.12 shows SEM pictures of original and oxidized CNFs. Most of the CNFs are cut into short ones after oxidation, but in the case of CNF-AS, majority of CNFs still remain relatively long, which indicates that acid mixture sonication is the treatment with least cutting effect on CNF lengths. Considering the previous analysis that the oxidation method with H_2SO_4/HNO_3 by bath sonication shows clearly the presence of COOH characteristic peaks in IR spectra and the highest amount of graphite structure from XPS analysis (high ratio of C=C

over C-H groups), it is chosen as the best method for oxidizing CNFs. In the following experiments, all the oxidation process of CNFs is achieved by acid mixture sonication at RT.

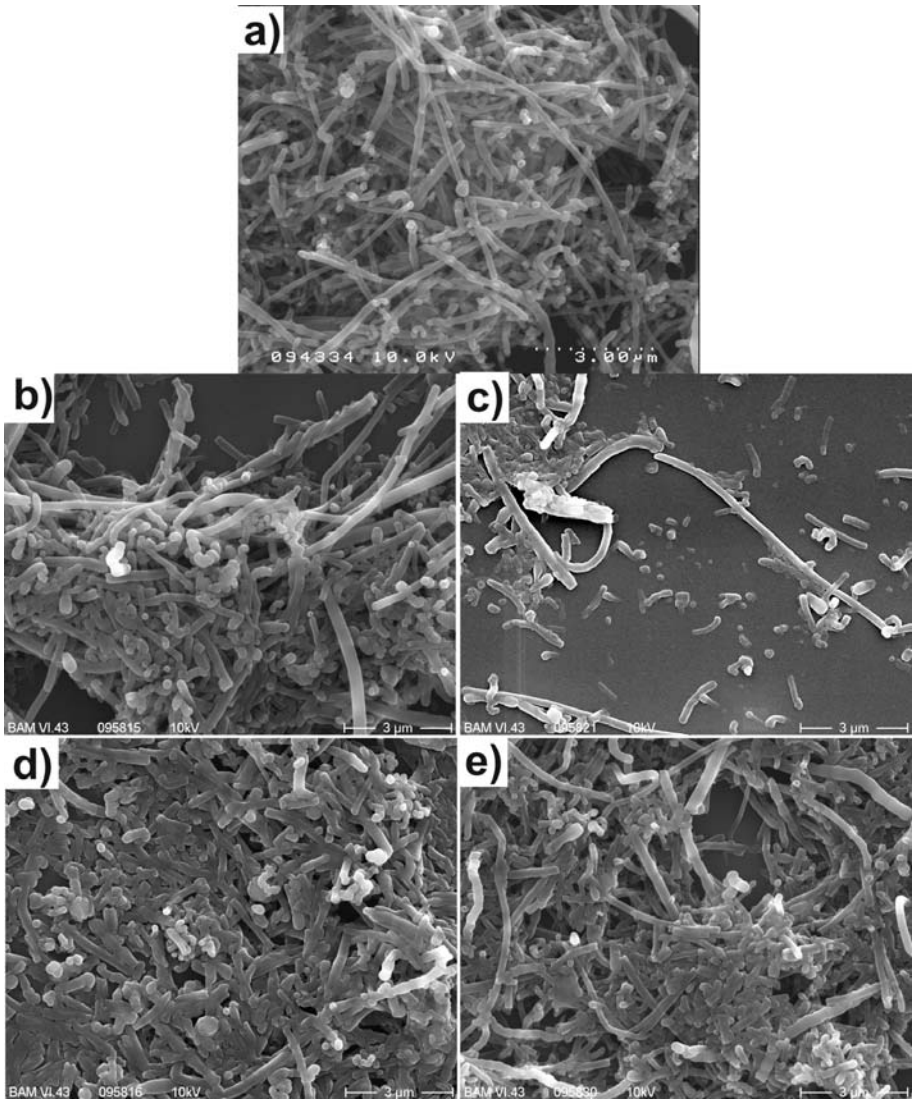

Figure 2.12 SEM pictures of original and oxidized CNFs by different methods: a) CNF-O, b) CNF-AS, c) CNF-AH, d) CNF-PMS, e) CNF-PMH.

2.4.2 Silanization of CNFs with glycidoxysilane

2.4.2.1 IR spectra

As seen from Figure 2.13, original CNFs (CNF-O) show only one characteristic band around 1583 cm^{-1}, which corresponds to the graphite structure [127]; while the oxidized CNFs (CNF-AS) have additonal peaks at 3429 cm^{-1} (O-H stretching), 2920 cm^{-1} (C-H sp^3 hybridization), 1725 cm^{-1} (C=O stretching), 1623 cm^{-1} (quinone groups), 1380 cm^{-1} (O-H bending) and 1070 cm^{-1} (C-O stretching) respectively, which confirms that the oxidation is effective. After the glycidoxysilanization, the intensity of peak from C-H sp^3 hybridization

increases and the peak position shifts a little (2899 cm^{-1}) due to the introduction of propyl and glycidoxy groups from GPTMS. Meanwhile, the O-H stretching peak broadens, and the intensity of O-H bending peak at 1380 cm^{-1} increases. Since GPTMS covalently bonds with CNFs via the reaction of hydrolyzed methoxy groups from silanes and hydroxyl groups from the oxidized CNFs [91], there are two possible reasons for the existence of O-H groups on CNF surface after silanization: the residue of O-H groups from carboxyl groups which not completely react with GPTMS and remaining O-H groups from the hydrolyzed GPTMS which are not covalently bonded with the CNF surface. The hydrolyzed Si-OH groups tend to crosslink with each other, therefore the existence of OH groups is mainly attributed to C-OH groups from carboxyl groups. The incomplete reaction between carboxyl groups and silanes suggests that the silanization yield is low. However, new peaks appear at 1460 cm^{-1}, 1060 cm^{-1}, and 875 cm^{-1}, are attributed to CH_2 scissoring from glycidoxy groups [128], Si-O stretching and epoxy ring [129, 130] respectively. Therefore from IR spectra, it is obvious that GPTMS is coupled onto the surface of CNFs. Although it is likely that epoxy ring reacts with COOH groups, it only happens with the addition of base catalyst or at a temperature higher than 200 °C [88, 131, 132]. In addition, the presence of epoxy ring peak also gives a direct proof that the main reaction takes place between Si-OH groups from the hydrolyzed silanes and carboxyl groups on CNFs.

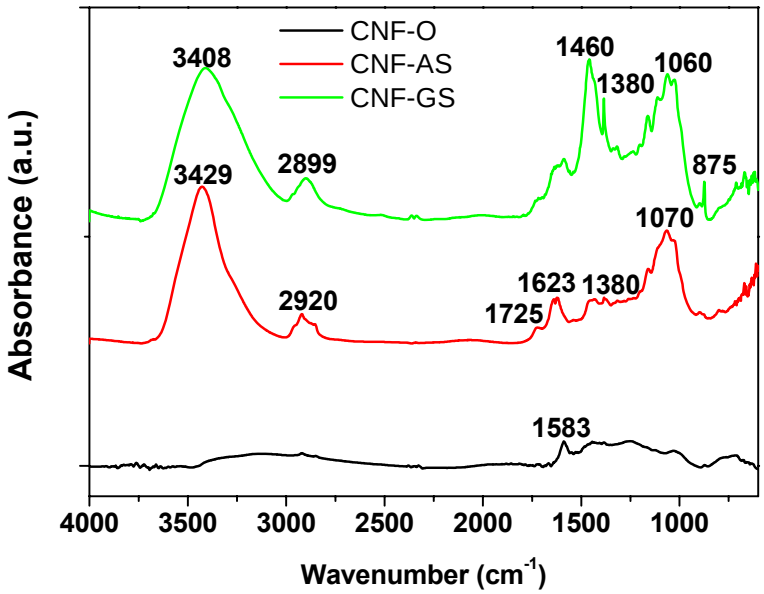

Figure 2.13 FTIR spectra of silanized CNFs (CNF-GS) compared with original CNFs (CNF-O) and oxidized CNFs (CNF-AS).

2.4.2.2 XPS analysis

XPS measurement was done to further verify the reaction (Table 2.3 and 2.4). Unfortunately, there is only a little increase of Si content after the silanization (from 0.2 % to 0.4 %). On the other hand, the relative percentage of functional groups shows that the surface C=C bonds decreases a lot after silanization (from 35 % to 22 %). It suggests that the chemical environment of CNF surface has changed. The increase of C-O-C groups from 10 % to 25 % after silanization due to the ether groups in glycidoxysilane also indicates that the surface chemistry changes after the silane coating process. Thus the little increase of Si content is probably because the Si is buried beneath the surface coating.

Table 2.3 XPS measurements of CNF surface composition.

	Concentration of elements in at%			
Sample	C	O	Si	S
CNF-O	96.4	3.3	-	0.3
CNF-AS	79.1	20.6	0.2	0.1
CNF-GS	82.0	17.5	0.4	0.1

Table 2.4 Relative percentage of functional groups from the deconvolution of XPS C 1s peak.

	Relative percentage of functional groups (%)						
Binding energy and assignation	C=C (284.6 eV)	C-C, C-H (285.0 eV)	C-O, C-N (286.0 eV)	C=O (287.0 -287.5 eV)	COOH, COOC (288.7-289.3 eV)	$\pi - \pi^*$ shake up of carbonyl (290.2-290.7 eV)	$\pi - \pi^*$ shake up of graphitic carbon (291.7 eV)
CNF-O	77	4	11	4	2	1	1
CNF-AS	35	37	10	7	10	1	-
CNF-GS	22	42	25	5	5	1	-

The Si 2p peak fitting is done to clarify the reaction mechanism. Due to the low Si content on the surface, the signal of Si 2p peak is rather rough (Figure 2.14). The methoxy groups from GPTMS first hydrolyze into OH groups due to the existence of trace amount of water in the ethanol solution, and then some hydrolyzed silanes can condense into small oligomers through Si-O-Si bonds and the free Si-OH groups attack the COOH groups on CNFs. The hydrogen from carboxyl groups reacts with the hydroxyl group from silanols to produce water and covalent ester bond O=C-O-Si is built at the interface. When the hydrolyzed silanes are only physically adsorbed onto the CNF surface, most Si will be in the form of Si-O-Si due to

the crosslinking of hydrolyzed Si-OH groups after self-condensation (Figure 2.15). Since the Si peak is completely fitted into the Si-O-C peak, indicating that the existence of Si is based on covalent bonds between Si-OH and COOH groups on CNFs.

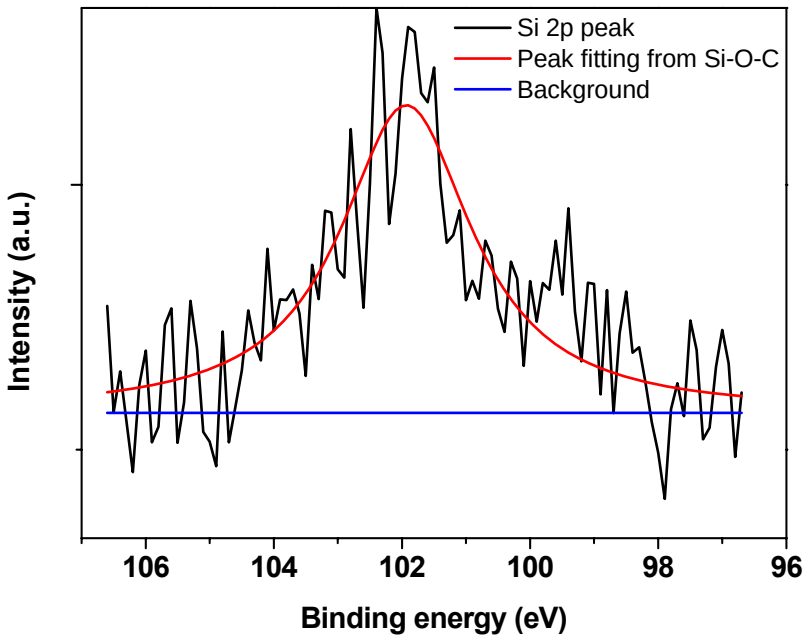

Figure 2.14 XPS Si 2p peak fitting of CNF-GS.

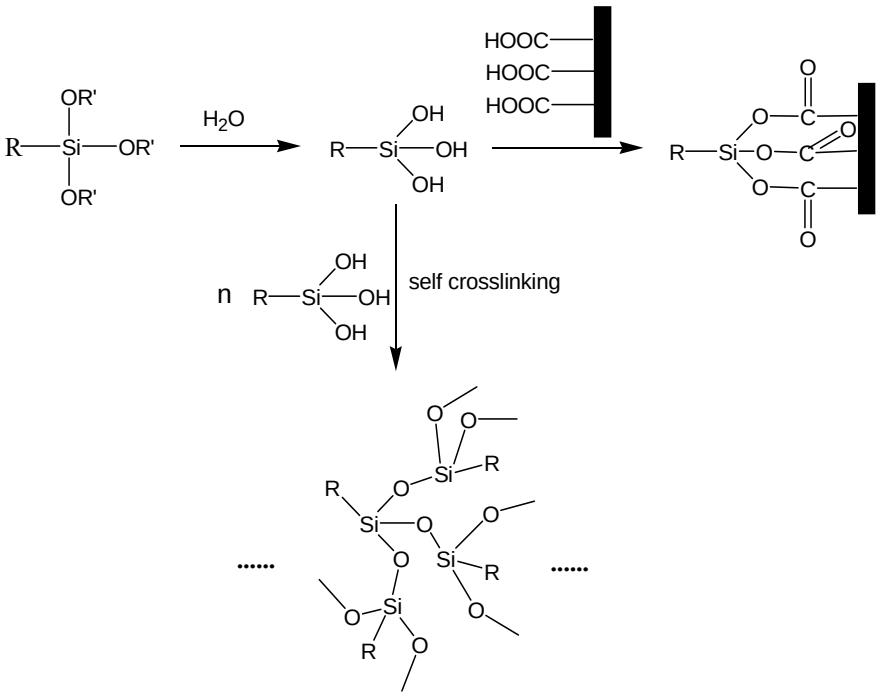

Figure 2.15 Scheme of the possible reactions between alkoxysilanes and CNFs.

2.4.2.3 SEM and EDX analysis

Surface morphology of CNFs was characterized by SEM (Figure 2.16). The diameter of original CNFs is in the range 60 - 180 nm, a little greater than the data from the producer. After oxidation, some nanofibers are cutted into short ones because of the stong acid aggression, but the tube morphology remains. With silanization, the appearance of CNFs changes little, suggesting this process is mild and non-destructive to the CNF structure. Some great particles except fibers exist in SEM pictures, which is attributed to the carbon particle impurity during the synthesis process of CNFs. Results of EDX measurements in Figure 2.16 d shows only one apparent peak of carbon for original CNFs, while after oxidation, an additional peak from oxygen appears. In the silanized sample CNF-GS, a further small peak at 1.7 keV corresponding to Si is visible, which verifies the existance of silane in the sample.

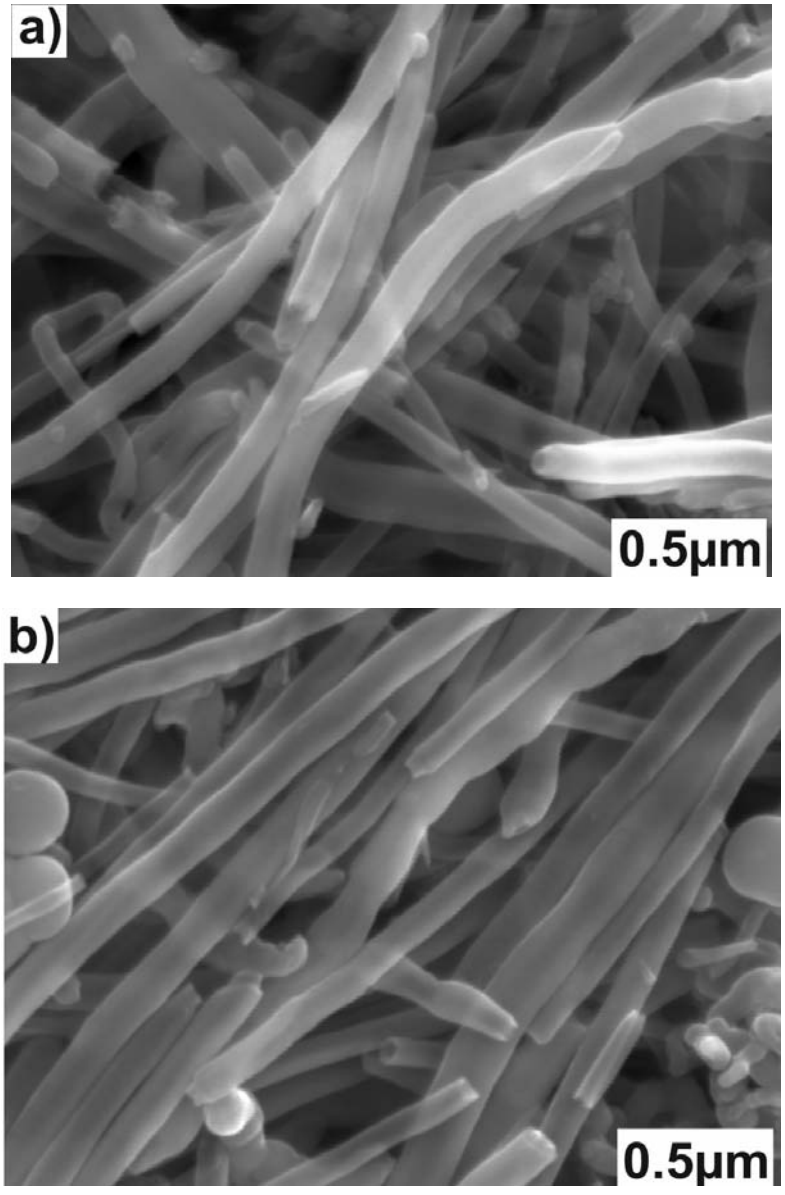

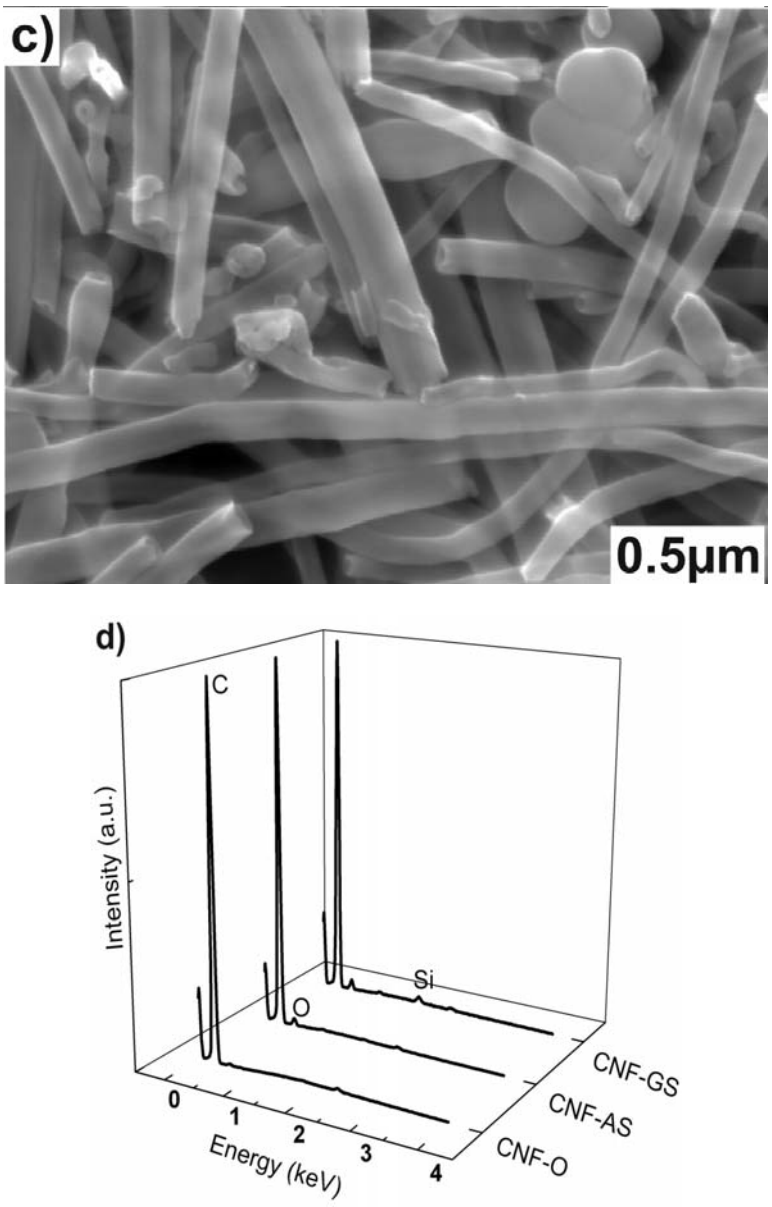

Figure 2.16 SEM of a) original CNFs (CNF-O), b) oxidized CNF (CNF-AS), c) silanized CNFs (CNF-GS); and d) EDX analysis of CNFs.

2.4.2.4 TGA measurements

TGA measurements were carried out to get quantitative information about Si content on CNFs (Figure 2.17). Compared to the weight residue of CNF-O (5.4 %) and CNF-AS (1.3 %), CNF-GS has a leftover of 3.6 %. Due to acid treatment, the amount of metal catalyst from the synthesis process is reduced, which results in a less residue after burning of CNFs. Assuming the complete oxidation of Si element in air environment, the 3.6 % residue is attributed to the sum of both oxide residue from metal catalyst in CNFs and SiO_2 from silane coating. By subtraction of 1.3 % residue from CNF-AS (corresponding to metal oxide), based on the Si element content in molecule SiO_2, the concentration of Si in CNF-GS is calculated to be

1.1 %. This value is comparable with results from Ma et al. [96]. Regarding also the EDX results given above, it is concluded that the performed silanization process is effective to introduce silicon onto CNF surface.

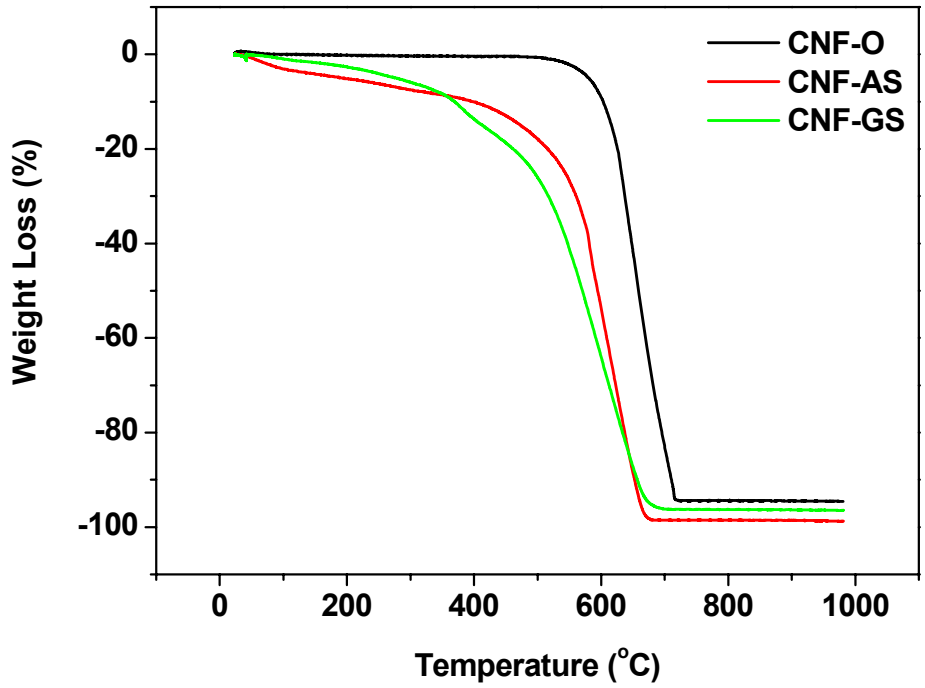

Figure 2.17 TGA measurements of silanized CNFs (CNF-GS) compared with original CNFs (CNF-O) and oxidized CNFs (CNF-AS).

2.4.2.5 Raman spectra

The ratio of I_G/I_D is constant after the oxidation process, but reduced from 1.37 to 1.27 after the silanization (Figure 2.18), suggesting that the surface graphitic structure is disturbed. In addition, the peak position of G band shifts up; the shoulder peak around 1620 cm^{-1} is apparent in CNF-GS. Those phenomena are caused by disorders from surface defects or functional groups coming from the silanization treatment.

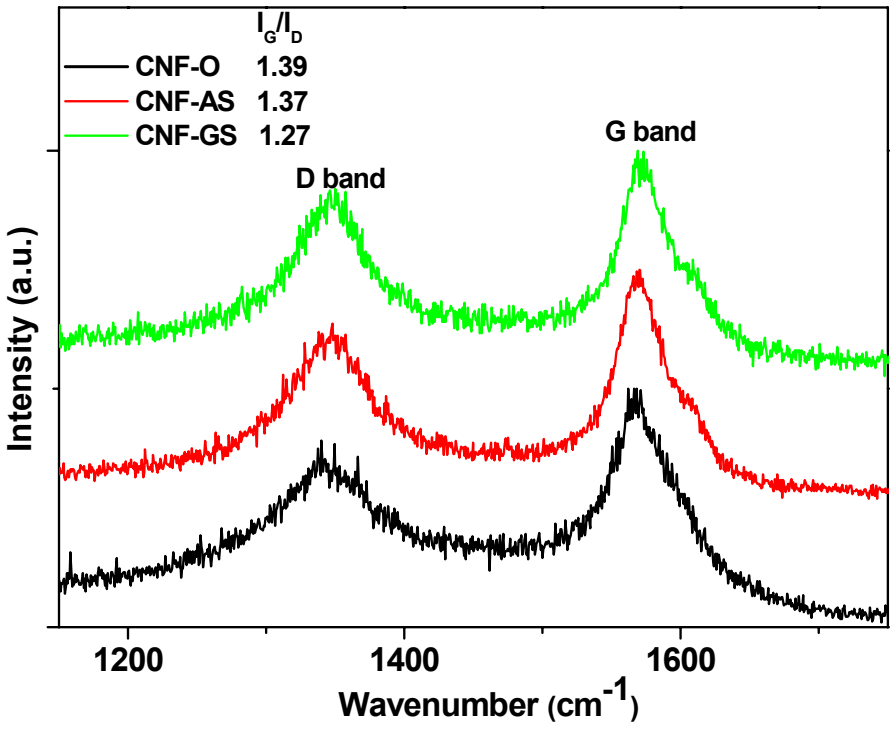

Figure 2.18 Raman spectra of CNF-GS compared with the original CNFs (CNF-O) and oxidized CNFs (CNF-AS).

2.4.2.6 Behavior of CNF suspension under electric field

In order to check the effect of silanization on the electrical conductivity of CNFs, an ethanol suspention of CNF-O and CNF-GS was prepared and set between two electrodes under high DC electric field (6×10^4 V m^{-1}). As shown in Figure 2.19, the original CNFs are aligned after 30 min exposure in the electric field, but the CNFs modified with glycidoxysilane remain disordered after half an hour. Under electric field, the CNFs are polarized and the electric charge is redistributed to the ends of CNFs. Thus under the external electric field, this polarization gives a torque which rotates the CNFs in the direction parellel to the electric field [133-135]. But after the surface modification, if CNFs are coated with a layer of insulating material, the conductivity of CNFs is decreased and they need long time to to be polarized and alignend under the electric field. So the failure of alignment after silanization suggests that the CNF surface contains some moieties which lower the electrical conductivity, and they are the silanes here.

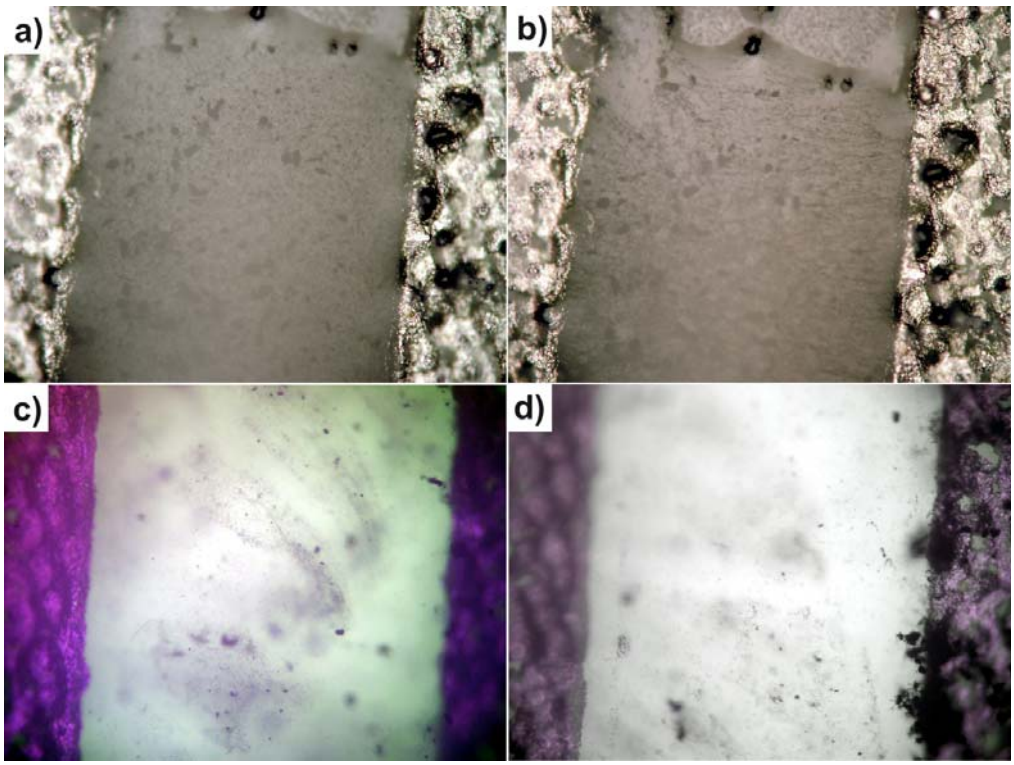

Figure 2.19 Optical microscopy of CNF ethanol suspension under AC electric field (6×10^4 V·m^{-1}): a) CNF-O, 0 min; b) CNF-O, 30 min; c) CNF-GS, 0 min; d) CNF-GS, 30 min. The magnification is 200×.

2.4.3 Silanization of CNFs with aminosilane

2.4.3.1 IR spectra

In sol gel chemistry, it is well known that the alcoholic hydroxyl groups react with alkoxysilanes easily. Since the silanization process with GPTMS by the reaction of carboxyl groups and hydrolyzed methoxy silanes through heating treatment introduces only a small amount of Si (1.1 wt% based on TGA, and 0.4 at% based on XPS) on CNFs, silanization process by reaction of alcoholic hydroxyl groups and methoxysilane was carried out in order to increase the silicon content on CNFs.

As shown in Figure 2.20, the original CNFs (CNF-O) sample presents a broad and weak band in the range from 1000 to 1500 cm^{-1}, which is referred to weak oxidation of the CNFs surface in the ambient environment. There is also a small peak at 1583 cm^{-1} corresponding to the graphite structures. No other specific peaks corresponding to functional groups appear in the spectrum. For CNFs oxidized by acid sonication (CNF-AS), new broad bands at ~ 3429 cm^{-1} and 1070 cm^{-1} are attributed to O-H and C-O stretching vibrations from carboxyl groups; weak band near 2920 cm^{-1} represents sp^3 C-H bonding; small peak at 1725 cm^{-1} is the

characteristic peak for C=O stretching in COOH; appearance of peak 1623 cm^{-1} is due to the intermediate oxidation products - quinone groups; 1380 cm^{-1} results from the O-H bending vibration from COOH groups. The vibration at ~ 3400 cm^{-1} can also be attributed to adsorbed water. However, before IR measurements, all the KBr and CNFs powder were dried 24 h at 120 °C to exclude the effect of water. Thus, IR results clearly indicate the effectiveness of oxidation for sample CNF-AS. In the reduced CNF-N sample, almost disappearance of the band at ~ 1725 cm^{-1} and the increased intensity of O-H stretching demonstrates the effective reduction of carboxyl groups into alcoholic groups (C-OH). After silanization, the apparent intensity increases at 1060 cm^{-1} and 2920 cm^{-1} is a direct evidence of Si-O stretching and methylene groups from the silicon coupling agent APTMS, respectively. But there is still an intensive and broad band from 3000 to 3600 cm^{-1} corresponding to hydroxyl groups (O-H). For the bonding of APTMS with CNF-N nanofibers, the first step is the hydrolysis of methoxy groups in the existence of trace amount of water with the catalysis of TEA [102, 136]; then the silanol groups (Si-OH) are adsorbed onto the CNFs; finally they react with the alcoholic groups (C-OH) on the surface of CNF-N sample. The C-OH groups are not completely converted to Si-O-C groups, thus the IR band (3429 cm^{-1}) corresponding to OH groups still exists [137].

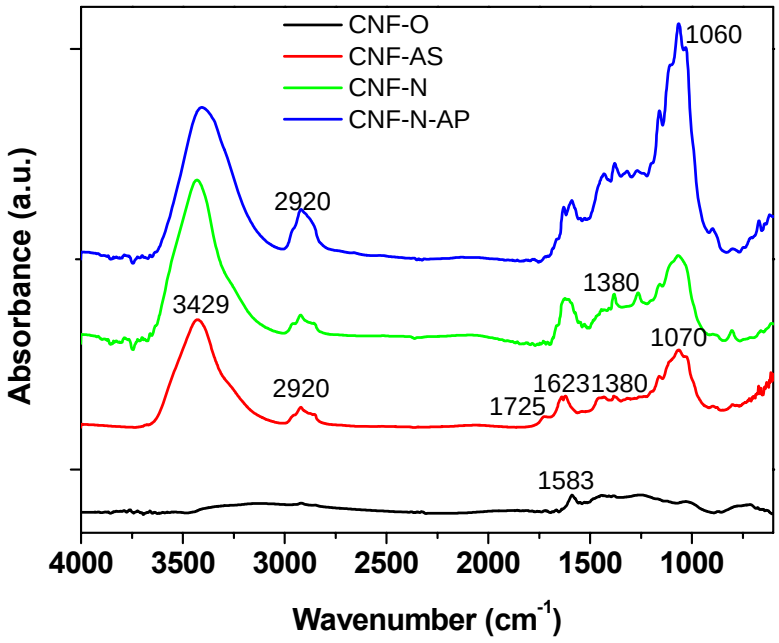

Figure 2.20 IR spectra of original CNFs and modified CNFs at different steps (CNF-O: original nanofibers; CNF-AS: oxidized CNFs after acid sonication; CNF-N: reduced CNFs by $NaBH_4/I_2$; CNF-N-AP: silanized CNFs with APTMS).

2.4.3.2 XPS analysis

XPS measurements (Table 2.5 and 2.6) show the surface concentration of atoms and functional groups on CNFs in original state and after each modification step. The C 1s peak was deconvoluted by Unifit program and the obtained seven subpeaks (peak A to G) were assigned to different chemical surroundings or species. The peak around 284.6 eV corresponds to the sp^2 hybridized graphite double bond (C=C), while the peak at 285 eV is due to the sp^3 hybridization of saturated structures on the surface (C-C, C-H). The content of oxygen increases a lot after oxidation (from 3.3 to 20.6 %), and through reduction decreases a little (from 20.6 to 15.6 %). The percentage of C=C structures decreases greatly while the amount of C-H, C-C sp^3 hybridization increases a lot in sample CNF-N suggesting the reduction process introduces many sp^3 hybridized carbon structures on the surface. The increase of relative percentage of C-OH groups from 10 % in CNF-AS to 18 % in CNF-N sample gives another direct hint that the reduction from COOH to C-OH is effective. However, the amount of carboxyl groups only decreases from 10 to 8 %, which suggests that not all the carboxyl groups are reduced. This result is different from IR findings which show almost disappearance of COOH groups. The reason may be that XPS measurement detects only up to a depth of 10 nm from the surface, while IR measurement represents properties of the whole sample, in which the amount of COOH groups is not high enough to be detected. In sample CNF-N-AP, the detection of Si element proves the success of silanization. Here the Si content is 1.1 at%, higher than that in CNF-GS (0.4 at%), suggesting this silanization method incorporates more Si on CNF surface. There are also trace amounts of S, Si, and Cl detected in CNF-O, CNF-AS, and CNF-N-AP samples, which may arise from contamination. The existence of Na element in CNF-N and CNF-N-AP samples is due to the residue from the washing process after reduction treatment.

Table 2.5 XPS measurements of CNF surface composition.

	Concentration of elements in at%						
Sample	**C**	**O**	**N**	**Si**	**S**	**Na**	**Cl**
CNF-O	**96.4**	**3.3**	**-**	**-**	**0.3**	**-**	**-**
CNF-AS	**79.1**	**20.6**	**-**	**0.2**	**0.1**	**-**	**-**
CNF-N	**83.4**	**15.6**	**-**	**-**	**-**	**1.0**	**-**
CNF-N-AP	**80.4**	**16.2**	**0.8**	**1.1**	**0.2**	**1.1**	**0.2**

Table 2.6 Relative percentage of functional groups from the deconvolution of XPS C 1s peak.

	Relative percentage of functional groups (%)						
	Peak A	Peak B	Peak C	Peak D	Peak E	Peak F	Peak G
	284.6 eV	285.0 eV	286.0 eV	287.0-287.5 eV	288.7-289.3 eV	290.2-290.7 eV	291.7 eV
CNF-O	77	4	11	4	2	1	1
CNF-AS	35	37	10	7	10	1	-
CNF-N	7	60	18	6	8	1	-
CNF-N-AP	9	58	18	7	7	1	-

Peak A: assigned to graphitic carbon (C=C)

Peak B: assigned to sp^3 hybridized carbon (C-C, C-H)

Peak C: phenolic, alcoholic hydroxyls, carbon nitrogen bond or ether oxygen (C-OH, C-O-C, C-N)

Peak D: carbonyl, amide groups (C=O, N-C=O)

Peak E: carboxyl groups or ester groups (COOH, COOC)

Peak F: π-π^* shake up peaks of carbonyl bonds

Peak G: π-π^* shake up peaks of graphitic carbon

Meanwhile the Si 2p peak fitting (Figure 2.21) demonstrates that most Si exists as Si-O-C (peak position at 101.4 eV, relative percentage 95 %) in the sample CNF-N-AP, and only 5 % Si is coming from Si-O-Si groups (peak position at around 104.1 eV), the crosslinking of hydrolyzed silanes, which gives a direct evidence that chemical silanization rather than physical adsorption dominates the interaction between CNFs and APTMS.

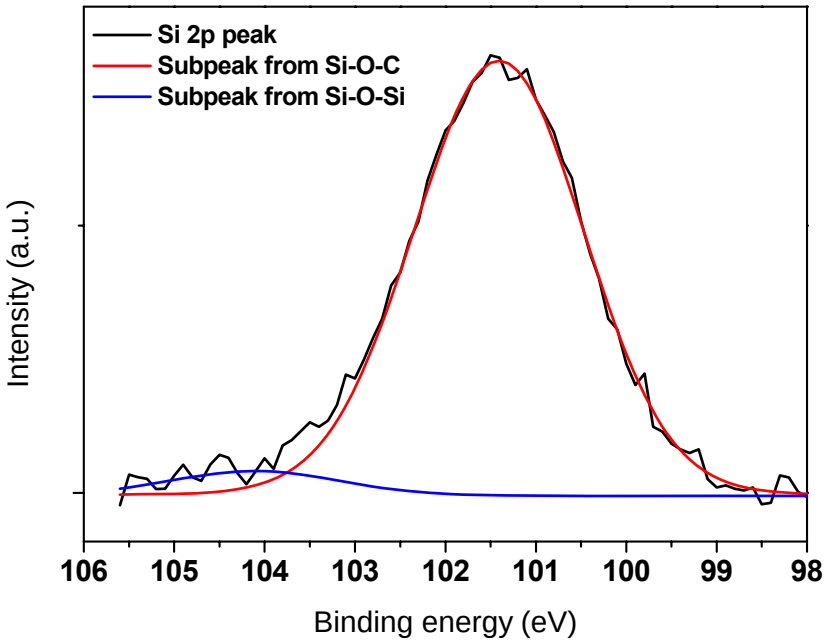

Figure 2.21 XPS Si 2p peak fitting of CNF-N-AP.

2.4.3.3 TGA measurements

TGA curves are depicted in Figure 2.22. The original nanofibers CNF-O have a weight loss of 94.6 % and the residue is 5.4 %, respectively. The higher weight loss of oxidized sample CNF-AS (98.7 %) suggests only 1.3 % residue is left. The additional weight loss of 4.1 % compared with CNF-O is due to the dissolution of metallic impurities by severe acid sonication treatment. After reduction treatment, the residue for CNF-N is 4.8 %. The increase of residue results from the contamination of NaOH in the washing process. The silanized CNFs (CNF-N-AP) has a leftover of 6.1 %. It is a contribution from both sodium oxide (incomplete washing in the reduction step, which is also indicated from XPS results: 1.1 at% of Na element exists in the CNF-N-AP sample) and silicon oxide residue (resulting from the oxidation of silanes on CNFs). Subtracted from the 4.8 % residue of the reduced sample CNF-N, only 1.3 % residue comes from the calcination of coated silanes on CNF-N-AP. Since air is constantly flowing through the device cabinet during the measurement, silanes should be completely oxidized to silica (1.3 %). The calculated bulk concentration of silicon in CNF-N-AP is around 0.6 wt%, lower than CNF-GS (1.1 wt%). Consideration of the XPS results that CNF-N-AP has a higher Si content (1.1 at%) than CNF-GS (0.4 at%), it is assumed that silane funtionalization occurs mostly on the sidewalls of CNFs in CNF-N-AP, while silanization takes place mainly on the opening ends of CNFs in sample CNF-GS.

Therefore higher content of Si is detected on the surface, but lower concentration of Si in the bulk sample CNF-N-AP as calculated from TGA results.

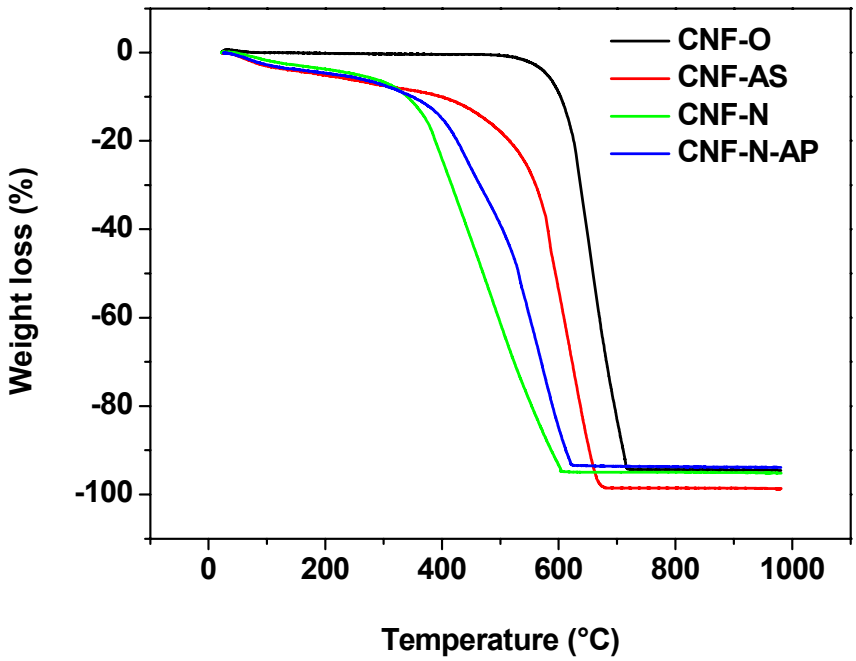

Figure 2.22 TGA measurements of silanized CNFs (CNF-N-AP) compared with original CNFs (CNF-O), oxidized CNFs (CNF-AS) and reduced CNFs (CNF-N).

2.4.3.4 Streaming potential measurements

The surface charge of CNFs was characterized by streaming potential measurements (Figure 2.23). The original CNFs have an isoelectric point (IEP) at pH = 4.2, while after oxidation process, CNF-AS possesses a negative streaming potential in the region of pH > 1.1 due to the existence of COOH groups on the surface. The reduced CNFs (CNF-N) have CH_2-OH groups on the surface, which are neutral functional groups preferably adsorbing OH^- than H^+ [138, 139]. As a result, the streaming potential of sample CNF-N is always negative at pH > 1.5 (IEP = 1.5). After the aminosilanization, the IEP of CNF-N-AP shifts to higher pH (pH = 2.0) and the streaming potential to smaller absolute values due to the protonation of amine groups on the surface. When the surface is dominated by NH_2 groups, the surface charge should be positive at pH 2. Thus it is an indication that the surface OH groups not completely bond to aminosilanes after the silanization. However, the concurrent existence of OH and NH_2 groups on the surface contributes to a higher value of IEP than CNF-N. The change of surface charges after each chemical treatment provides another evidence for the successful surface modification.

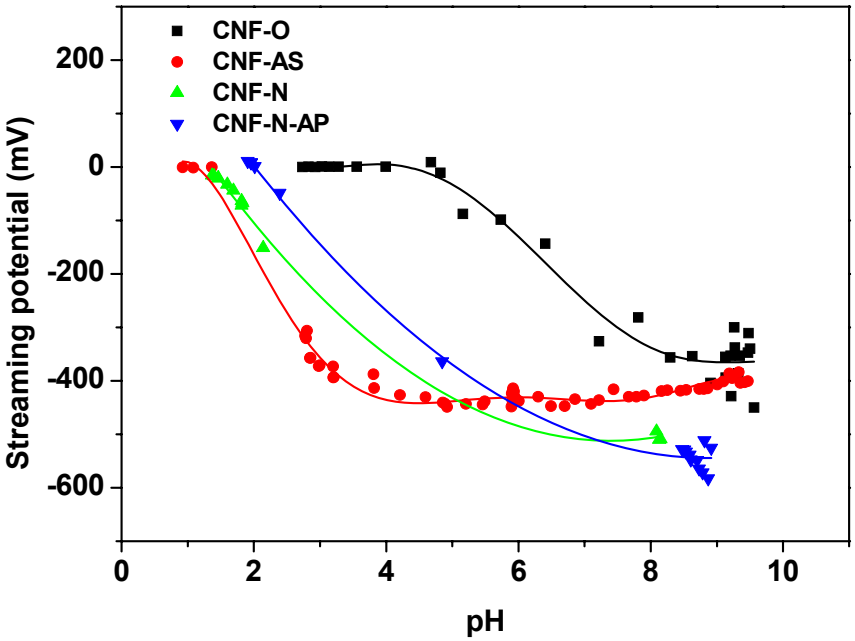

Figure 2.23 Streaming potential of CNFs versus pH after each chemical treatment in the aminosilanization procedure.

2.4.3.5 Raman spectra

Raman spectra of the nanofibers show two bands at 1568 cm^{-1} (G band) and 1342 cm^{-1} (D band) (Figure 2.24). The width of G band is related to the size distribution of CNFs and that of D band to the degree of graphitization. The ratio of intensity of G band to D band reflects the concentration of defects. Here the ratios of I_G/I_D for CNF-O, CNF-AS, CNF-N and CNF-N-AP are 1.39, 1.37, 1.53 and 1.57, respectively. The consistent ratio before and after oxidation demonstrates that the severe acid sonication brings few surface defects onto the nanofibers. After the reduction process, the increase of the ratio indicates a more graphitized structure on CNFs [100].

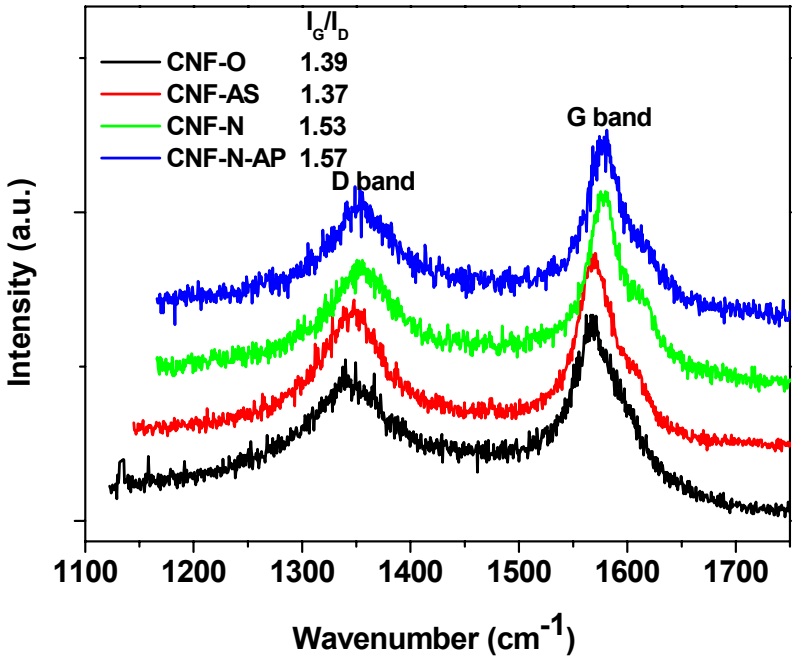

Figure 2.24 Raman spectra of CNF-N-AP compared with the original CNFs (CNF-O), oxidized CNFs (CNF-AS) and reduced CNFs (CNF-N).

2.4.4 Silanization of CNFs with isocyanatesilane and aminosilane

2.4.4.1 IR spectra

3-isocyanatopropyltriethoxysilane (IPTES) was used because of the easy reaction between N=C=O groups from IPTES and COOH groups on the oxidized CNFs. Since the Si-O stretching bands (peak position at around 1060 cm^{-1}) and C-O stretching bands (peak position at around 1070 cm^{-1}) in IR spectra overlap, it is plausible to evaluate the efficiency of silanization from the absolute peak intensity. However, as shown in Figure 2.25, the ratio of the peak intensity of O-H stretching (3429 cm^{-1}) over that of Si-O stretching (1060 cm^{-1}) decreases in the first silanized sample (CNF-I) compared to the oxidized sample (CNF-AS), which indicates the effective silanization. After the second silanization with aminosilane (CNF-I-AP), a new peak at around 1265 cm^{-1} appears, corresponding to the Si-C stretching. Although after the first silanization, the Si-C covalent bond already exists on the surface, perhaps the amount is not great enough to be detected by IR. The second silanization introduces much more Si-C bonds on the surface so that they can be detected in the IR spectra. From the above analysis, it is concluded that the two-silanization treatment is successful.

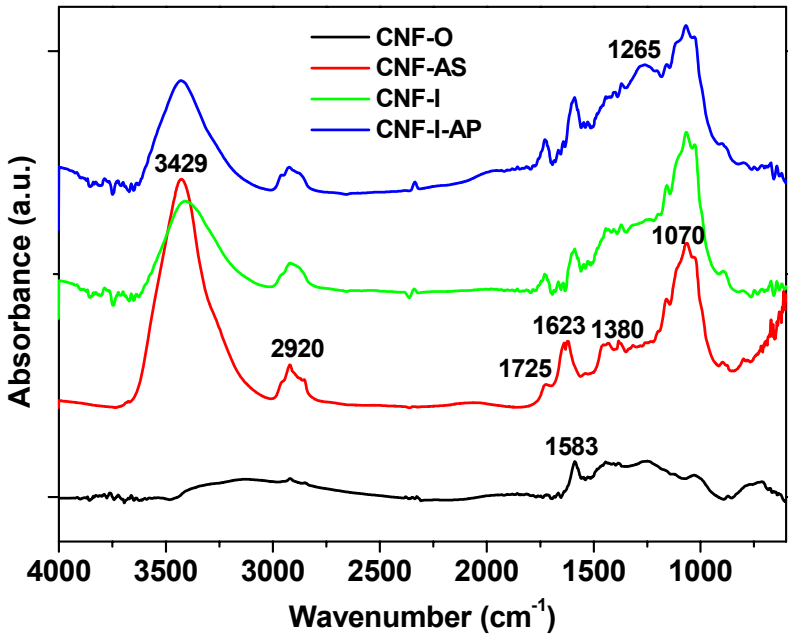

Figure 2.25 IR spectra of silanized CNFs (CNF-I, sample after the first silanization; CNF-I-AP, sample after the second silanization) compared with original CNFs (CNF-O) and oxidized CNFs (CNF-AS).

2.4.4.2 XPS analysis

XPS measurements (Table 2.7 and 2.8) show the effective oxidation from CNF-O to CNF-AS, which has been discussed in previous sections. The increase of Si and N content after each silanization step, especially after the second silanization is apparent in Table 2.7. Though little change in Si content is detected after the first silanization (CNF-I), the relative percentage of C-O groups increases from 10 % to 17 % due to the introduction of OCH_2CH_3 groups from IPTES on CNFs. After the further silanization with 3-aminopropyltrimethoxysilane (APTMS), the area percentage of this peak increases up to 21 % due to the introduction of C-N groups, suggesting the success of second silanization. The great increase of the content of Si and N after the second silanization indicates that the first silanization is helpful for the second silanization with APTMS. The increased ratio of the relative percentage of sp^2 to sp^3 hybridization after silanization is unexpected. Perhaps during the silanization treatment, the adsorbed but not covalently bonded sp^3 hybridized functional groups on the CNF surface were removed through the purification procedure.

Table 2.7 XPS measurements of CNF surface composition.

	Concentration of elements in at%						
Sample	C	O	N	Si	S	Cl	F
CNF-O	96.4	3.3	-	-	0.3	-	-
CNF-AS	79.1	20.6	-	0.2	0.1	-	-
CNF-I	77.9	20.6	1.1	0.2	0.2	-	-
CNF-I-AP	64.8	23.0	5.3	6.4	-	0.3	0.2

Table 2.8 Relative percentage of functional groups from the deconvolution of XPS C 1s peak.

Binding energy and assignation	Relative percentage of functional groups (%)						
	C=C (284.6 eV)	C-C, C-H (285.0 eV)	C-O, C-N (286.0 eV)	C=O (287.0 -287.5 eV)	COOH, COOC (288.7-289.3 eV)	π - π^* shake up of carbonyl (290.2-290.7 eV)	π - π^* shake up of graphitic carbon (291.7 eV)
CNF-O	77	4	11	4	2	1	1
CNF-AS	35	37	10	7	10	1	-
CNF-I	58	7	17	7	9	2	-
CNF-I-AP	64	1	21	8	5	1	-

The Si 2p peak fitting of CNF-I indicates only one peak at around 101.9 eV corresponding to Si-O-C state, which is due to the non-hydrolyzed IPTES (Figure 2.26). After the second silanization (CNF-I-AP), the Si-O-Si bonds should have dominated the Si state in the sample, which arise from the reaction between Si-OH groups hydrolyzed from IPTES on the first silanized CNFs (CNF-I) and Si-OH groups from the hydrolysis of the second silane (APTMS). However, it is not the case and the Si-O-C bonds still dominate the Si state on the surface (relative percentage 99 %, Figure 2.27). A possible explanation can be that the carboxyl groups on CNFs react partially with the isocyanate groups from IPTES. The residue carboxyl groups further react with silanol groups from the hydrolyzed APTMS and form Si-O-C covalent bonds on the surface. The Si content increases tremendously after the second silanization (from 0.2 at% to 6.4 at%). This is probably because the existence of IPTES, which is beneficial for the further adsorption of silanes on the surface, facilitates the second silanization.

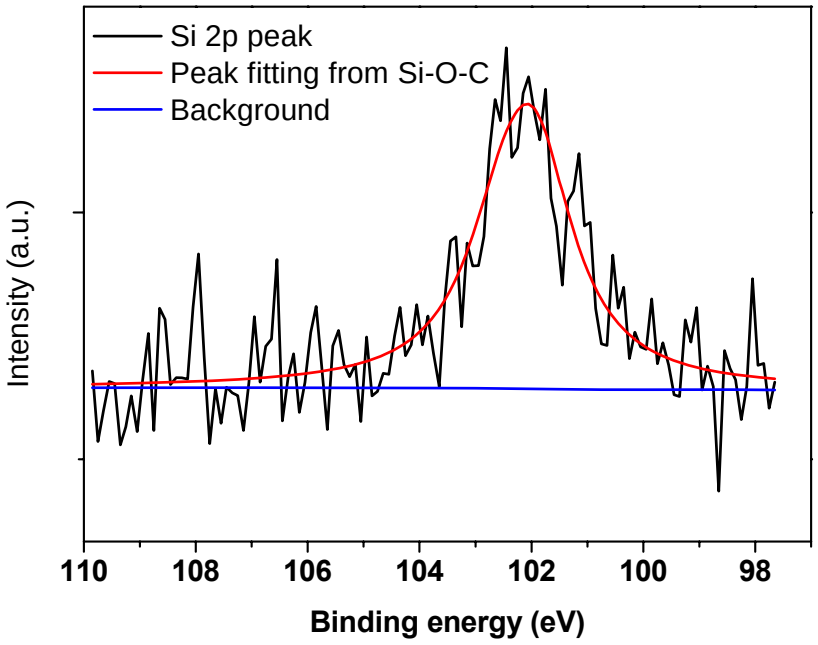

Figure 2.26 XPS Si 2p peak fitting of CNF-I.

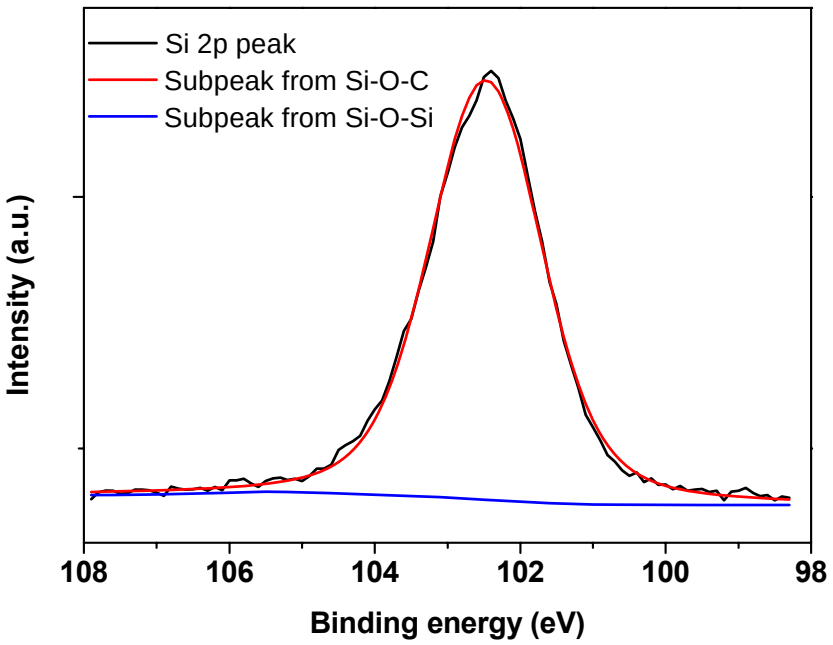

Figure 2.27 XPS Si 2p peak fitting of CNF-I-AP.

2.4.4.3 TGA measurements

As before, the weight loss of silanized CNFs is measured through TGA in air environment (Figure 2.28). The residue after the acid treatment (CNF-AS), after the first silanization

(CNF-I) and the second silanization (CNF-I-AP) are 1.3 %, 3.0 % and 8.6 % respectively. The content of silicon is calculated again based on the assumption of the complete combustion of sample in air environment. After the first silanization, the silicon content is 0.8 %; after the second silanization, the silicon content is 3.4 %.

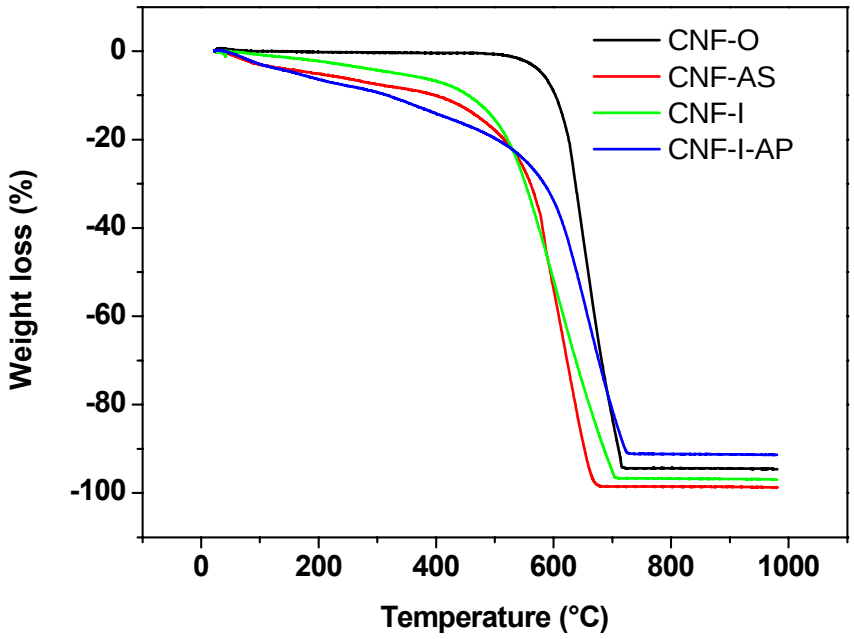

Figure 2.28 TGA measurements of silanized CNFs (CNF-I and CNF-I-AP) compared with original CNFs (CNF-O) and oxidized CNFs (CNF-AS).

2.4.4.4 Streaming potential measurements

The streaming potential results are shown in Figure 2.29. The original CNFs have an isoelectric point (IEP) at pH = 4.2. The surface charge of CNF-AS is negative due to the existence of COOH groups on the surface in the range of pH >1.1. After the first silanization process, the surface is terminated with neutral ethoxy groups, which adsorb OH^- more easily than H^+. As a result, the streaming potential of sample CNF-I is always negative in the measured pH range. The second silanization introduces NH_2 on the surface, which changes the surface potential from negative to positive at pH = 6.8. This is because the amine groups are protonated by H^+ at low pH value. The positive streaming potential at pH lower than 6.8 indicates that this two-silanization process introduces more amine groups on CNF surface than the single aminosilanization process discussed in section 2.4.3.4 so that the sign of the surface charge alters. It coincides well with the detection of much more Si and N compared to the other two silanizations (CNF-GS and CNF-N-AP) in XPS analysis.

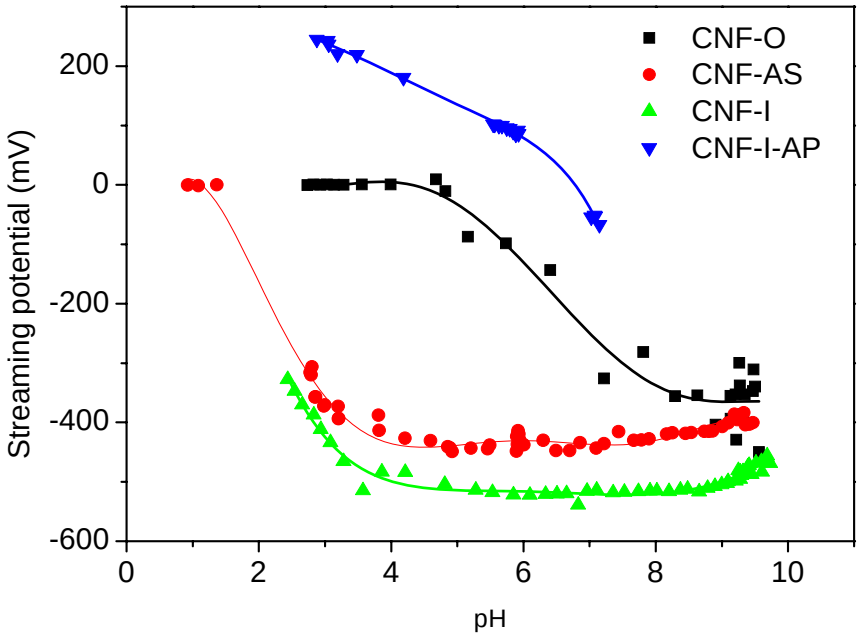

Figure 2.29 Streaming potential of CNFs versus pH after each chemical treatment in the two-silanization procedure.

2.4.4.5 XRD results

From the XRD spectra (Figure 2.30), the interlayer space between graphene layers (d_{002}) is calculated based on the (002) peak located at about $2\theta = 26$ °. After the acid oxidation treatment, the peak position shifts to lower values, which suggests the interlayer distance d_{002} is expanded. This perhaps results from the herringbone structure of CNFs, which enables some intercalation of functional groups into the interstices between graphitic layers. The size of crystallite along the c axis (L_c) indicates the degree of graphitization of CNFs. The values of d_{002} and L_c are listed in Table 2.9. After the oxidation treatment, further silanization process has no apparent effect on both the crystalline size and the interlayer space, which suggests that the silanization is non-destructive to the structure of graphitic crystallite.

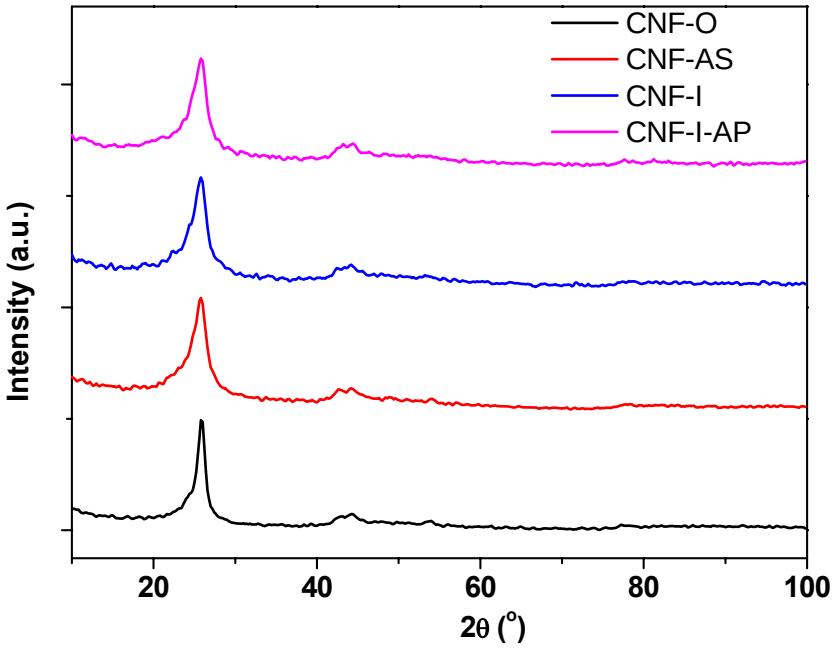

Figure 2.30 XRD patterns of CNFs before and after chemical treatments in the two-silanization procedure.

Table 2.9 Summary of XRD results of CNFs before and after chemical treatments in the two-silanization procedure.

Sample	Angle 2θ (°)	d_{002} value (Å)	L_C (nm)	Number of layers (L_C /d_{002})
CNF-O	26.085	3.416	11.8	35
CNF-AS	25.971	3.431	5.5	16
CNF-I	25.967	3.431	5.9	17
CNF-I-AP	26.000	3.427	5.5	16

2.4.4.6 Raman spectra

The ratio of I_G/I_D remains almost unchanged before and after silanization (Figure 2.31). It means that the graphitization is generally unaffected by the silanization procedure, which coincides with the XRD results. The peak position of the G band shifts to higher wavenumber after silanization, which is attributed to the effective functionalization; the shoulder peak at

1620 cm^{-1} appears after the silanization, suggesting existence of some surface defects. However, their amount is not tremendous enough to have great influence on the ratio of I_G/I_D.

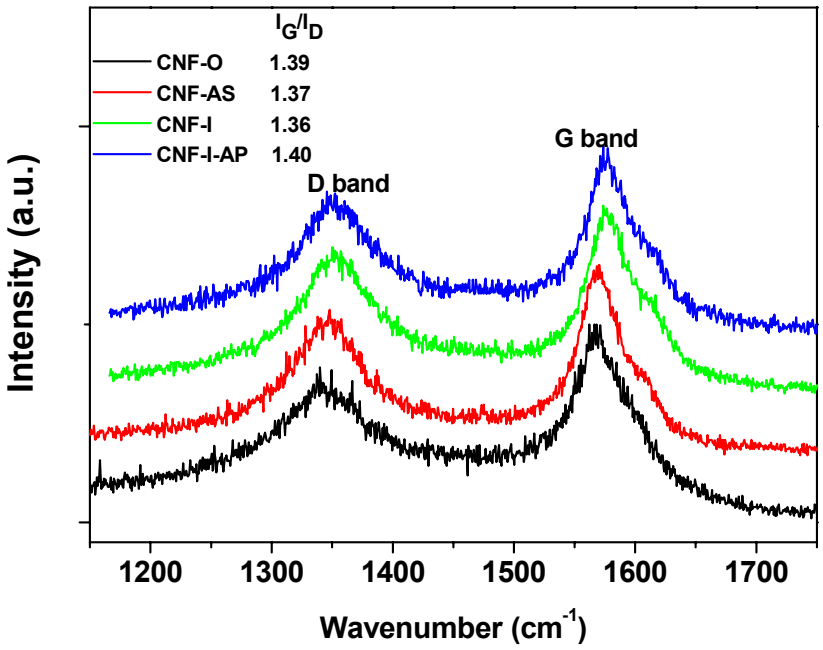

Figure 2.31 Raman spectra of silanized CNFs (CNF-I, CNF-I-AP) compared with original CNFs (CNF-O) and oxidized CNFs (CNF-AS).

2.4.5 Oxidation of MWCNTs

2.4.5.1 IR spectra

The oxidization treatments for CNFs indicate that by heating treatment in the acid mixture of H_2SO_4/HNO_3 (CNF-AH), the graphitic structure is largely disturbed, and by $KMnO_4/H_2SO_4$ sonication (CNF-PMS) carbonyl groups are not detectable in IR spectra. Thus for the oxidation of MWCNTs, only the sonication treatment in the acid mixture (MWCNT-AS) and the heating treatment in $KMnO_4/H_2SO_4$ (MWCNT-PMH) were tried on MWCNTs. In IR spectra (Figure 2.32), the pristine MWCNT has already shown peaks corresponding to C-H sp^3 hybridization (2892 cm^{-1}), O-H groups (3430 cm^{-1}), oxygen containing functional groups (1630 and 1056 cm^{-1}), which are attributed to the oxidation in the ambient environment. MWCNT-AS demonstrates new peaks at 1725 cm^{-1} and 1382 cm^{-1} due to carbonyl stretching and hydroxyl bending from carboxyl groups respectively. Also the peaks corresponding to C-H sp^3 symmetric and asymmetric stretching at 2853 and 2920 cm^{-1} become more apparent. In sample MWCNT-PMH, the characteristic peaks of carbonyl stretching and C-H sp^3

stretching are also confirmed. Thus both oxidation processes are capable to introduce carboxyl groups on the surface.

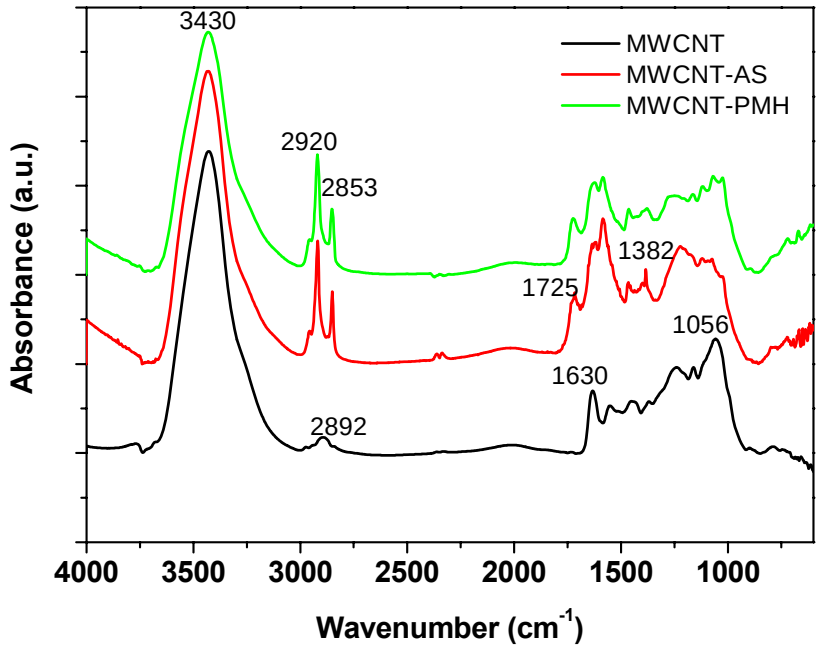

Figure 2.32 IR spectra of pristine MWCNTs (MWCNT) and oxidized MWCNTs (MWCNT-AS, MWCNT-PMH).

2.4.5.2 Raman spectra

The oxidation process was further characterized through Raman spectra to see the effect of the oxidation on the surface graphitic structure (Figure 2.33). After the acid oxidation (MWCNT-AS), the I_G/I_D ratio decreases from 1.33 to 0.94, indicating the disturbance of the surface structure; however, with sample MWCNT-PMH, this ratio is 1.35, comparable to the pristine MWCNT. Thus the permanganate and sulfuric acid heating treatment is a milder oxidation procedure which keeps the graphitic structure of nanotubes. It is chosen as the oxidation method for MWCNTs in the later experiments.

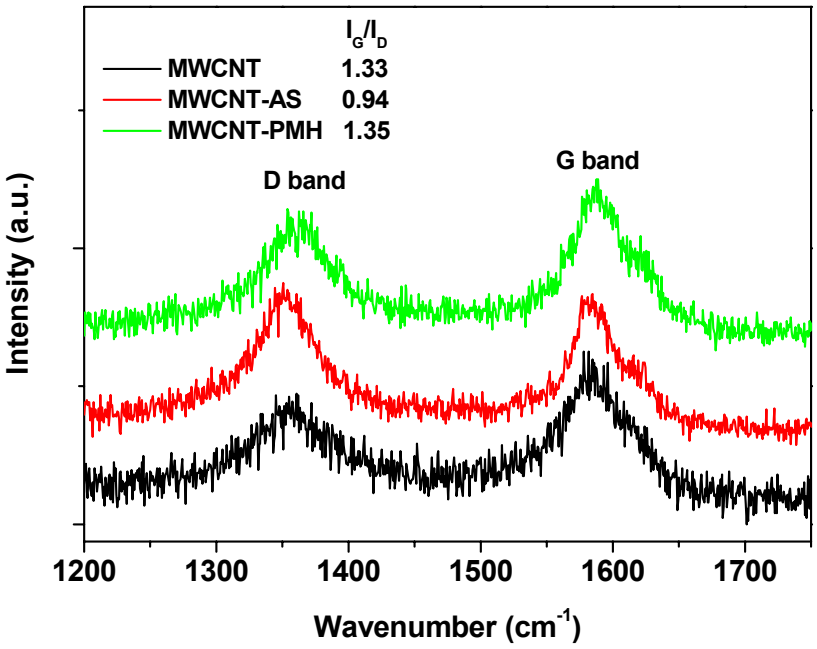

Figure 2.33 Raman spectra of pristine MWCNTs (MWCNT) and oxidized MWCNTs (MWCNT-AS, MWCNT-PMH).

2.4.6 Silanization of MWCNTs with aminosilane

2.4.6.1 IR spectra

The aminosilanization of MWCNTs is done in the similar way as CNFs. First MWCNTs are oxidized by dilute sulfuric acid and potassium permanganate at high temperature, and then reduced by iodine and sodium borohydride, and finally silanized with APTMS. Instead of concentrated H_2SO_4 and HNO_3, mixture of $KMNO_4$ and H_2SO_4 are selected for milder oxidation to remain as many graphitic structures as possible. The FTIR spectra are shown in Figure 2.34. For pristine MWCNTs , there are bands at 3430, 2892, 1630, and 1056 cm^{-1}, which corresponds to O-H stretching, C-H stretching, quinone groups and C-O stretching respectively due to the oxidation by air. After the oxidation treatment, a new peak at around 1725 cm^{-1} attributed to the C=O stretching in COOH groups appears, and the peak intensity of C-H stretching (2920 and 2853 cm^{-1}) increases, which are indications of successful oxidation. For the reduced sample MWCNT-PMN-N, the higher intensity at 1382 cm^{-1} comes from O-H bending in alcoholic groups (C-OH); higher intensity of the peak at around 1060 cm^{-1} (C-O stretching) and the disappearance of the C=O stretching at around 1725 cm^{-1} verifies that the COOH groups are reduced into C-OH groups. After the silanization, the peak corresponding to C-OH bending almost disappears. However, the intensity of the peak at

around 1060 - 1070 cm^{-1} related to Si-O stretching is quite low. Therefore further evidence is required to prove the silanization.

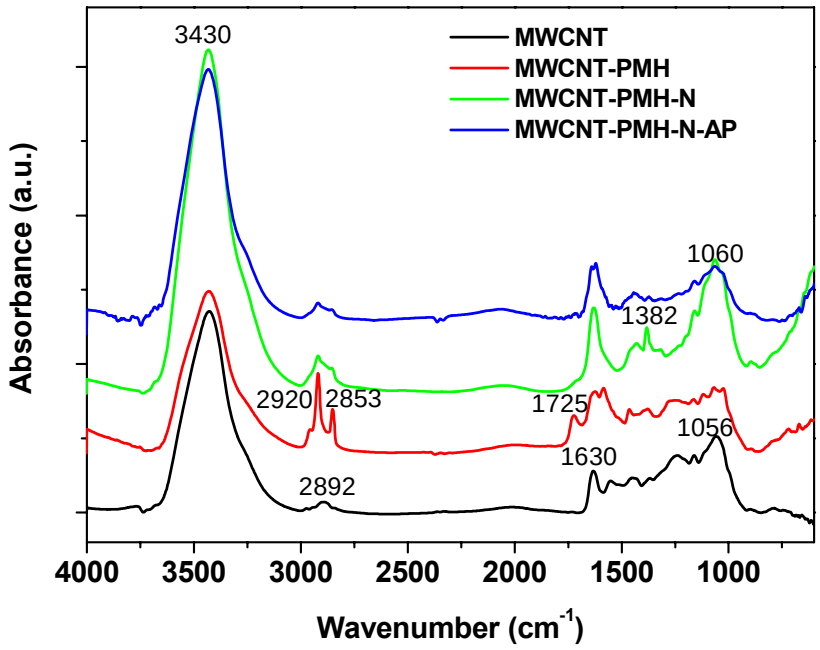

Figure 2.34 IR spectra of pristine MWCNTs and modified MWCNTs (MWCNT: pristine MWCNTs; MWCNT-PMH: oxidized MWCNTs; MWCNT-PMH-N: reduced MWCNTs; MWCNT-PMH-N-AP: silanized MWCNTs with APTMS).

2.4.6.2 XPS analysis

XPS measurements (Table 2.10 and 2.11) show that the content of oxygen increases from 4.0 % to 7.6 % after the oxidation. The detection of N and Fe from the original CNTs is reasonable because the nanotubes were prepared from mixture of benzene and acetonitrile with ferrocene as catalyst. But after the silanization, the increase of N content from 1.2 % to 2.4 % and the detection of 1.4 % Si are indications that the aminosilane is coated onto the surface. From the decrease of the relative ratio between C=C and C-C, C-H groups in C 1s peak deconvolution, it is concluded that the surface chemical environment changes a lot after each chemical treatment. Also the relative area percentage of the peak at 286.0 eV increases from 19 % to 28 % after silanization due to the introduction of C-N groups from APTMS. But the area percentage of the peak corresponding to C=O and (C=O)-N groups also increases from 6 % to 11 %, arising from the probable reaction of COOH groups on the surface of CNTs with NH_2 groups in the silane. Therefore the silanization of MWCNTs with aminosilane may have a mechanism different from the aminosilanization of CNFs (CNF-N-AP).

Table 2.10 XPS measurements of MWCNT surface composition.

Concentration of elements in at%							
Sample	**C**	**O**	**N**	**Fe**	**Cl**	**Na**	**Si**
MWCNT	**93.0**	**4.0**	**2.7**	**0.3**		**-**	**-**
MWCNT-PMH	**90.7**	**7.6**	**1.4**	**0.1**	**0.2**	**-**	**-**
MWCNT-PMH-N	**89.7**	**8.4**	**1.2**	**-**	**-**	**0.7**	**-**
MWCNT-PMH-N-AP	**86.4**	**9.8**	**2.4**	**-**	**-**	**-**	**1.4**

Table 2.11 Relative percentage of functional groups from XPS C 1s peak deconvolution.

Relative percentage of functional groups (%)							
	Peak A 284.6 eV	**Peak B 285.0 eV**	**Peak C 286.0 eV**	**Peak D 287.0-287.5 eV**	**Peak E 288.7-289.3 eV**	**Peak F 290.2-290.7 eV**	**Peak G 291.7 eV**
MWCNT	**64**	**14**	**13**	**4**	**2**	**2**	**1**
MWCNT-PMH	**55**	**18**	**16**	**5**	**3**	**2**	**1**
MWCNT-PMH-N	**49**	**21**	**19**	**6**	**2**	**2**	**1**
MWCNT-PMH-N-AP	**6**	**47**	**28**	**11**	**4**	**3**	**1**

Peak A: assigned to graphitic carbon (C=C)

Peak B: assigned to sp^3 hybridized carbon (C-C, C-H)

Peak C: phenolic, alcoholic hydroxyls, carbon nitrogen bond or ether oxygen (C-OH, C-O-C, C-N)

Peak D: carbonyl, amide groups (C=O, N-C=O)

Peak E: carboxyl groups or ester groups (COOH, COOC)

Peak F: π- π^* shake up peaks of carbonyl bonds

Peak G: π- π^* shake up peaks of graphitic carbon

To quantify C-OH and C-NH_2 groups on MWCNT-PMH-N and MWCNT-PMH-N-AP respectively, MWCNT-PMH-N was derivatized with TFAA and MWCNT-PMH-N-AP with TFBA respectively (Figure 2.35). TFBA is specific with primary amine and does not react with other nitrogen functional groups. Therefore it is possible to determine the relative amount of C-NH_2 groups on MWCNT-PMH-N-AP.

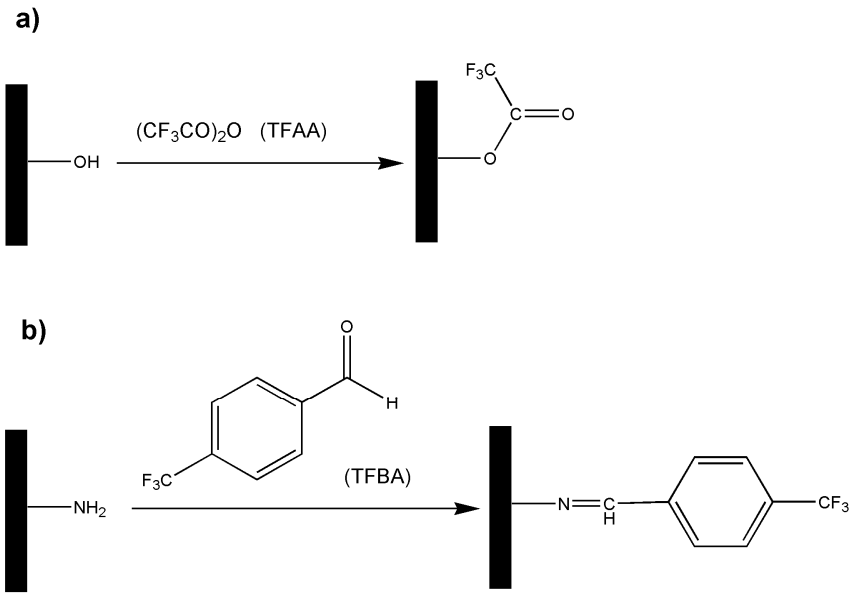

Figure 2.35 Scheme for the derivatization of a) MWCNT-PMH-N with TFAA and b) MWCNT-PMH-N-AP with TFBA.

XPS measurements were done with the derivatized samples (Table 2.12). The relative percentage of C-OH groups on non-derivatized MWCNT-PMH-N can be determined based on equation 6; the relative percentage of C-NH_2 groups on non-derivatized MWCNT-PMH-N-AP can be determined by equation 7 [140]

$$X_{OH} = \frac{100 n_F}{3n_C - 2n_F} \qquad (6)$$

$$X_{NH_2} = \frac{100 n_F}{3n_C - 8n_F} \qquad (7)$$

where X_{OH} is the relative percentage of C-OH groups (%), X_{NH_2} is the relative percentage of C-NH_2 group (%), n_F is the atom percentage of fluorine after derivatization, n_C is the atom percentage of carbon after derivatization.

Table 2.12 XPS measurements of MWCNT surface composition after derivatization.

	Concentration of elements in at%							
Sample	**C**	**O**	**N**	**F**	**Cl**	**Si**	**Na**	**Zn**
derivatized MWCNT-PMH-N	**85.7**	**5.9**	**1.6**	**5.0**	**-**	**-**	**1.1**	**0.7**
derivatized MWCNT-PMH-N-AP	**87.6**	**6.9**	**1.8**	**1.5**	**0.2**	**1.7**	**0.3**	**-**

From the data in Table 2.12, the relative percentage of C-OH groups on MWCNT-PMH-N is calculated to be 2 %, while the total relative percentage of C-OH and C-O-C groups is 19 % (Table 2.11), suggesting that only about 10 % of C-O moieties exists as C-OH state on the surface of MWCNT-PMH-N. The relative percentage of C-NH_2 groups is calculated to be 1 %, while the total relative percentage of C-O-C, C-OH and C-N groups is 28 % (Table 2.11). Therefore, the derivatized XPS indicates that only trace amount of nitrogen exists as primary amine (NH_2); most nitrogen exists as protonated amine (amine groups are easily protonated with hydrogen ions from water in the ambient environment), amide groups (considering the XPS results in Table 2.11)), etc. on the MWCNT surface.

The Si 2p peak fitting demonstrates that the Si-O-Si dominates the Si state in MWCNT-N-AP (peak at around 103.1 eV, relative percentage 98 %), different from the aminosilanized CNFs (CNF-N-AP), in which the Si-O-C state is dominant. There are two plausible reasons: (1) the APTMS silane is only physically adsorbed on the MWCNT surface; (2) the APTMS silane is covalently bonded onto the surface through amide bonds between carboxyl groups and amine groups. Afterwards the either adsorbed or covalently bonded aminosilanes hydrolyze into silanols and crosslink with each other to form Si-O-Si bonds on the surface.

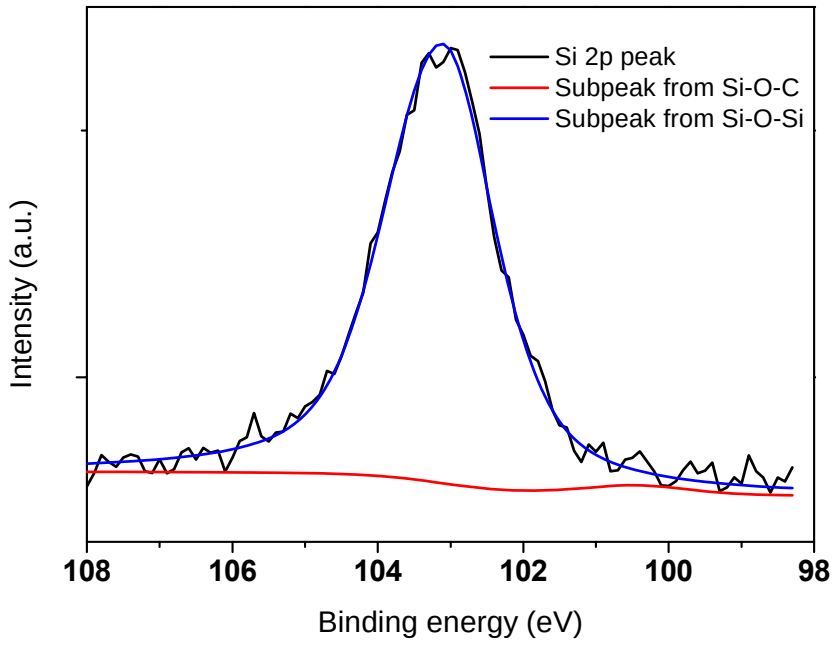

Figure 2.36 XPS Si 2p peak fitting of MWCNT-PMH-N-AP.

2.4.6.3 Raman spectra

I_G/I_D ratios of the samples MWCNT, MWCNT-PMH, MWCNT-PMH-N and MWCNT-PMH-N-AP are 1.33, 1.35, 1.49 and 1.33 respectively (Figure 2.37). It follows the same trend as the aminosilanized procedure for CNFs, which shows that the reduction of nanofiller (CNF-N or MWCNT-PMH-N) increases the surface graphitization. However, in MWCNT-PMH-N-AP the ratio decreases due to the amorphous silane molecules on the surface.

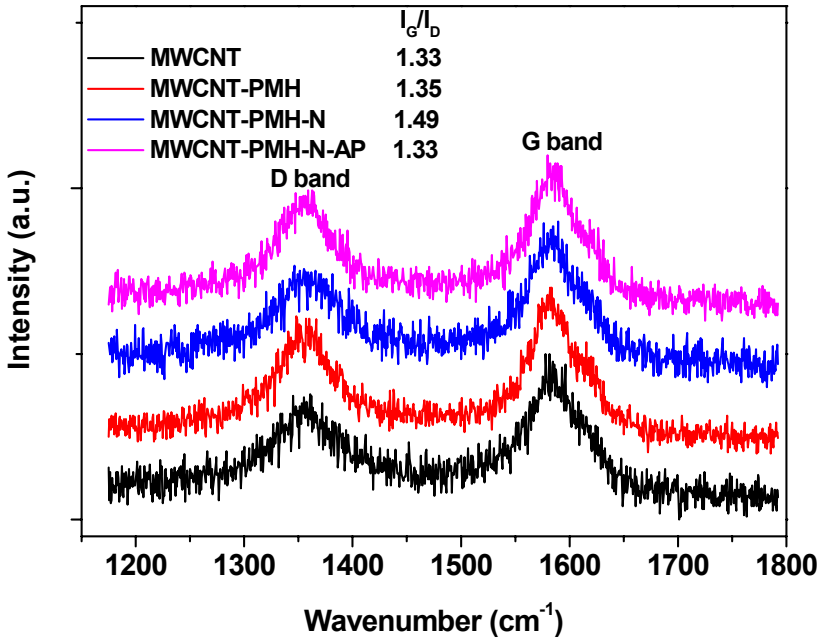

Figure 2.37 Raman spectra of MWCNT-PMH-N-AP compared with pristine MWCNTs (MWCNT), oxidized MWCNTs (MWCNT-PMH) and reduced MWCNTs (MWCNT-PMH-N).

2.5 Summary

Oxidation by acid mixture of H_2SO_4/HNO_3 or $KMnO_4/H_2SO_4$ was carried out to find the optimal condition for the introduction of oxygenated groups on CNFs or CNTs. The oxidation process was characterized by IR, XPS, SEM and Raman spectra. The oxidation method with mixture of H_2SO_4/HNO_3 by bath sonication was chosen as the best way for CNF oxidation, while the oxidation with $KMnO_4/H_2SO_4$ by heating treatment was optimal for MWCNTs. The silanization of CNFs was carried out with three different procedures. For the silanization with GPTMS, IR, XPS, EDX were used to verify the chemical reaction, and Raman spectra indicated that the silanization process introduced surface defects on the graphitic structures.

TGA confirmed 1.1 wt% Si in the silanized sample CNF-GS. Different behaviors of ethanol suspensions of CNF-GS and CNF-O under DC electric field indicated that the silanization process decreased the electrical conductivity of CNFs. XPS Si 2p peak fitting gave direct evidence that the silanization took place through covalent bonds between hydrolyzed glycidoxysilanes and carboxyl groups. Silanization through first reduction of carboxyl groups into alcoholic groups and then reaction of C-OH groups with silanol groups from hydrolyzed APTMS was verified by XPS analysis (1.1 at% Si on the surface, higher than 0.4 at% Si on CNF-GS). However, the bulk concentration of Si calculated from TGA results in CNF-N-AP was 0.6 wt%, lower than CNF-GS (1.1 wt%). Thus it was presumed that these Si moieties were mostly attached onto the sidewalls of CNFs rather than onto the ends of CNFs, which was contrary to CNF-GS. Most Si existed on the CNF surface as Si-O-C groups, which confirmed chemically covalent bonds between silanes and CNFs. IR spectra confirmed the appearance of Si-O stretching on CNF-N-AP after silanization; the change of IEP in streaming potential measurements gave further evidence that the alteration of surface charge was due to the attachment of aminosilanes onto CNFs. It was worth to note that Raman spectra showed that the process to reduce the carboxyl groups on oxidized CNFs into alcoholic hydroxyl groups improved the graphitization of CNF-N in some extent. Perhaps it was due to the repeated washing procedure with acid and base after the reduction treatment. The two consecutive silanizations with IPTES and APTMS were carried out to further improve the yield of silicon on CNFs. The ratio of the peak intensity of Si-O stretching to O-H stretching in IR spectra increased after the first silanization. After the second silanization, the intensity of Si-C peak increased, arising from the APTMS coating on the surface. XPS C 1s peak fitting indicated that the relative percentage of C-O and C-N groups increased after both silanizations, suggesting the surface silanization took place. XPS Si 2p peak fitting indicated that both IPTES and APTMS silanes were covalently bonded onto the CNF surface. XRD showed that the two - silanization procedure had no effect on the crystallization and interlayer distance of CNFs, which was consistent with Raman results. Streaming potential and TGA measurements confirmed that the content of silanes was the most on CNF-I-AP compared to the other two silanized CNFs (CNF-GS and CNF-N-AP). In order to investigate the different effects of silanization on CNFs and MWCNTs, the silanization with aminosilane was also performed with MWCNTs. The oxidation of MWCNTs was realized by heat treatment with $KMnO_4/H_2SO_4$ (MWCNT-PMH). IR spectra verified the effective oxidation process. Further XPS analysis confirmed the aminosilane coating on the surface of MWCNT-PMH-N-AP. The relative percentage of C-OH groups on MWCNT-PMH-N was determined to be 2 %; the

relative percentage of C-NH_2 groups on MWCNT-PMH-N-AP was 1 %. Different from CNF-N-AP, XPS Si 2p peak fitting from MWCNT-PMH-N-AP indicated that the silane either physically adsorbed on the surface or reacted with carboxyl groups through amide bonds. Raman spectra indicated that the surface graphitic structures of MWCNTs were intact after each chemical treatment.

3 CNFs/epoxy and MWCNTs/epoxy composites

3.1 Preparation of composites

3.1.1 Materials

Original CNFs and silanized CNFs were the same as those used in Chapter 2. Epoxy resin EPON 828 was purchased from Hexion Specialty Chemicals Inc., Houston, Texas, USA, and hardener (poly(propylene glycol) bis(2-aminopropyl ether)) was from Sigma-Aldrich, Steinheim, Germany. Acetone (98 %) was bought from AppliChem GmbH, Darmstadt, Germany.

3.1.2 CNFs/epoxy composites

CNF-O and CNF-N-AP were dispersed in polymer resin EPON 828 by the procedure shown in Figure 3.1. First a certain amount of CNFs according to the desired concentration of CNFs in epoxy composite was dispersed in acetone by ultrasonic probe for 5 min, and then a corresponding amount of epoxy resin was added into the suspension and sonicated again with ultrasonic probe for another 5 min. After CNFs were homogeneously mixed with epoxy resin, acetone was removed by rotary evaporation. Then the mixture of CNFs and epoxy resin was left in a flask under vacuum at 60 °C over night to remove possible residue of acetone. Finally hardener ((poly(propylene glycol) bis (2-aminopropyl ether)) was added into the system (weight ratio between resin and hardener was 100:55). The mixture was then pumped in a vacuum desiccator for 2 h to remove the trapped air bubbles. Finally CNFs/epoxy composite was casting into preformed molds and kept at RT overnight. The liquid mixture was cured for first 30 min at 80 °C and then 2 h at 115 °C on the next day. To prepare samples for measurements of electrical and thermal conductivity, round propylene molds were used (diameter 30 - 50 mm, thickness 1 - 5 mm); for DMA measurements, stainless rectangular molds were used (85 mm × 10 mm); for tensile strength measurements, silicone molds with dog-bone shape were used (50 mm × 5 mm for the effective measuring area).

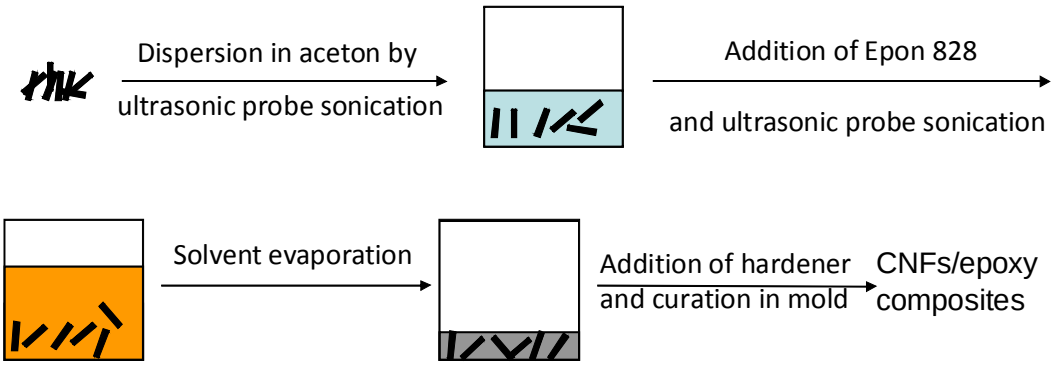

Figure 3.1 Scheme for the preparation of CNFs/epoxy nanocomposites.

3.1.3 MWCNTs/epoxy composites

The preparation of 0.5 wt% unaligned MWCNTs/epoxy composites was similar as section 3.1.2 with some minor changes. 100 mg of MWCNT or MWCNT-N-AP was put into a beaker and dispersed in 20 ml acetone by ultrasonic probe for 2 min. Then 12.839 g EPON 828 was added into the above mixture, followed by manually stirring with a glass stick and ultrasonic probe sonication for another 5 min. The mixture was transferred into a flask (the beaker was rinsed with acetone in order to collect all the material) for evaporating acetone completely with a rotary evaporator. Afterwards, the liquid suspension was put into another beaker, stirred for 2 h with heating at 60 °C to insure that all the acetone was evaporated. On the next day, 7.061 g hardener (poly(propylene glycol) bis(2-aminopropyl ether)) was manually mixed with the resin by a glass stick and the air bubbles were removed by carefully pumping in a desiccator**.** Then the mixture was poured into the mold and cured at 80 °C for 30 min, and then 115 °C for 1 h (for unaligned MWCNT/epoxy and MWCNT-PMH-N-AP/epoxy composites).

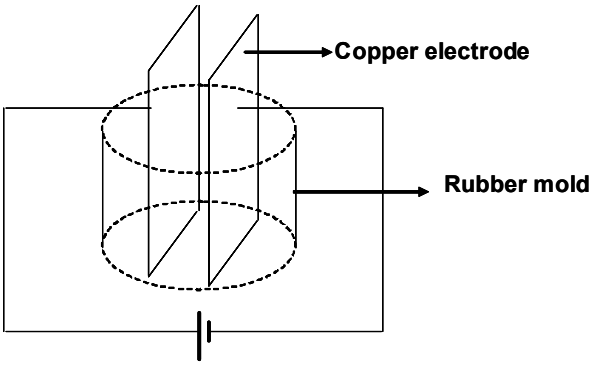

Figure 3.2 Sketch for the alignment of MWCNTs in epoxy resin.

Preparation of the aligned MWCNTs/epoxy composites: the liquid mixture of epoxy resin and hardner was prepared exactly in the same way as above. Then it was poured into a rubber mold and the scheme for alignment is shown in Figure 3.2. Two rectangular copper electrodes

with a dimension of 50 mm × 20 mm and a thickness of 1 mm stand parallel with each other in the pre-mixed MWCNTs/epoxy liquid with a distance of 1 cm. A sinusoidal AC power supply was applied between the two electrodes. The peak voltage and the frequency of the sinusoidal electric field are 200 V and 10 kHz respectively. The maximal AC electric field between the electrodes is 2×10^4 V m^{-1}. The sample was under electric field for 1 h. Then it was cured in situ first at 80 °C for 30 min, and later at 115 °C for 1 h. The experimental set-up is demonstrated in Figure 3.3.

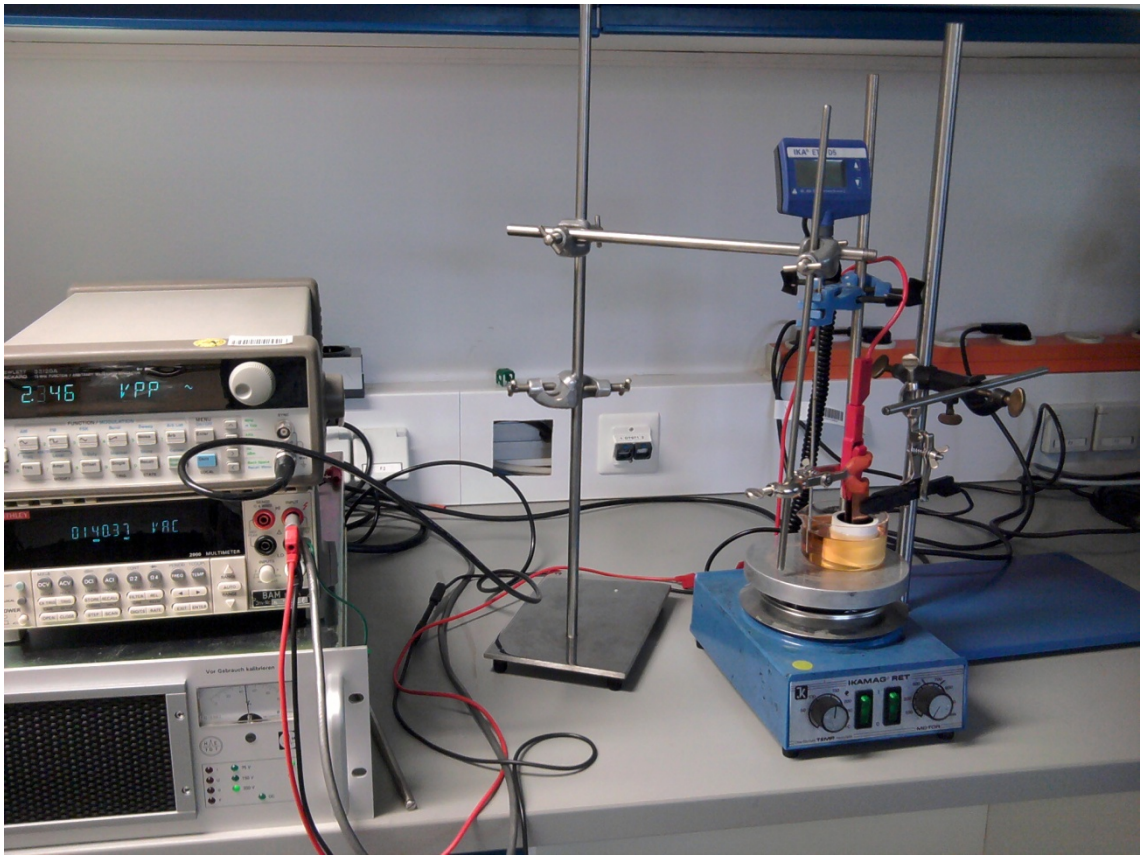

Figure 3.3 Picture of the set-up for the preparation of aligned MWCNTs/epoxy composites.

3.2 Characterization

Morphology of the composites was characterized by SEM (Hitachi S-4100 and Zeiss Gemini Supra 40). Alternative current (AC) electrical conductivity of epoxy composites was calculated from direct measurements of electrical resistance of epoxy composites tablets using a LCR meter HP 4284A and an impedance analyzer HP 4194A with sample holder HP16451B under 1 V in the frequency range of 10^5 - 1.5×10^7 Hz. AC electrical conductivity of pure CNF powder tablets (40 mg powder pressed by a hydraulic press at 40 MPa; diameter of tablets was 7.9 mm) was calculated by direct measurements of the electrical resistance under the same conditions but with different sample holder HP 16089B. Direct current (DC) electrical

conductivity of composites was calculated by direct measurements of the electrical resistivity on the high resistance meter HP 4339B with HP 16008B resistivity cell. Thermal conductivity of composites was measured based on hot disk method on HotDisk Thermal Constants Analyser TPS 1500. DMA measurements were done on DMA 2980 from TA instruments at a frequency of 1Hz and in the temperature range from RT to 100 °C with the heating rate of 2 K/min. Tensile shear strength of composites was measured according to EN 1465 [141]. The scheme of the measurement is shown in Figure 3.4. Two stainless steel substrates were cleaned first by oxalic acid/H_2SO_4 mixture, and then they were glued together by CNFs/epoxy resin composites, finally cured at 115 °C for 1h. Mechanical load was applied at both ends to measure the shear strength.

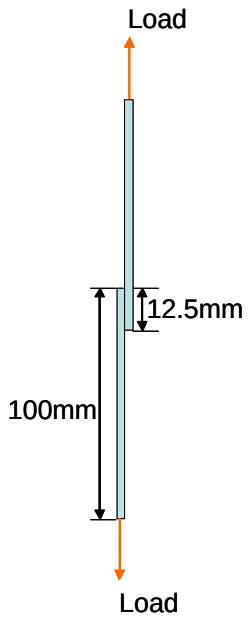

Figure 3.4 Scheme for the measurement of the tensile shear strength based on EN 1465.

3.3 Results and discussion

3.3.1 Morphology of CNFs/epoxy composites

3.3.1.1 Comparison of CNF-GS/epoxy with CNF-O/epoxy composites

Fracture surfaces of CNFs/epoxy composites were characterized by SEM, as shown in Figure 3.5. Both 1 wt% and 3 wt% CNF-O/epoxy composites contain great aggregations of CNFs in the matrix, and most nanofibers are pulled out from the matrix. The modified CNFs (CNF-GS) are better dispersed in the matrix and no apparent pulling out of fibers from the epoxy polymer is visible, which is a hint of stronger interfacial force between fillers and matrices. The improved dispersion of CNFs comes from the change of surface chemistry. Silane coating makes CNFs easily wetted by organic solvents and liquid epoxy resin.

Furthermore, the epoxy groups can react further with the amine groups in the hardener [97], which enhances the interfacial adhesion between fillers and polymer matrices. However, the 10 wt% silanized CNFs/epoxy composites showed great agglomeration of fillers (Figure 3.5 e), indicating that CNFs are not able to disperse uniformly in the matrix at high concentration even after the surface silanization.

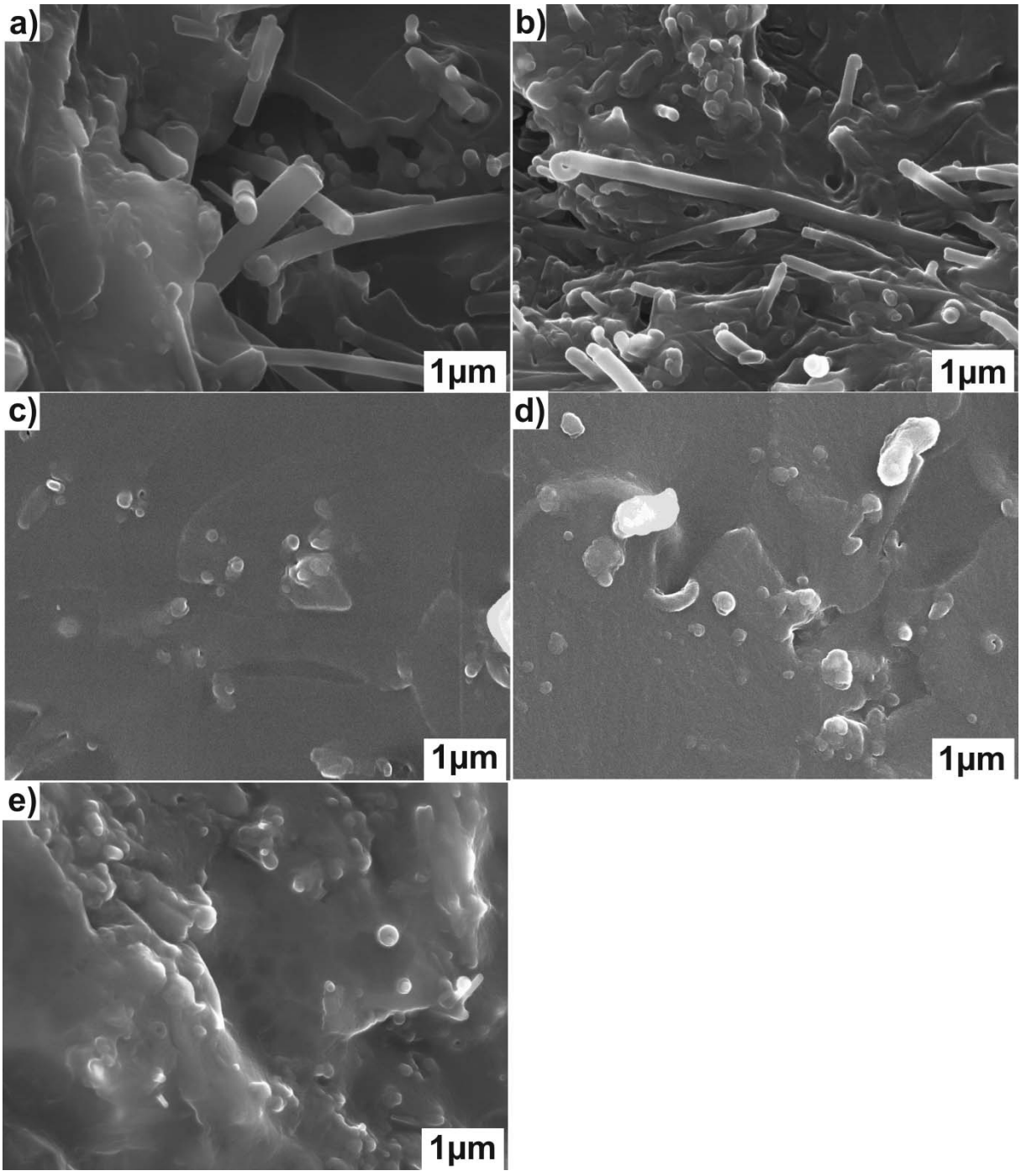

Figure 3.5 SEM pictures of composites a) 1 wt% CNF-O/epoxy b) 3 wt% CNF-O/epoxy and c) 1 wt% CNF-GS/epoxy d) 3 wt% CNF-GS/epoxy e) 10 wt% CNF-GS/epoxy.

3.3.1.2 Comparison of CNF-N-AP/epoxy with CNF-O/epoxy composites

SEM pictures of CNF-O/epoxy composites in Figure 3.6 a show that the original CNFs with a concentration of 2 wt% in an epoxy resin are agglomerated. The bright spots correspond to CNFs, and the dark gray “river” or “clay” is the polymer matrix. Seen from enlarged microscopic picture (Figure 3.6 b), there are lots of extruded CNFs on the sample, which suggests original CNFs are easy to pull out from the matrix due to weak interfacial force between fillers and the matrix. In contrast, the CNF-N-AP/epoxy composites show homogeneous dispersion of the nanofibers (Figure 3.6 c). Most fillers are inset into the matrix without apparent pulling out (Figure 3.6 d). Therefore the surface silanization process renders better dispersion of the nanofibers and stronger adhesion between the nanofibers and the epoxy matrix, which was also observed by Shen et al. [142].

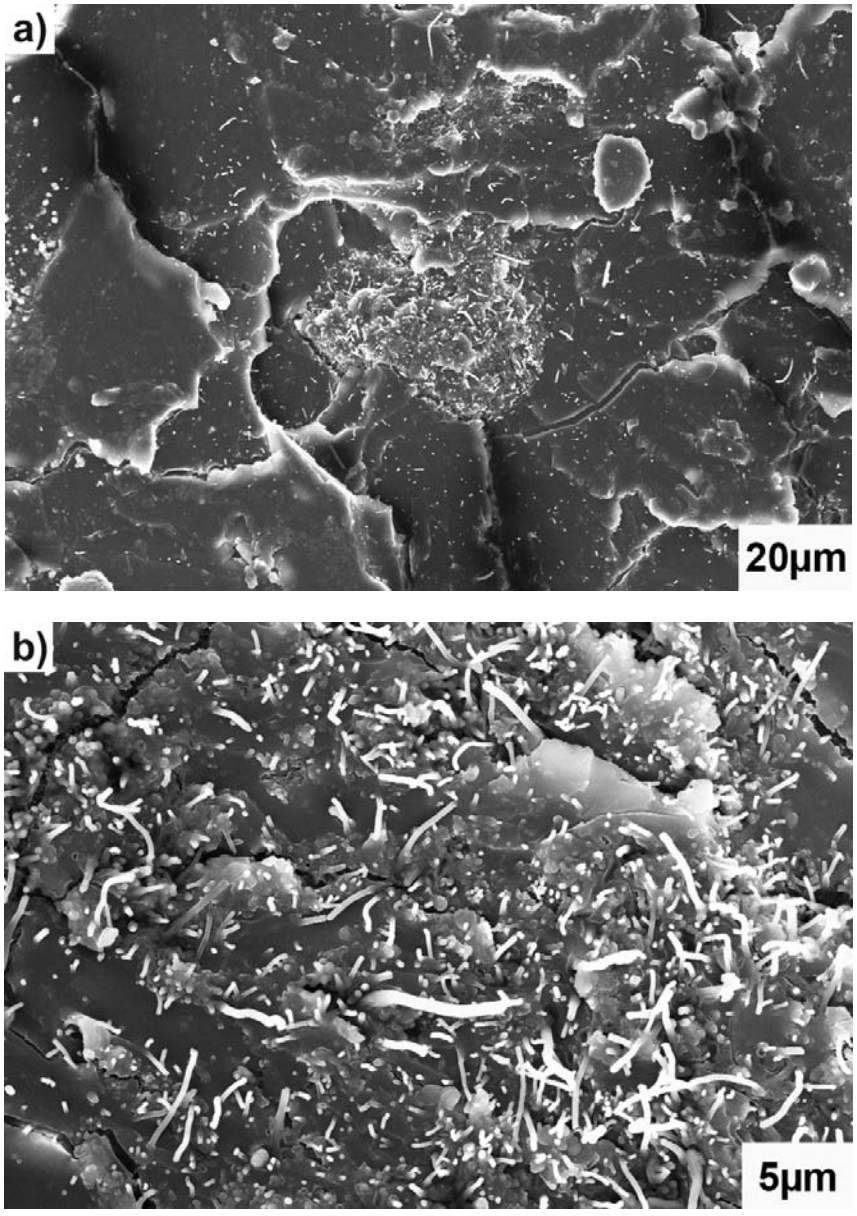

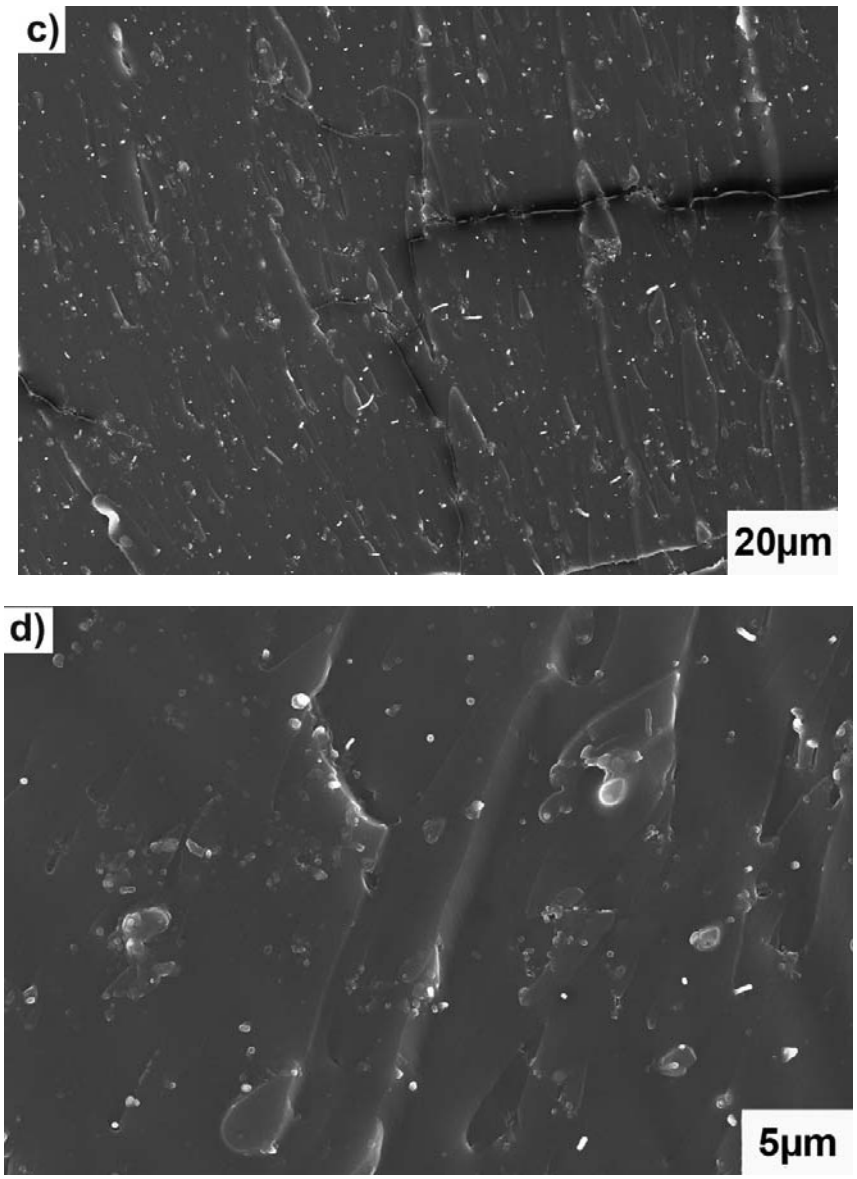

Figure 3.6 SEM pictures of epoxy composites containing 2 wt% CNFs a) CNF-O/epoxy composite; b) magnified picture from a); c) CNF-N-AP/epoxy composite; d) magnified picture from c).

3.3.1.3 Comparison of CNF-I-AP/epoxy with CNF-O/epoxy composites

Epoxy composites containing CNF-I-AP show homogeneous distribution of CNFs in large area, while the original CNFs in epoxy composites are highly agglomerated (Figure 3.7). It confirms again that the surface silanization is helpful to uniformly distribute the CNFs in the epoxy matrix because of both better wetting of epoxy on CNFs and greater space repulsion between CNFs coming from the surface functional groups

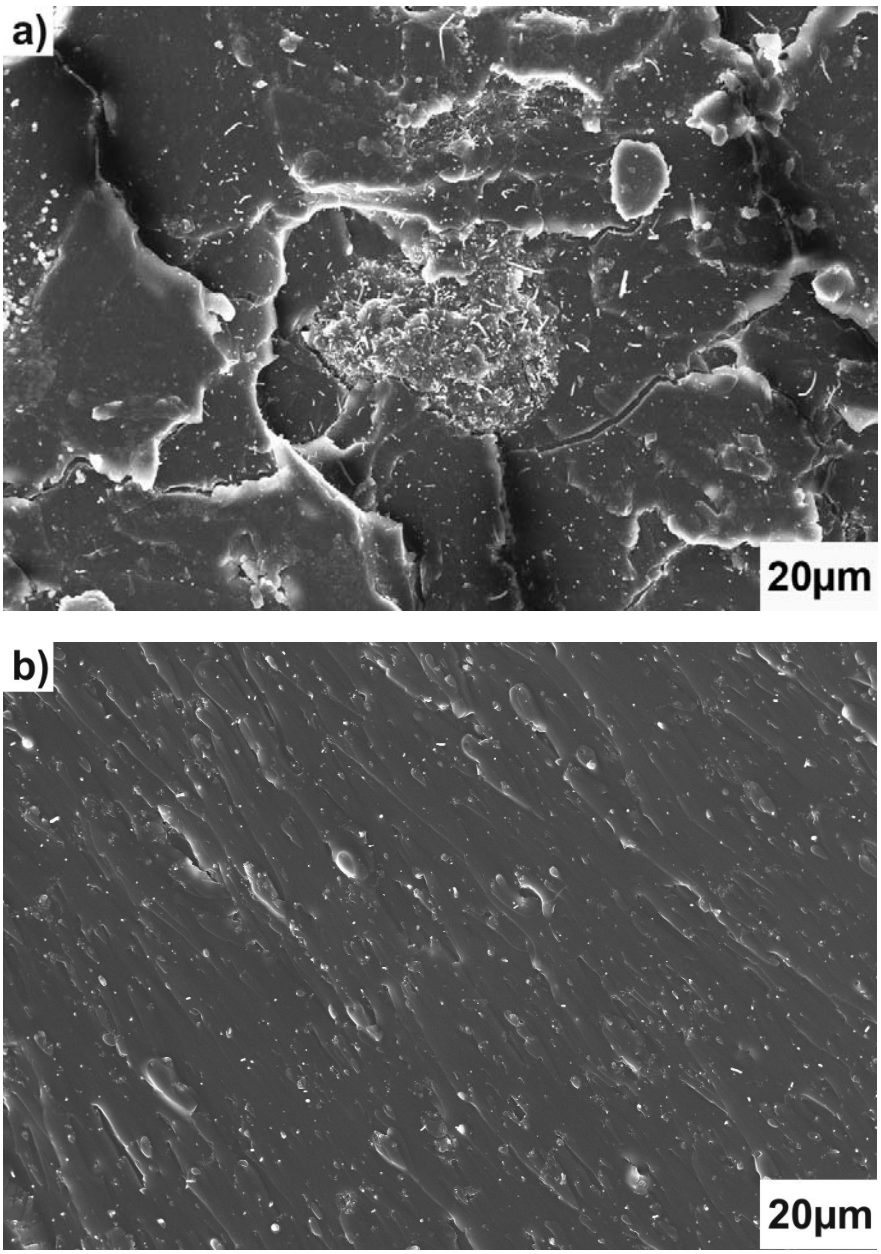

Figure 3.7 SEM pictures of composites a) 2 wt% CNF-O/epoxy b) 2 wt% CNF-I-AP/epoxy.

3.3.1.4 Summary of the morphology characterization

The original CNFs were highly agglomerated in the epoxy polymer. It was demonstrated that silanization process improved the distribution and the dispersion state of CNFs in the matrix. Moreover, the less pulling out of fibers from matrices and fewer voids in composites indicated that silane coating on CNF surface was beneficial to increase the adhesion between fillers and matrices, which would enable the efficient transfer of the mechanical load from polymer matrices to CNFs for achieving a higher mechanical strength of polymer composites.

3.3.2 Mechanical properties of CNFs/epoxy composites

3.3.2.1 DMA anylysis of CNF-GS/epoxy and CNF-O/epoxy composites

The results of dynamic mechanical analysis (DMA), which was performed to evaluate viscoelastic properties such as storage modulus and glass transition temperature (T_g) of the composites are manifested in Table 3.1 and Figure 3.8. In contradiction to an expected reinforcement of mechanical properties of a polymer by the infusion of CNFs, an opposite effect on composites was observed for original CNFs. Obviously, the infusion of CNF-O results in a weakening of the polymer matrix. Therefore the mechanical properties of CNF-O/epoxy composites deteriorate. On the other hand, epoxy composites containing silanized CNFs (CNF-GS) have higher storage modulus than pure epoxy polymer at RT. 1 wt% CNF-GS/epoxy composite exhibits a 20 % increase of storage modulus than the pure epoxy matrix; while those containing original CNFs (CNF-O) show lower storage modulus than the pure polymer. The enhancement of storage modulus may arise from a reaction of the surface epoxy ring with the amine group in the hardener. During the curing process, the hardener (poly (propylene glycol) bis (2-aminopropyl ether)) reacts not only with the epoxy resin EPON 828, but also with the epoxy groups on CNFs, forming covalent bonds between fillers and matrices. As a result, the mechanical load on composites is effectively transferred from the epoxy matrix to fillers, so that a higher storage modulus is achieved with silanized CNFs/epoxy composites. In contrast, original CNFs have no chemical interaction with the epoxy resin or the hardener, which demonstrates no reinforcement role on the mechanical property.

Tan δ is the ratio of loss modulus over storage modulus of a material. The peak position from the curve of tan δ versus temperature indicates the glass transmission temperature (T_g) of the material, as shown in Figure 3.8 b. T_g of both CNF-O/epoxy and CNF-GS/epoxy composites is lower than that of the pure epoxy polymer. The results are comparable with the data given by Shen [142], Barrera [143], and Prolongo [65] et al., whereas other researchers found an increase of glass transmission temperature [66-68, 97, 98, 144]. This behavior is not jet fully understood and various explanations have been given. It is assumed that the addition of CNF disturbs the formation of a cross-linked polymer matrix or a non-stoichiometric ratio of resin and hardener can result in a weaker composite. Defects due to air bubbles or agglomeration of CNFs in the matrix hindering the formation of polymer network were presumed in [65, 142, 143]. Therefore the T_g decrease of original CNFs/epoxy composites may come from the aggregates of fillers in the matrix (as shown in Figure 3.5). For silanized CNFs, the existence

of excess epoxy groups on CNF surface lowers the stoichiometric ratio between hardener and epoxy resin, which will result in less crosslinking of the polymer and thus T_g decreases.

Table 3.1 Storage modulus at RT and the glass transition temperature (T_g) of the pure epoxy polymer and epoxy composites.

Composition	Storage modulus at RT (MPa)	T_g (°C)
Pure epoxy	2317	55.3
1 wt% CNF-O/epoxy	2283	51.2
2 wt% CNF-O/epoxy	2202	52.7
1 wt% CNF-GS/epoxy	2831	51.8
2 wt% CNF-GS/epoxy	2561	51.2

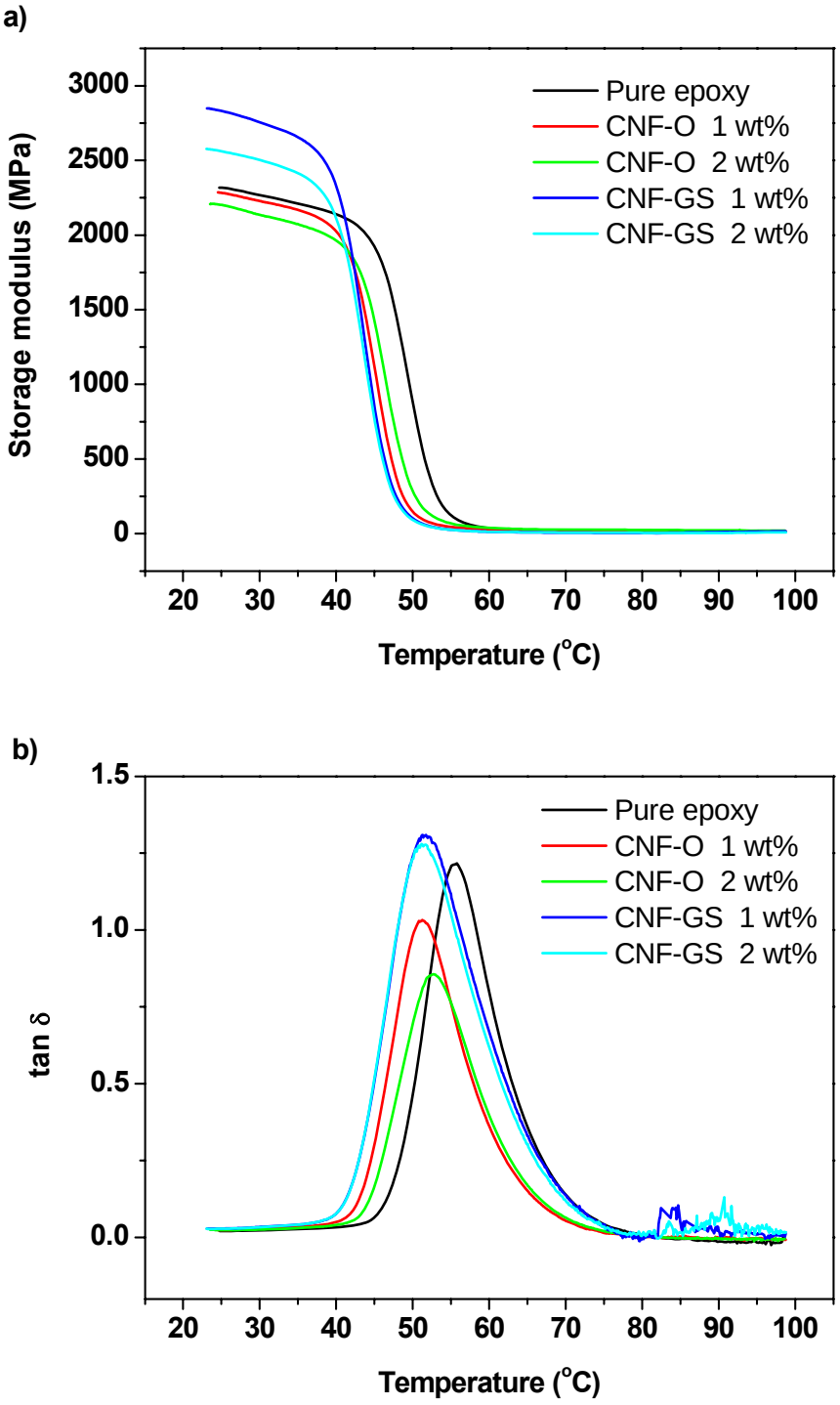

Figure 3.8 Dynamic mechanical analysis: a) variation of storage modulus with temperature for epoxy composites filled with CNFs; b) variation of tan δ with temperature for epoxy composites filled with CNFs.

3.3.2.2 Mechanical strength of CNF-N-AP/epoxy compared with CNF-O/epoxy composites

The mechanical strength measurements verify enhanced interaction between aminosilanized CNFs (CNF-N-AP) and the epoxy matrix (Figure 3.9). Both tensile and shear strength measurements show that the original fiber CNF-O deteriorates the strength of epoxy composites, especially in the shear strength measurements. The poor interaction between CNF-O and matrix limits the load transfer from matrix to CNFs, thus the more CNFs in the polymer, the more voids between fillers and epoxy. As a result, lower strength occurs. Moreover, due to high viscosity, it was impossible to remove all air bubbles from the premixed epoxy composites in order to prepare CNF-O/epoxy composites with 10 wt% nanofibers. This is also an indication of the lower surface energy of CNF-O compared to silanized CNF-N-AP, which is easier to be wetted by acetone in the dispersion step. The introduction of silanized CNF-N-AP fibers keeps the strength of polymer composites at a relative high value as the pure epoxy. It results from two effects. Polar aminosilanes facilitate better dispersion of CNFs in the epoxy matrix and amine functional groups react with the epoxy resin during the curing process, which strengthen the effective mechanical load transfer from polymer matrix to fillers. The phenomenon that the value of tensile strength of CNF-N-AP reinforced composite (about 47 MPa) is more than twice as that of shear strength (about 22 MPa) is noticeable. For the shear strength measurement, two parallel surface-pretreated stainless steel substrates with a certain overlapped area on one end were glued together by epoxy composites. Then load was applied to the other end of both substrates and pulled in the opposite direction. Due to the existence of the substrate, the occurred fracture was generally a combination of the peeling of the composite from substrates and the internal tensile fracture of the composite itself. Thus the measured shear strength which indicates the tensile properties of the epoxy as adhesives is normally lower than the tensile strength measured directly.

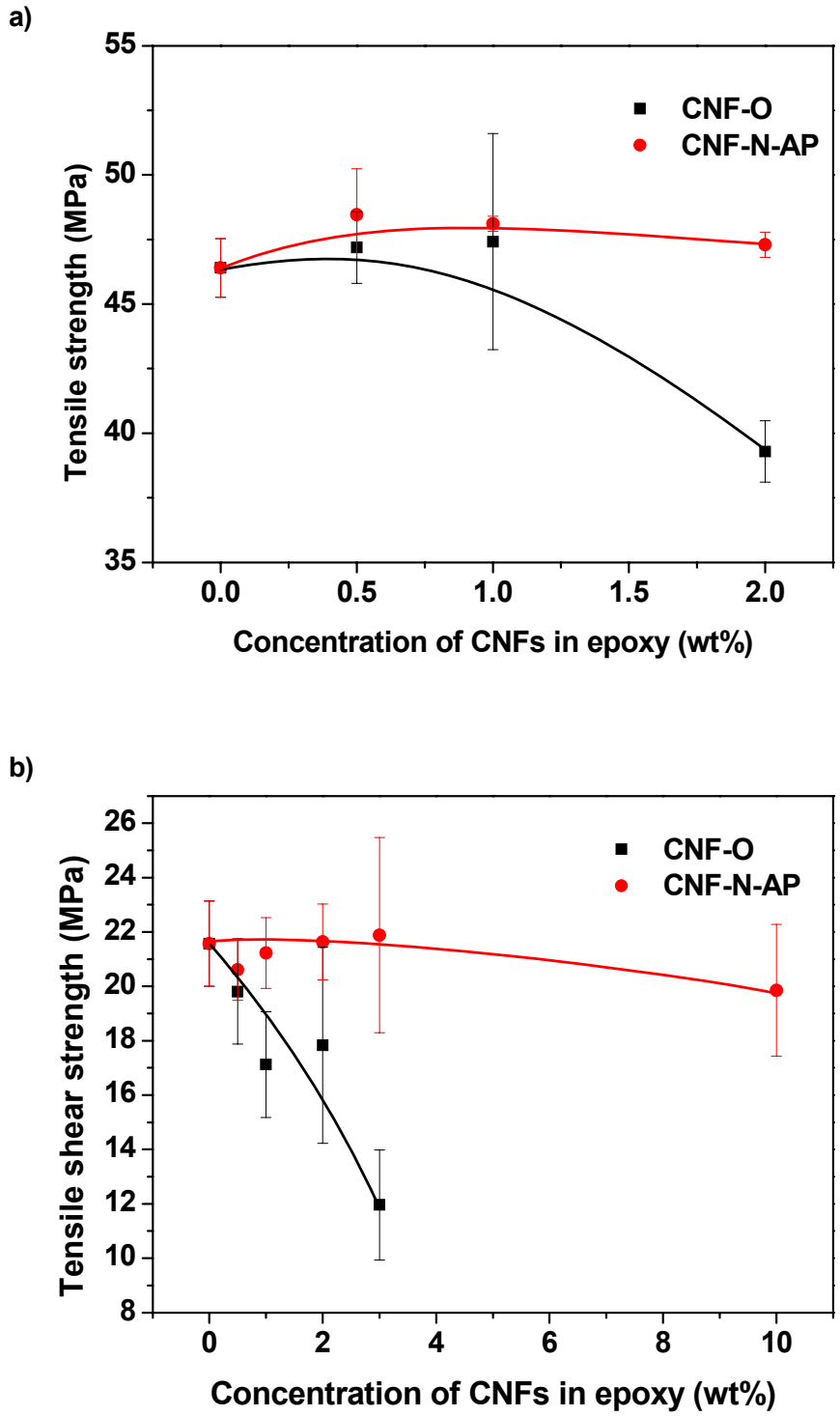

Figure 3.9 Dependence of a) tensile strength and b) tensile shear strength on the CNF loading of epoxy composites.

3.3.2.3 Shear strength of CNF-I-AP/epoxy compared with CNF-O/epoxy composites

Similar as the CNF-N-AP/epoxy composites, the shear strength of CNF-I-AP/epoxy composites also remains comparable with the pure epoxy polymer, while the shear strength of

original CNF-O/epoxy composites shows a rapid decrease (Figure 3.10). It suggests that the surface modification improved the interfacial force between fillers and epoxy polymers, which enables the mechanical load transfer from matrices to CNFs.

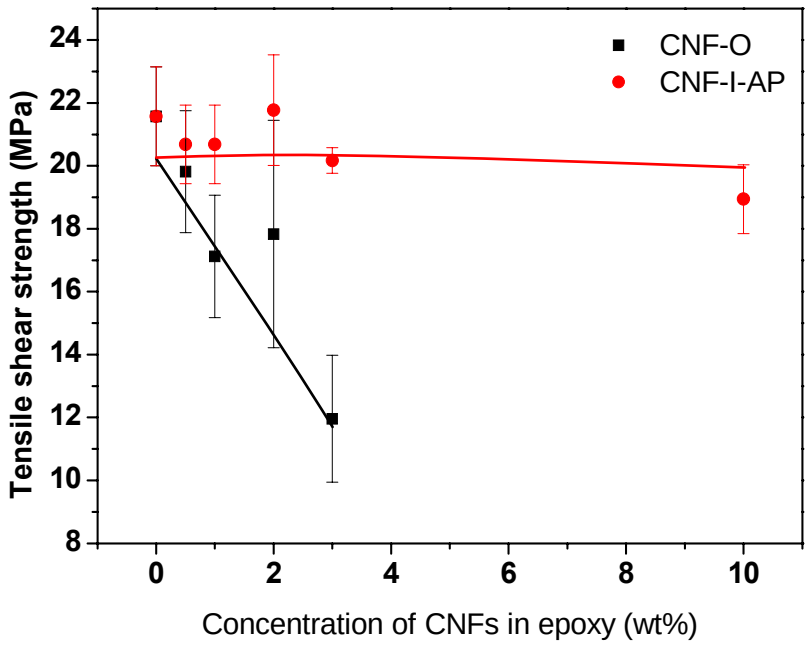

Figure 3.10 Dependence of the tensile shear strength on CNF loading for CNF-I-AP/epoxy composites compared with that for CNF-O/epoxy composites.

3.3.2.4 Summary of the mechanical properties

DMA measurements indicate that the silanization with glycidoxysilane increases the storage modulus of composites due to enhanced interfacial adhesion between fillers and epoxy polymer, while the original CNF-O shows negative effects on the mechanical behavior. In tensile testing, original fiber CNF-O deteriorates the strength of epoxy composites due to the poor interaction between CNF-O and the matrix. The introduction of aminosilanized fibers (CNF-N-AP, CNF-I-AP) keeps the tensile shear strength of epoxy composites at a relative high value as the pure polymer. It is attributed to two reasons: better dispersion of CNFs in the epoxy matrix and the amine groups on CNF surface further react with the epoxy resin during the curing treatment, which enhances the interfacial force between fillers and matrices, consequently enabling the effective mechanical load transfer from epoxy matrices to CNFs.

3.3.3 Electrical conductivities of CNFs/epoxy composites

3.3.3.1 Electrical conductivities of CNF-GS/epoxy composites

The dependence of DC electrical conductivity of CNFs/epoxy composites on CNF loading is plotted in Figure 3.11 a. Due to several factors (such as distribution and dispersion state of CNFs in the resin) affecting the electrical conductivity [26], neither apparent percolation phenomenon nor linear dependence of filler concentration due to tunneling effect is visible for DC electrical conductivity. However, the silanized CNFs/epoxy composites show lower conductivity than the original CNFs/epoxy composites at the same concentration. Especially for 2 wt% CNF-GS/epoxy composites, the conductivity is 50 times lower than 2 wt% CNF-O/epoxy composites. For 10 wt% loading, only CNF-GS/epoxy composite could be prepared because a pore-free composite containing 10 wt% CNF-O is unable to obtain due to its high viscosity. The DC conductivity of 10 wt% CNF-GS/epoxy composite is 1.05×10^{-12} $S\cdot m^{-1}$ (not shown in the figure). This value is much higher than the pure epoxy polymer (8.62×10^{-15} $S\cdot m^{-1}$). Normally insulating adhesives used in die attach have an electrical conductivity around 1×10^{-14} $S\cdot m^{-1}$. According to the given results, the uppermost concentration of silanized CNFs in epoxy resin is 3 wt%, which still keeps the conductivity of composites in that low range. Composites containing 3 wt% CNFs show lower conductivity than 2 wt% for both original and silanized CNFs, which is an indication of aggregation at higher CNF concentration, as shown in SEM (Figure 3.5 b and 3.5 d).

The AC electrical conductivity of composites is shown in Figure 3.11 b and 3.11 c. It is apparent that with respect to the same weight concentration of CNFs at certain frequency, CNF-GS/epoxy composites always have a lower electrical conductivity than CNF-O/epoxy composites. The lower conductivity of composites containing 3 wt% fillers than 2 wt% fillers coincides with the results of DC electrical conductivity shown in Figure 3.11 a.

a)

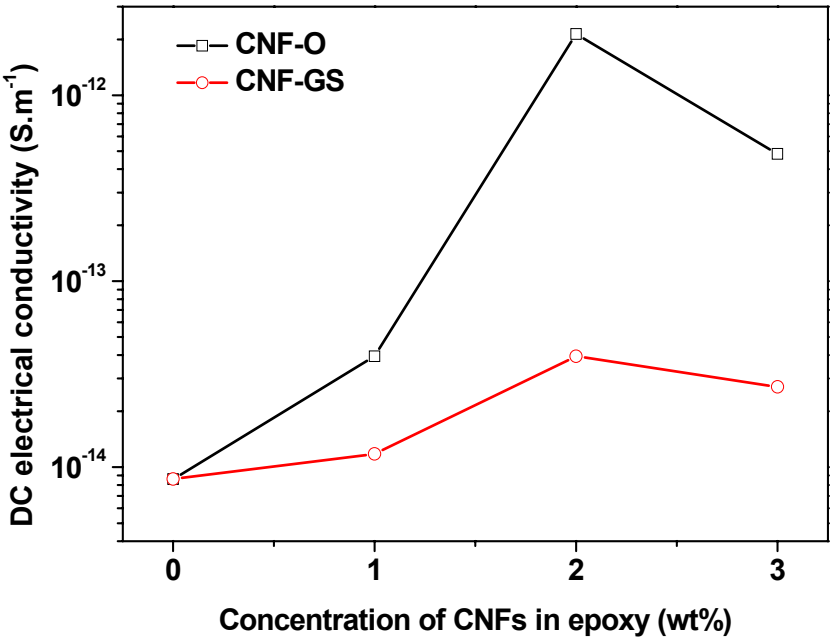
CNF-O
CNF-GS
DC electrical conductivity (S.m-1)
10-12
10-13
10-14
0
1
2
3
Concentration of CNFs in epoxy (wt%)

b)

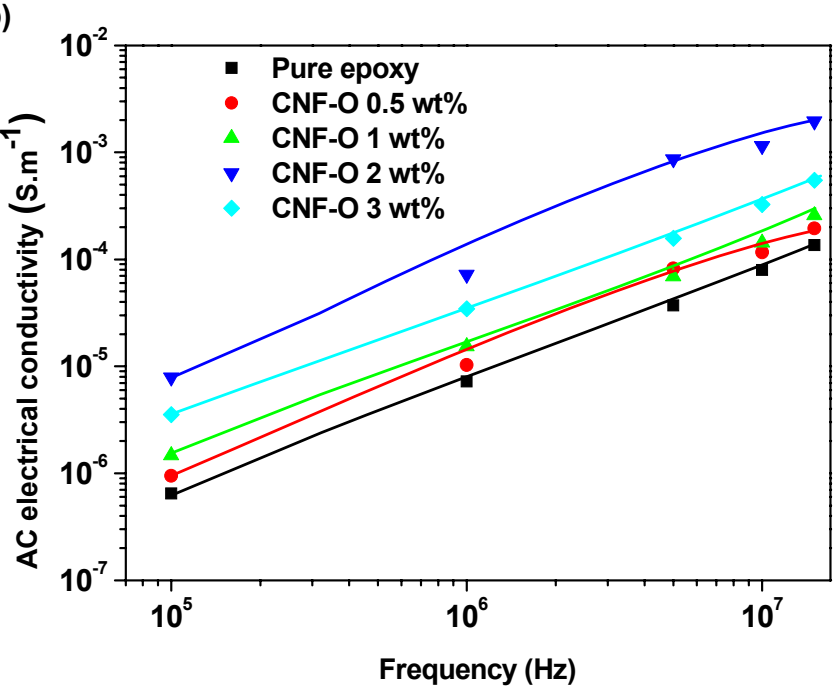
Pure epoxy
CNF-O 0.5 wt%
CNF-O 1 wt%
CNF-O 2 wt%
CNF-O 3 wt%
AC electrical conductivity (S.m-1)
10-2
10-3
10-4
10-5
10-6
10-7
105
106
107
Frequency (Hz)

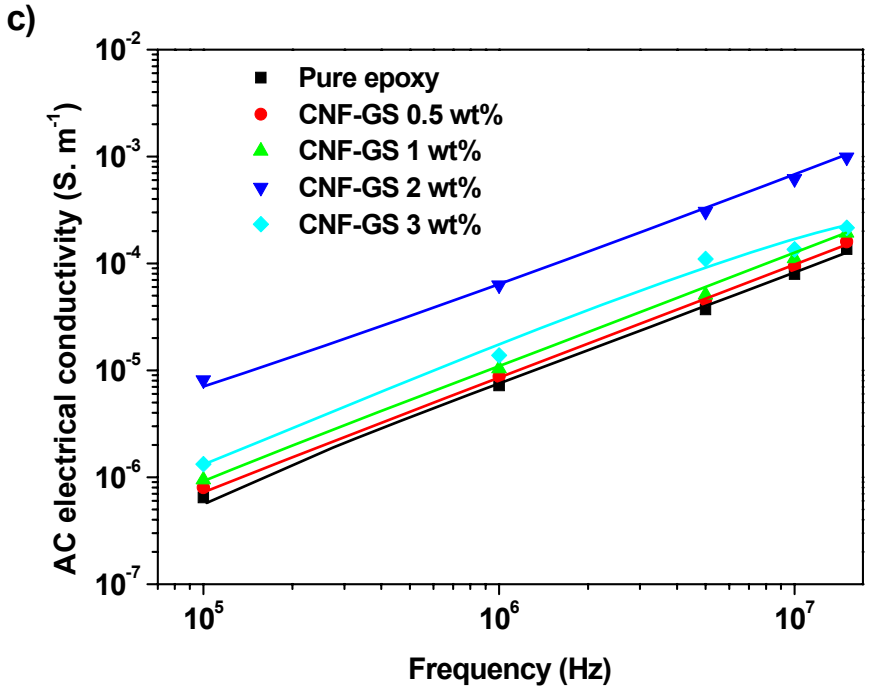

Figure 3.11 a) DC electrical conductivity of epoxy composites versus the weight concentration of CNFs; b) dependence of the AC electrical conductivity on the frequency for CNF-O/epoxy composites; c) dependence of the AC electrical conductivity on the frequency for CNF-GS/epoxy composites.

3.3.3.2 Electrical conductivities of CNF-N-AP/epoxy composites

Surface functionalization of CNFs with aminosilane lowers the electrical conductivity of CNFs/epoxy composites (shown in Figure 3.12). AC conductivity of both CNF-O/epoxy composites and CNF-N-AP/epoxy follows the same tendency (Figure 3.12 a and 3.12 b): at fixed concentration, the conductivity of CNFs increases with frequency; at fixed frequency, the conductivity rises up with the concentration of CNFs in composites. The exception that the 3 wt% CNF-O/epoxy composite has lower conductivity than the composite with 2 wt% CNF loading is due to the aggregation of CNFs at high concentration. In the measured frequency range, all epoxy composites containing silanized CNF possess a conductivity of about one order of magnitude lower than original CNF-O/epoxy composites with the same concentrations. Measurements of AC conductivity on pure CNFs powder tablets also confirm that the surface modification decreases the electrical conductivity for about 16 times in comparison to original CNF (from 830 to 50 $S \cdot m^{-1}$) in the frequency range of 20 - 10^6 Hz. Thus, it can be concluded that the lower electrical conductivity of silanized CNF/epoxy composites compared to original CNF-O/epoxy composites is attributed to the surface

wrapping of organic silanes, which diminishes the chance of direct contacts between electrically conductive CNFs [16].

The dependence of the DC conductivity on CNF concentration is consistent with the findings in the AC conductivity, verifying the reduction of conductivity after surface modification (Figure 3.12 c). The results indicate that the electrical properties of CNFs filled epoxy composites are dominated by the insulating epoxy matrix. A percolation behavior observed by other researchers [145] is not seen here. Original CNFs show bad distribution and dispersion in the matrix based on SEM pictures, which is the main reason why composites demonstrate insulating properties rather than drastically increased conductivity after a certain percolation threshold [26]. For silanized CNFs, they are immersed into the polymer matrix and insulated from each other by the surface silane coating, so no conductive networks of fibers can be formed in the matrix, as reported also by Ma and coworkers for silanized CNTs [97].

a)

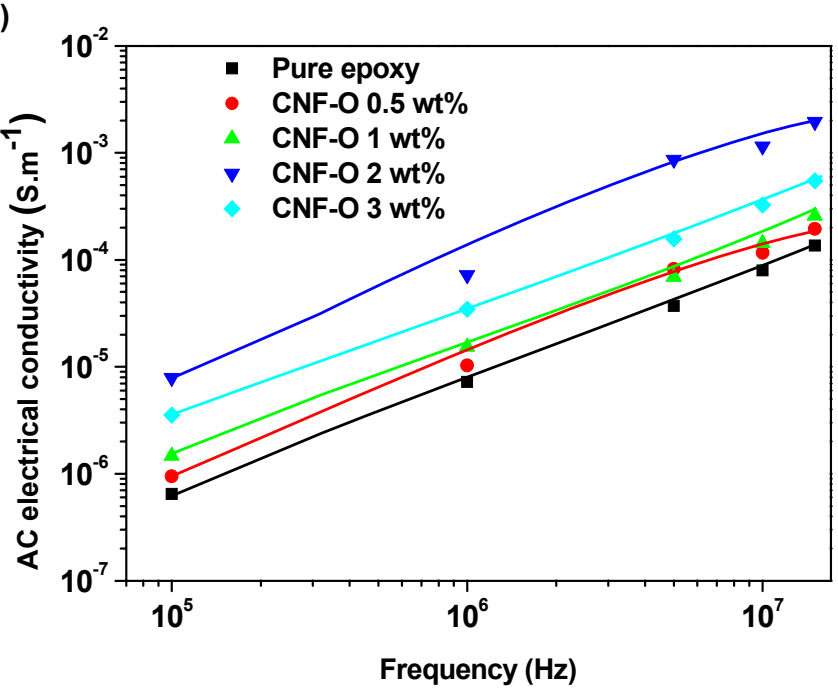
Pure epoxy
CNF-O 0.5 wt%
CNF-O 1 wt%
CNF-O 2 wt%
CNF-O 3 wt%
AC electrical conductivity (S.m-1)
Frequency (Hz)

b)

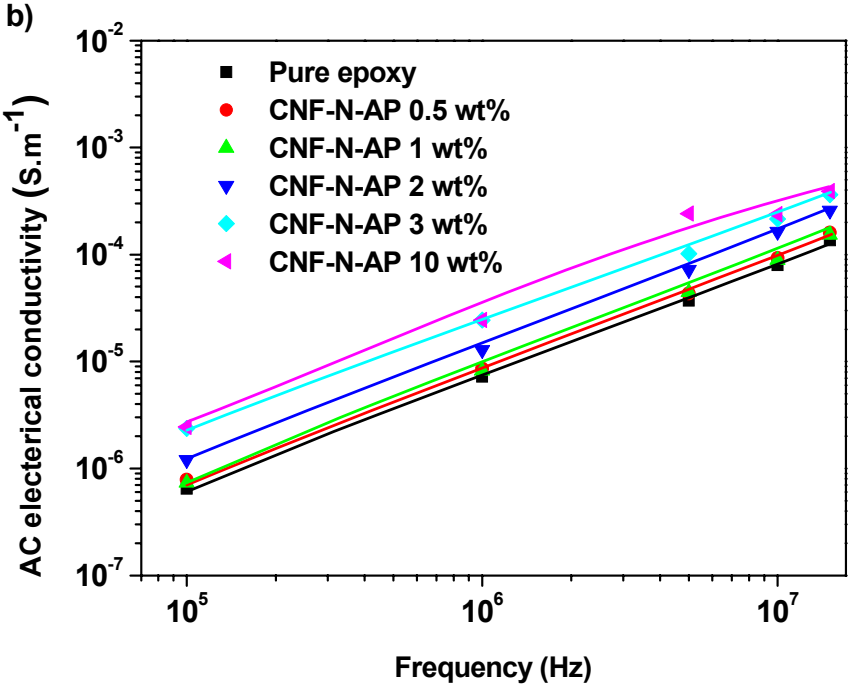
Pure epoxy
CNF-N-AP 0.5 wt%
CNF-N-AP 1 wt%
CNF-N-AP 2 wt%
CNF-N-AP 3 wt%
CNF-N-AP 10 wt%
AC electerical conductivity (S.m-1)
Frequency (Hz)

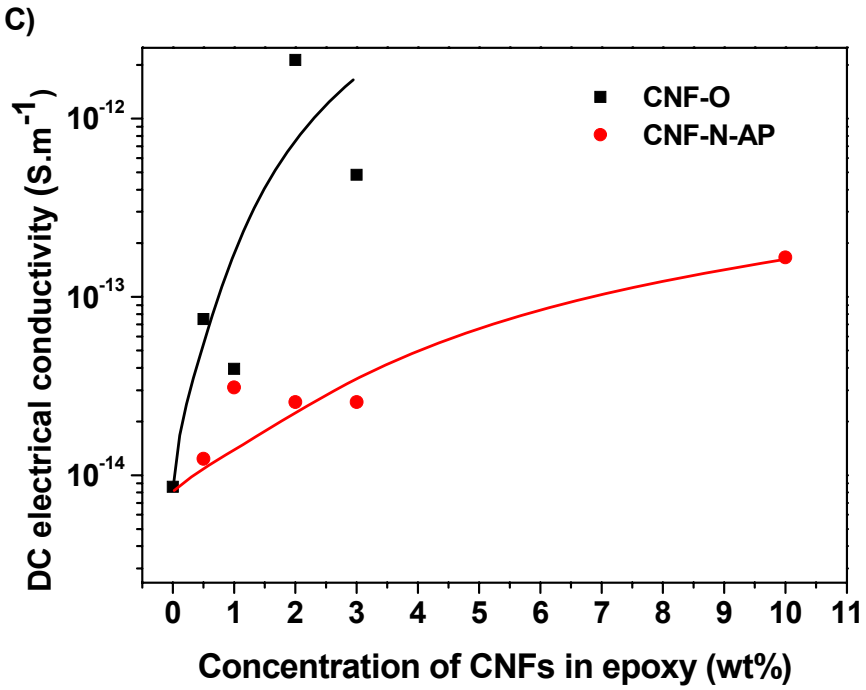

Figure 3.12 Dependence of the AC electrical conductivity on the frequency for a) CNF-O/epoxy composites and b) CNF-N-AP/epoxy composites; c) dependence of the DC electrical conductivity of epoxy composites on the weight concentration of CNFs.

3.3.3.3 Electrical conductivities of CNF-I-AP/epoxy composites

The AC electrical conductivity of CNF-I-AP/epoxy composites is lower than CNF-O/epoxy composites with the same CNF concentration at each measured frequency (Figure 3.13). Especially 10 wt% CNF-I-AP/epoxy composite still keep the electrical conductivity at a level comparable with 3 wt% CNF-O/epoxy composite. It indicates that the silane coating effectively diminishes the electrical conductivity of CNFs/epoxy composites.

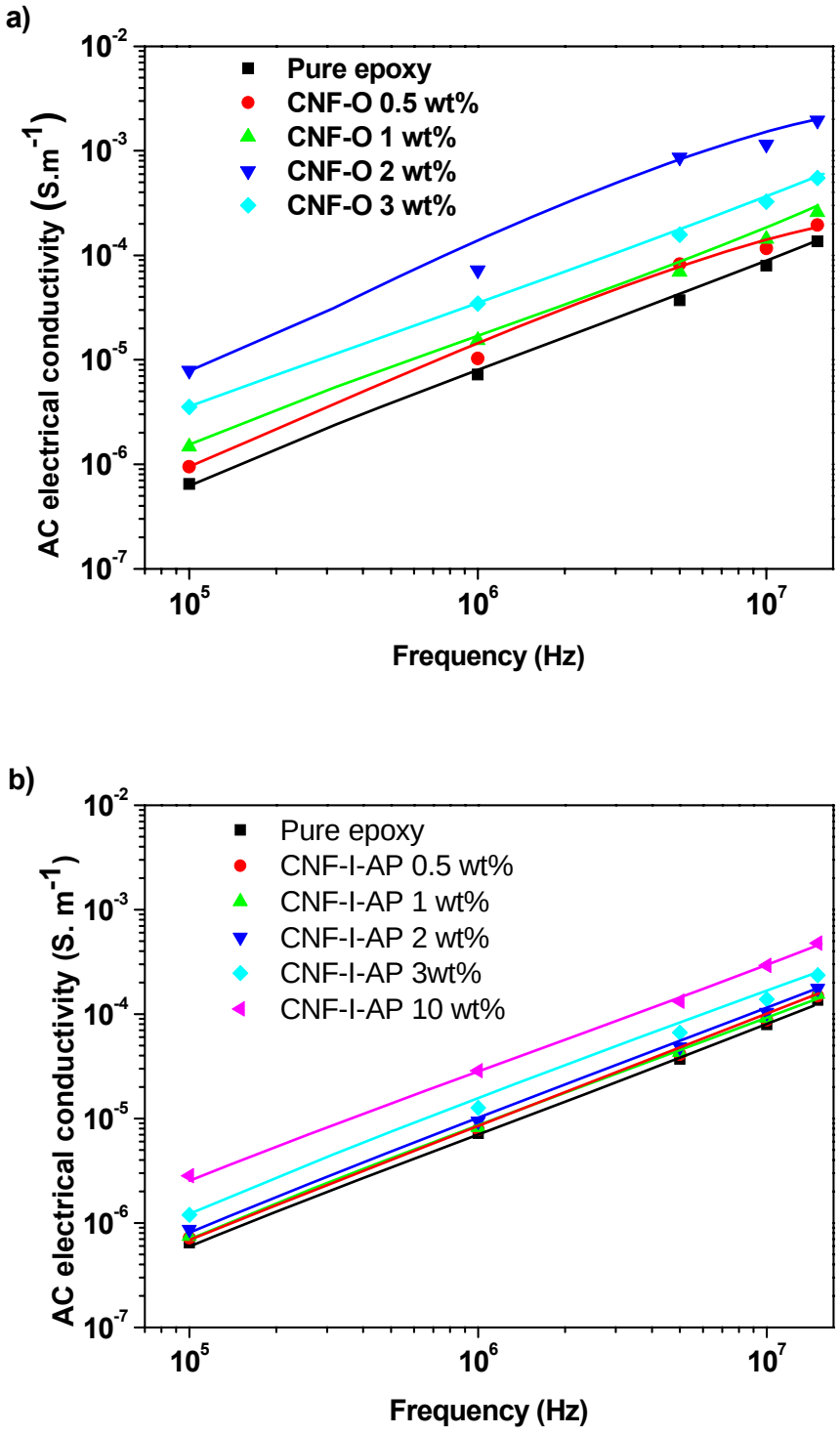

Figure 3.13 Dependence of the AC electrical conductivity on the frequency for a) CNF-I-AP/epoxy composites compared with that for b) CNF-O/epoxy composites.

3.3.3.4 Summary of the electrical conductivities

With the same CNF loading, all epoxy composites containing silanized CNFs possess an AC conductivity of about one order of magnitude lower than the original CNF-O/epoxy

composites in the measured frequency range. For aminosilane terminated CNFs (Figure 3.12 b and Figure 3.13 b), CNF-I-AP/epoxy composites showed comparable AC electrical conductivities with CNF-N-AP/epoxy composites up to 2 wt% CNF loading. But at 3 wt% loading, the conductivity was lower than the CNF-N-AP/epoxy composites, probably arising from the thicker insulating silane coating on the surface.

Measurements of the AC conductivity of CNF powder tablets also confirm that the surface modification decreases the electrical conductivity of silanized CNFs significantly compared to original CNFs in the frequency range of 20 - 10^6 Hz (Figure 3.14). CNF-O has a constant conductivity of about 830 $S \cdot m^{-1}$, about 7 times higher than CNF-GS (110 $S \cdot m^{-1}$), while CNF-N-AP and CNF-I-AP have conductivity of about 50 $S \cdot m^{-1}$ and 10 $S \cdot m^{-1}$ respectively. The silane coating is insulating; the polar functional groups from silanes result in higher repulsion among fibers and inhibit their direct contacts with each other. Thus a lower conductivity is observed for silanized CNFs than original CNFs. Here the electrical conductivity of CNFs is nearly independent on the frequency over a large range, but after reaching a certain frequency, the conductivity decreases due to skin effect induced by the high frequency AC electric field. This phenomenon was also observed in CNTs and can be explained by Drude model [146, 147].

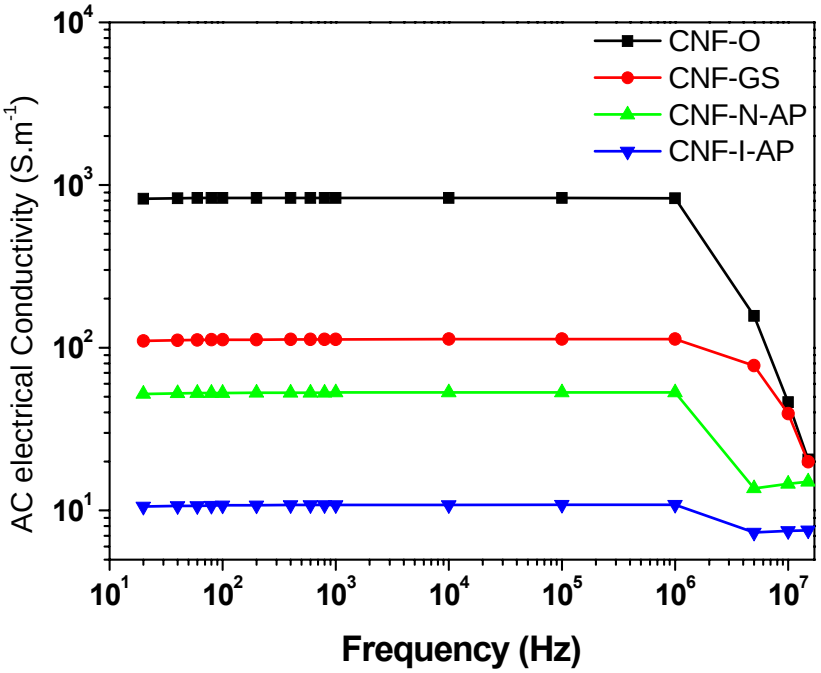

Figure 3.14 Dependence of the AC electrical conductivity of pure CNF powders on the frequency.

3.3.4 Thermal conductivities of CNFs/epoxy composites

3.3.4.1 Thermal conductivities of CNF-GS/epoxy composites

Silanized CNFs improved the thermal conductivity of epoxy composites better than original CNFs (Figure 3.15). However, the improvement seems to be disappointing (about 16 % for 2 wt% CNF loading) considering the superior thermal conductivity of CNFs (1950 $W \cdot m^{-1} \cdot K^{-1}$).

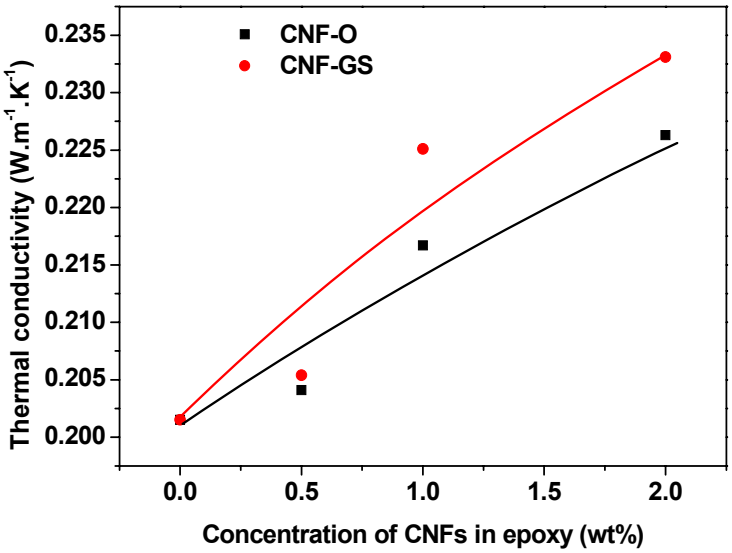

Figure 3.15 Dependence of the thermal conductivity on the weight concentration of CNFs for CNF-GS/epoxy composites compared with that for CNF-O/epoxy composites.

To understand the reason behind this behavior, the experimental data is compared with the theoretical simulation. The enhancement of the thermal conductivity both for original and silanized CNFs/epoxy composites versus the concentration of CNFs is shown in Figure 3.16. The increase of thermal conductivity of composites due to the infusion of highly thermal conductive fillers into a polymer matrix can be described by mixing formulas from Agari et al. as below [148], which is based on an assumption of a geometric mean

$$\log\lambda_C = v_{CNF} C_2 \log\lambda_{CNF} + (1 - v_{CNF}) \log(C_1 \lambda_{EP})$$

where λ_C is the thermal conductivity of the composite; λ_{EP} is the thermal conductivity of the pure epoxy polymer (according to our measurement, it is 0.2015 $W \cdot m^{-1} \cdot K^{-1}$); λ_{CNF} is the thermal conductivity of CNFs (according to different given values from literature, it is taken as 20 $W \cdot m^{-1} \cdot K^{-1}$ [69], 200 $W \cdot m^{-1} \cdot K^{-1}$ [149] and 2000 $W \cdot m^{-1} \cdot K^{-1}$ [150] respectively); v_{CNF} is the volume content of CNFs in the composite; C_1 is a coefficient which reflects the structure

of polymer; C_2 is a coefficient indicating the ease of fillers forming conductive paths in the matrix.

Based on the assumption from Agari, C_1 is 1 for carbon fibers in polymers. For the simulation in Figure 3.16, C_2 is also assumed to be 1. Although the dispersion state and surface modification is not regarded, Figure 3.16 shows that a theoretical fitting closest to the experimental data is obtained with the λ_{CNF} value of 2000 $W \cdot m^{-1} \cdot K^{-1}$. The experimental data are higher than the theoretical values due to the assumption of $C_2 = 1$. The real dispersion state and the aspect ratio of CNFs can make the value of $C_2 > 1$, which will increase the theoretical thermal conductivity. The experimental thermal conductivity increases from 0.2015 $W \cdot m^{-1} \cdot K^{-1}$ for the pure epoxy polymer to 0.2331 $W \cdot m^{-1} \cdot K^{-1}$ for 2 wt% CNF-GS/epoxy composites, an enhancement of 16 %, higher than that of the 2 wt% CNF-O/epoxy composites (12 %). These results indicate that the surface silanization of CNFs, instead of decreasing the thermal conductivity of composites due to more phonon scattering as reported by other researchers [151], enhances the thermal conductivity because of better dispersion of CNFs in the matrix and improved interfacial adhesion between fibers and the epoxy polymer [152]. The silane coating on CNF surface may introduce more phonon scattering centers which can increase the interfacial thermal resistance, but the better CNF dispersion and interfacial interaction between fillers and matrices facilitate the heat transport. At low concentration, the effect of the CNF dispersion and the interfacial adhesion dominates; at high concentration, the influence of phonon scattering prevails. Thus the 3 wt% CNF-GS/epoxy composite has lower thermal conductivity than the composite with 2 wt% CNF-GS, resulting from more phonon scattering centers and filler aggregations at higher concentration.

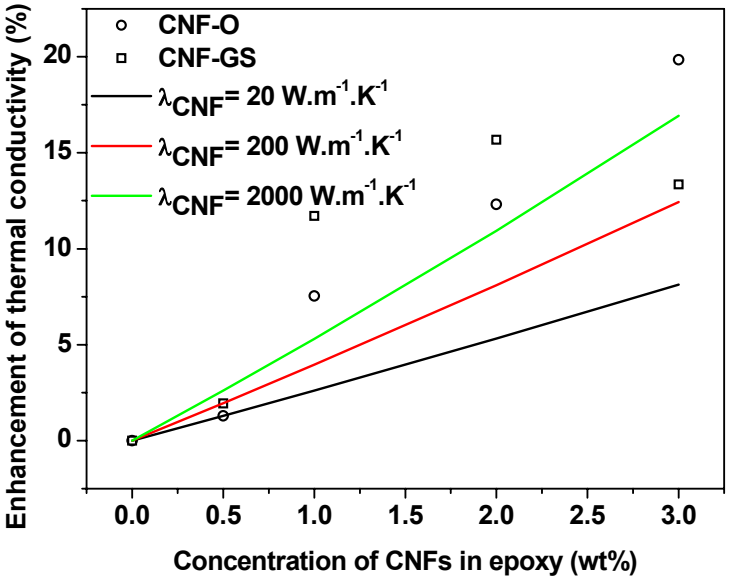

Figure 3.16 Enhancement of the thermal conductivity compared to the pure epoxy polymer as a function of CNF loading. The empty circles represent the thermal conductivity enhancement of composites containing original CNFs (CNF-O); the empty squares represent the thermal conductivity enhancement of composites containing silanized CNFs (CNF-GS); straight lines are fitted values based on Agari model.

3.3.4.2 Thermal conductivities of CNF-N-AP/epoxy composites

The thermal conductivity of aminosilanized CNFs/epoxy composites remains at a satisfactory level (Figure 3.17). Thermal conductivity of epoxy composites depends on the aspect ratio, thermal conductivity, dispersion of CNFs and interfacial thermal resistance between CNFs and epoxy [153]. Although the silanization may increase the interfacial thermal resistance due to more phonon scattering centers caused by the amorphous silanes, the modification facilitates the dispersion of CNFs and interfacial heat transport [152]. As a result, the thermal conductivity of CNF-N-AP/epoxy composites still remains at a comparable or even higher value than the original CNF-O/epoxy composites.

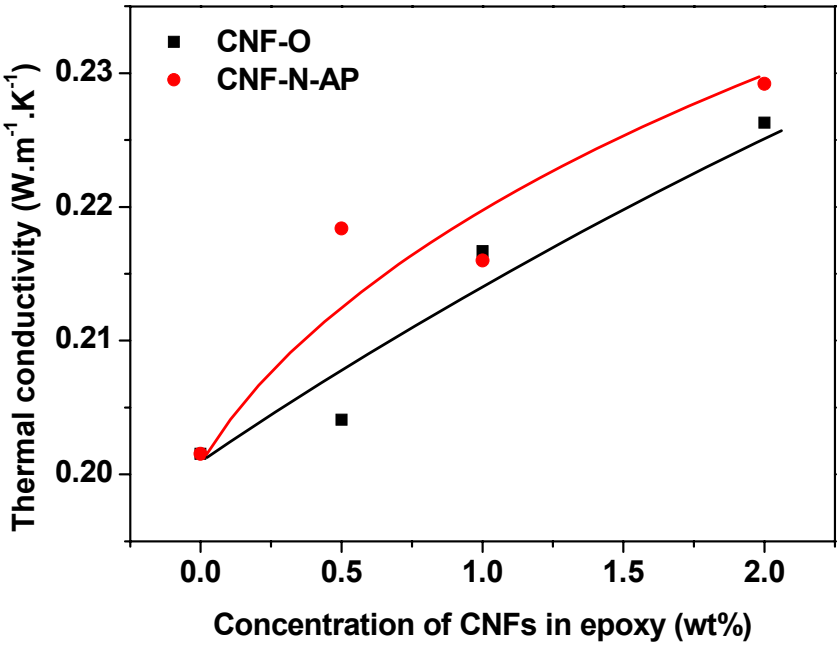

Figure 3.17 Dependence of the thermal conductivity on the weight concentration of CNFs for CNF-N-AP/epoxy composites compared with that for CNF-O/epoxy composites.

3.3.4.3 Thermal conductivities of CNF-I-AP/epoxy composites

The introduction of CNF-I-AP into the epoxy polymer increases the thermal conductivity of composites (Figure 3.18). However, compared to the original CNFs (CNF-O), the enhancement is lower for composites containing CNF-I-AP, which differs from the previous silanizations (CNF-GS and CNF-N-AP), demonstrating better improvements of the thermal conductivity of composites than CNF-O. Considering that the pure CNF-I-AP powder has a much lower AC electrical conductivity than CNF-GS and CNF-N-AP (Figure 3.14) and a relatively higher silicon content (3.4 wt%) calculated from TGA measurements compared to the other two modifications (CNF-GS, 1.1 wt% and CNF-N-AP, 0.6 wt%), the lower thermal conductivity is probably due to the thicker silane layer on the surface, which scatters more phonons and thus hinders the heat transport.

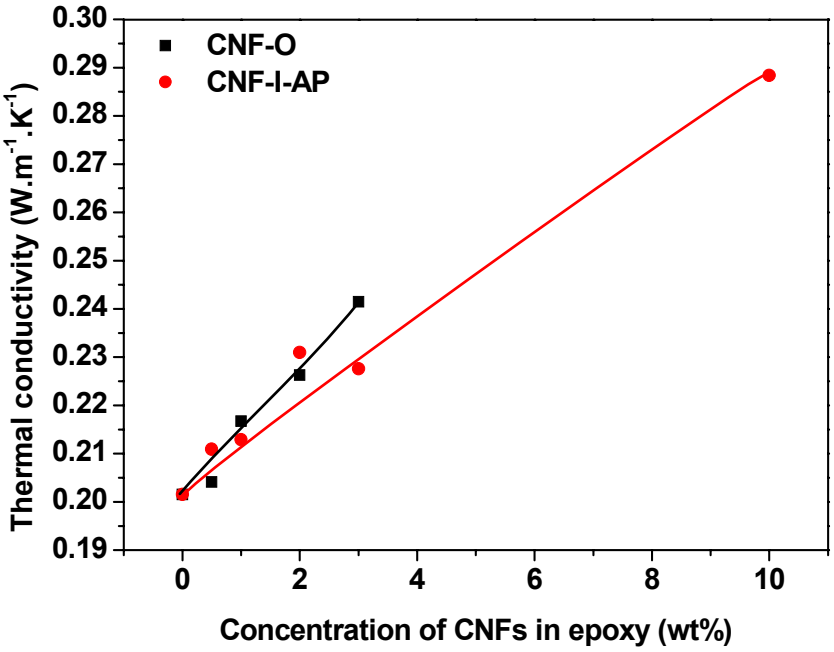

Figure 3.18 Dependence of the thermal conductivity on the weight concentration of CNFs for CNF-I-AP/epoxy composites compared with that for CNF-O/epoxy composites.

3.3.4.4 Summary of the thermal conductivities

Thermal conductivity of composites increased with the CNF loading. It depended on many factors such as aspect ratio, thermal conductivity and dispersion of CNFs, and interfacial thermal resistance between CNFs and epoxy polymer. On one hand, the silanization with glycidoxysilane (CNF-GS) and aminosilane (CNF-N-AP) probably introduced bigger interfacial thermal resistance due to more scattering centers from the surface functional groups; on the other hand, the modification improved interfacial heat transport because of the covalent bonds between fillers and polymer matrices. The predominant effect from the latter resulted in a higher thermal conductivity of silanized CNF/epoxy composites than that of original CNF-O/epoxy composites with the same CNF loading. However, the thermal conductivity of CNF-I-AP/epoxy composites was lower than that of the original CNFs/epoxy composites, which was attributed to the more phonon scattering centers from thicker silane coating.

3.3.5 Electrical conductivities of MWCNTs/epoxy composites

Macroscopic composites with anisotropy were prepared to investigate the influence of MWCNT silanization on the properties of composites.

As shown in Figure 3.19, the electrical conductivity of MWCNTs/epoxy composites demonstrates the typical behavior as a dielectric material - the conductivity increases linearly with the frequency in the high frequency range [133]. Compared to unaligned MWCNT/epoxy composites, unaligned MWCNT-PMH-N-AP/epoxy composites show about 100 times lower electrical conductivity at 400 Hz, which indicates that the insulating silane coating on the CNT surface hinders the electron transport in CNTs and thus the electrical conductivity of composites. In addition, the electrical conductivity in the direction parallel to the electric field is always higher than that across the electric field for both pristine and silanized CNTs/epoxy composites, demonstrating an anisotropic electrical property. This phenomenon is especially apparent in composites containing MWCNT-PMH-N-AP.

At frequency 1×10^{5} Hz, the 0.5 wt% unaligned MWCNT/epoxy composite has a conductivity of 1.9×10^{-5} $S\cdot m^{-1}$; the 0.5 wt% unaligned MWCNT-PMH-N-AP/epoxy composite possesses a conductivity of 8.0×10^{-7} $S\cdot m^{-1}$, 23 times lower than the former. At the same frequency, the conductivity of 0.5 wt% CNF-O/epoxy composite is 9.4×10^{-7} $S\cdot m^{-1}$ and that of 0.5 wt% CNF-N-AP/epoxy composite is 7.9×10^{-7} $S\cdot m^{-1}$, with a decrease of only 16 % than the former (Figure 3.12). Therefore with the same filler loading, pristine MWCNTs/epoxy composites are more conductive than original CNFs/epoxy composites; the same silanization has greater effects on the electrical conductivity of composites with MWCNTs than with CNFs.

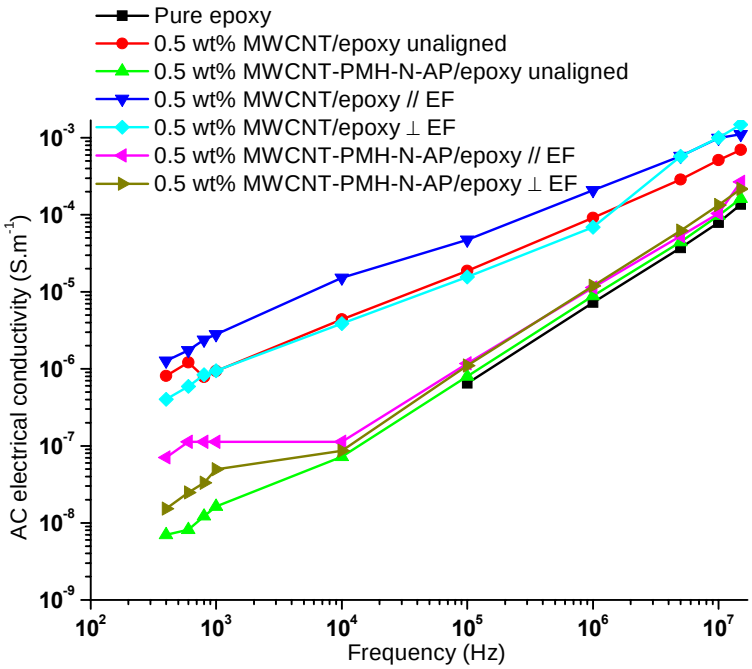

Figure 3.19 Dependence of AC electrical conductivity on frequency for MWCNTs/epoxy composites.

3.4 Summary

Physical properties such as mechanical properties, electrical conductivity and thermal conductivity of epoxy composites containing either original or silanized CNFs were measured. Silanization with glycidoxysilane improved the storage modulus of epoxy composites; however, the glass transition temperature of composites was lower than the pure epoxy polymer. The non-stoichiometric ratio between hardner and epoxy resin arising from the excessive epoxy groups introduced on CNF-GS resulted in a lower crosslinking density of the polymer and thus the decreased glass transition temperature. The electrical conductivity of CNF-GS/epoxy composites was lower than the original CNF-O/epoxy composites, but the thermal conductivity of CNF-GS/epoxy was higher than CNF-O/epoxy composites. The DC electrical conductivity increased with CNF loading, with some exceptions at higher CNF concentration due to unavoidable aggregates of both CNF-O and CNF-GS. The tensile strength of CNF-N-AP/epoxy and CNF-I-AP/epoxy composites remained at a relatively high value as the pure epoxy polymer, while the CNF-O/epoxy composites showed lower mechanical strength than the pure epoxy polymer. At the same frequency, the AC electrical conductivity of CNF-N-AP/epoxy composites was one order of magnitude lower than CNF-O/epoxy composites with the same CNF loading. The DC conductivity of CNF-N-AP/epoxy composites was significantly lower than CNF-O/epoxy composites with the same CNF loading. The thermal conductivity of CNF-N-AP/epoxy composites was higher than CNF-O/epoxy composites with the same CNF loading. The functional groups on CNFs brought more phonon scattering centers, which increased the interfacial thermal resistance; in contrast, the possible covalent bonds between CNFs and epoxy polymer improved the interfacial heat transport. Both factors took into effect and from the results of thermal conductivities, it was concluded that the latter was the dominant role determining the thermal property of composites with CNF-GS or CNF-N-AP. The AC electrical conductivity of CNF-I-AP/epoxy composites was also lower than that of CNF-O/epoxy composites. It was unexpected that the silanized CNF-I-AP/epoxy composites showed a lower thermal conductivity than CNF-O/epoxy composites. The reason could be that the amorphous silane coating scattered more phonons, which drastically increased the interfacial thermal resistance. Anisotropic MWCNT/epoxy composites were prepared by electrical alignment of MWCNTs in epoxy resin and further in situ curation. The direction parallel to the electric field had always higher conductivity than the direction across the electric field for both pristine MWCNT/epoxy composites and silanized MWCNT-PMH-N-AP/epoxy composites.

4 Conclusion and discussion

4.1 Conclusion of the experimental results

Surface silanization was carried out on oxidized CNFs to bridge the nanofiller with the epoxy polymer matrix. In order to do that, different oxidation methods were carried out on CNFs to find the optimal condition for the introduction of carboxyl groups on the graphitic surface. According to IR spectra, except for the oxidation in the mixture of $KMnO_4/H_2SO_4$ under bath sonication (CNF-PMS), the other three oxidation methods, including in the mixture of concentrated H_2SO_4/HNO_3 under bath sonication (CNF-AS), in the mixture of concentrated H_2SO_4/HNO_3 under heating treatment (CNF-AH) and in the mixture of $KMnO_4/H_2SO_4$ under heating treatment (CNF-PMH), were effective to introduce carboxyl groups on CNFs. XPS analysis demonstrated that the relative percentage of carboxyl groups on CNF surface was quite low (5 - 9 %), consistent with the results from other researchers. In addition, the oxidation method with acid mixture under bath sonication (CNF-AS) kept the greatest ratio of C-C sp^2 hybridization to C-H sp^3 hybridization. The SEM pictures gave a direct impression that CNF-AS kept the largest aspect ratio. Considering the Raman result that the graphitization of CNF-AS remained in a large extent compared to original CNFs (CNF-O), bath sonication of CNFs in the mixture of concentrated H_2SO_4/HNO_3 was chosen as the optimal method to oxidize CNFs in the experiments.

In the silanization process with 3-glycidoxypropyltrimethoxysilane, the oxidized CNFs reacted with the silanes at refluxing condition (CNF-GS). The chemical functional groups were characterized by IR, and the existence of Si on CNFs was verified by XPS and EDX. XPS Si 2p peak fitting also confirmed the covalent bonding between CNFs and silanes. The bulk concentration of Si was calculated based on TGA results. Raman spectra showed that the silanization introduced small disturbances of the surface graphitic structures on CNFs.

Due to the small amount of Si detectable in XPS and TGA for CNF-GS, another silanization based on the reaction between the alcoholic hydroxyl group and 3-aminopropyltrimethoxysilane was carried out to improve the yield of silanization. Carboxyl groups on oxidized CNFs were first reduced into alcoholic hydroxyl groups by the combination of $NaBH_4$ and I_2; then CNFs terminated with alcoholic hydroxyl groups covalently reacted with the aminosilane (CNF-N-AP). IR measurements confirmed the existence of functional groups on CNFs after each chemical treatment. However, the silane

content detected from TGA and XPS analysis was still under expectation. TGA showed lower bulk content of Si in CNF-N-AP than that in CNF-GS, but XPS indicated a higher surface concentration of Si in CNF-N-AP than that in CNF-GS. Therefore it was assumed that the silanization with 3-glycidoxypropyltrimethoxysilane took place mainly at the open ends of the CNFs, while the silanization with 3-aminopropyltrimethoxysilane occurred on the sidewalls of CNFs. The interaction between CNFs and silanes was mainly through the covalent bonding instead of the physical adsorption based on the Si 2p peak fitting in XPS analysis. Raman spectra indicated that the reduction procedure before silanization increased the graphitization of CNFs. The change of IEP of CNFs in streaming potential measurements provided an additional evidence for the silanization.

To further increase the Si content on CNFs, the silanization procedure with two-silanes was performed. First 3-isocyanatopropyltriethoxysilane reacted with the carboxyl groups on oxidized CNFs at RT due to the readiness of isocyanate groups to covalently bond with carboxyl groups (CNF-I); then 3-aminopropyltrimethoxysilane condensed on CNF-I and reacted again with the carboxyl groups on the surface for the second silanization (CNF-I-AP). IR spectra verified the first silanization. After the second silanization, the silicon content increased significantly based on TGA and XPS analysis. XPS Si 2p peak fitting confirmed the covalent bonds between silanes and CNFs for the both silanizations. Raman spectra indicated that the graphitization of CNFs before and after silanizations was constant, consistent with the XRD results, which demonstrated that the crystalline size and the interlayer space of CNFs remained unchanged in the two-silanization treatment. Streaming potential measurements showed a higher IEP of CNF-I-AP than CNF-N-AP due to more amine groups on the surface.

In order to compare the effect of the same silanization on CNFs and MWCNTs, the silanization with 3-aminopropyltrimethoxysilane was transferred onto MWCNTs. The oxidation of MWCNTs was done by a mild oxidation in the mixture of potassium permanganate and dilute sulfuric acid under heating treatment instead of in the mixture of concentrated sulfuric acid and nitric acid under bath sonication in order to preserve as much graphitization as possible for MWCNTs. IR spectra confirmed the appearance of carboxyl groups and Raman spectra demonstrated the constant graphitization after the oxidation. The effective reduction from carboxyl groups to alcoholic hydroxyl groups was verified by IR spectra. The detection of Si in XPS confirmed the silanization. However, different from the aminosilanization of CNFs (CNF-N-AP), in which the covalent bonding between silanol groups from hydrolyzed silanes and hydroxyl groups from CNFs was the main reaction

mechanism, the physical adsorption or the amide bonding between amine groups in silanes and carboxyl groups on CNFs was the possible silanization mechanism for silanized MWCNTs (MWCNT-PMH-N-AP). The chemical derivatization with TFAA was used to quantify the surface C-OH groups after the reduction process (MWCNT-PMH-N). It was found that the relative percentage of C-OH groups was quite low. MWCNT-PMH-N-AP was derivatized with TFBA to get quantitative information about the C-NH_2 groups on the surface. Most nitrogen existed as protonated amine or amide groups rather than primary amine (NH_2) on silanized MWCNTs. The silanization had no effects on the graphitization of MWCNTs based on Raman spectra.

The original and silanized CNFs or MWCNTs were then embedded into epoxy polymer to investigate their influence on the physical properties of epoxy composites.

The morphology of the fracture surface of CNFs/epoxy composites was characterized by SEM. The original CNF-O/epoxy composites always showed great aggregates. Moreover, the incapability to prepare 10 wt% CNF-O/epoxy composites due to high viscosity and unavoidable voids in the composites demonstrated that original CNFs with very low surface energy were difficult to be wetted by the epoxy resin with a relatively higher surface energy. In contrast, silanization enhanced the surface energy of CNFs due to organic functional groups on the surface, which improved the compatibility of fibers with matrices and thus the wetting behavior of epoxy on fibers. For CNF-GS/epoxy composites with small CNF loading, CNFs distributed uniformly in the epoxy matrix; but at high concentration the dispersion of CNFs was still unsatisfactory because of great agglomeration. CNF-N-AP/epoxy composites and CNF-I-AP/epoxy composites also demonstrated better distribution of CNFs compared to original CNF-O/epoxy composites with the same CNF loading. Therefore, all three silanization procedures improved the dispersion and distribution of CNFs in the matrix. Furthermore, the fracture surface of epoxy composites from SEM showed less pulling out of silanized CNFs from the matrix than that of original CNFs, which proved that the silanized CNFs had stronger interfacial force with the matrix.

Dynamical mechanical analysis of CNF-GS/epoxy composites was performed to evaluate the reinforcement role of CNFs on the epoxy polymer. The storage modulus of CNF-GS/epoxy composites was about 20 % higher than that of the pure polymer, while CNF-O/epoxy composites had a lower storage modulus than the pure epoxy polymer. However, due to the excessive epoxy groups on CNF-GS, which broke the supposed stoichiometric ratio between hardener and epoxy resin and thus lowered the crosslinking density of the epoxy polymer, the

glass transition temperature of CNF-GS/epoxy composites was lower compared to the pure epoxy polymer. Tensile testing of CNF-N-AP/epoxy composites and CNF-I-AP/epoxy composites showed better results than that of CNF-O/epoxy composites. Therefore, the mechanical properties of CNF-GS/epoxy, CNF-N-AP/epoxy and CNF-I-AP/epoxy composites were improved due to the better interfacial adhesion between fillers and epoxy matrices.

Both DC and AC electrical conductivities of CNFs/epoxy composites were measured to investigate the effect of the silanization on the electron transport of composites. AC conductivity of CNF-GS/epoxy composites was always lower than that of CNF-O/epoxy composites with the same CNF loading at certain frequency. The DC electrical conductivity of 2 wt% CNF-GS/epoxy composite was 50 times lower than that of CNF-O/epoxy composite. The electrical conductivity of composites increased with the CNF loading except at high concentration with the agglomeration of CNFs. The AC conductivity of CNF-N-AP/epoxy composites was almost one order of magnitude lower than the CNF-O/epoxy composites with the same concentration. Measurements of the DC conductivity also confirmed that the aminosilane coating on CNFs diminished the conductivity of epoxy composites. The AC conductivity of CNF-I-AP/epoxy composites showed the similar tendency as that of CNF-N-AP/epoxy composites, but with a smaller electrical conductivity at 3 wt% loading compared to the CNF-N-AP/epoxy composite because of the thicker silane coating on the surface. In order to find the reason why silanized CNFs/epoxy composites possessed lower conductivities than original CNF-O/epoxy composites, the AC conductivity of pure CNF powders was measured. It was found that in the frequency range of 20 – 10^6 Hz, CNF-GS had a conductivity of 7 times lower than CNF-O; for CNF-N-AP, its conductivity was 16 times smaller than CNF-O; the conductivity of CNF-I-AP was about 80 times lower than CNF-O. The lower was the conductivity of pure CNF powders; the more organic silanes were on CNFs, which hindered the direct contact of conductive CNFs and accordingly decreased the electrical conductivity. It coincided well with the XPS analysis, which demonstrated that CNF-GS contained least Si element on the surface, while CNF-I-AP the most and CNF-N-AP in the middle.

The thermal conductivity of composites containing CNF-GS or CNF-N-AP was higher than those containing original CNFs, but the results were far below expectation. The main reason for the moderate improvement of the thermal conductivity was attributed to the great interfacial resistance between CNFs and polymer matrices. The silanization could decrease

the interfacial thermal resistance by bridging fillers and matrices through covalent bonds, but the organic silanes on the CNF surface introduced more phonon scattering centers at the interface, which would increase the interfacial thermal resistance. The thermal conductivity of CNF-GS/epoxy and CNF-N-AP/epoxy composites was still higher than CNF-O/epoxy composites, suggesting that the former factor dominated. However, the thermal conductivity of CNF-I-AP/epoxy composites was lower than CNF-O/epoxy composites, probably because the thicker silane coating on CNF-I-AP introduced many more phonon scattering centers and consequently increased the interfacial thermal resistance tremendously.

Anisotropic composites in centimeter scale were obtained by the alignment of MWCNTs in the epoxy resin under AC electric field. It provided the possibility to measure their electrical conductivities macroscopically. The electrical conductivity of MWCNTs/epoxy composites was higher in the direction parallel to the electric field than across the electric field. At the same filler loading, composites with pristine MWCNTs had higher electrical conductivity than those with original CNFs. The silanization of MWCNTs changed the electrical conductivity of composites in a greater degree than that of CNFs.

4.2 Overall discussion

With regard to the performed chemical treatments and the obtained results, there are still some open questions to debate:

- What was the reason for the low silicon content on silanized CNFs?

  Different procedures were carried out on CNFs to increase the silane content on CNFs. However, the amount of silane was still small due to the inertness of carbon double bonds. The carbon double bond consists of one σ bond, which is formed by the overlapping of two sp^2 hybridized orbitals, and one π bond, which originates from the overlapping of two 2p orbitals. It is more difficult to open a carbon double bond than a single bond due to its higher strength. Furthermore, the carbon atoms in graphitic CNFs or CNTs arrange in a hexagonal lattice resembling the structure of a conjugated aromatic ring. The π electrons are highly delocalized and conjugate with each other in the ring, which results in a very high resistivity against chemical treatments. Therefore, the surface oxidation and the further silanization take place only in a low degree.

- Why was it impossible to observe the percolation behavior of the electrical conductivity?

  From SEM pictures, it was apparent that the silanization improves the distribution and dispersion of CNFs in the composites. However, there were always aggregates of pristine and silanized CNFs in the bulk matrix, which hindered the formation of conductive networks in composites. Due to those unavoidable agglomerations of nanofillers in a macroscopic scale, the percolation phenomenon was not visible in the experiments.

- Why was the thermal conductivity of composites still low with the addition of silanized CNFs?

  The improvement of the thermal conductivity of CNFs/epoxy composites was relatively small with the consideration of the good heat transport of CNFs. The thermal conductivity of composites is affected greatly by the interfacial thermal resistance. The frequency of phonons in the matrix and fillers mismatches each other, resulting in a great interfacial thermal resistance inhibiting the heat transport. The phonon scattering on fillers also contributes to the interfacial thermal resistance. Though the silanization of CNFs improves the adhesion between fillers and epoxy polymer, which facilitates the heat transport, the enhancement is limited compared to the huge interfacial thermal resistance.

Further discussions about the answers to questions in section 1.5:

- Is it possible to distinguish the chemical silanization from the physical adsorption of silanes on carbon nanofillers?

  From the Si 2p peak fitting in XPS, the chemical silanization can be distinguished from the physical adsorption of silanes. And the amount of functional groups is also semi-quantified from XPS C 1s peak deconvolution. Silanes used in this work were alkoxysilanes, which readily hydrolyzed into silanols in ethanol solution with trace amount of water. If silanols physically adsorb onto the carbon nanofillers, only the peak attributed to the Si-O-Si groups should be apparent. When silanol groups in the hydrolyzed silanes further covalently react with hydroxyl groups on CNFs, the peak corresponding to Si-O-C groups will be visible. For CNF-GS and CNF-N-AP, the predominant chemical state of Si was the Si-O-C moiety. In the case of the two-silanization treatment, the reaction took place through amide linkage in the first silanization (CNF-I), therefore the Si in CNF-I existed as Si-O-C state; during the second silanization, hydrolyzed APTMS reacted further with the carboxyl group on CNF-I to form the Si-O-C group.

- Will the graphitic structure of CNFs or CNTs be damaged due to modification processes?

  According to XPS C 1s peak deconvolution, it is found that the strong acid oxidation has no effect on the ratio of carbon sp^2 to sp^3 hybridization, suggesting that the surface graphitic structure is not damaged. Silanization process introduces amorphous organic functional groups on the surface, which may affect the graphitic structure. Raman spectra showed that the ratio of the intensity of G band over D band (I_G/I_D) was relatively constant before (CNF-O, 1.39) and after the oxidation treatment (CNF-AS, 1.37). After different silanizations, CNF-GS had lower I_G/I_D (1.27) than CNF-O; CNF-N-AP had higher I_G/I_D (1.57) than CNF-O; while CNF-I-AP had an I_G/I_D value (1.40) comparable with CNF-AS. Therefore, the graphitic structures of CNFs remain mostly intact with only minor disturbances on the uppermost surface (thinner than 10 nm), which is also verified from the change of the ratio of carbon sp^2 to sp^3 hybridization in XPS analysis.

- What's the effect of silanizations on the properties of carbon nanofillers?

  The necessary oxidation treatment of CNFs or CNTs before silanization cuts some of the nanofillers into short ones, diminishing their aspect ratio, which as a result may influence

their physical properties. The silanization processes introduce insulating silanes onto the surface of carbon nanofillers, which decrease the intrinsic electrical conductivity of the graphitic carbon nanofillers. Depending on the amount of silanes on the surface, the electrical conductivity of silanized CNFs can be reduced up to 80-fold than that of the original CNFs. The surface wrapping of organic silanes brings more phonon scattering centers for heat transport, which may decrease the thermal conductivity of nanofillers. However, the surface modification improves the wetting property of fillers and consequently the dispersion and distribution of fillers in the epoxy matrix.

- Is it successful to alter the properties of CNFs/epoxy or CNTs/epoxy composites through silanization?

  Silanizations of CNFs improve mechanical properties of the epoxy composites compared to the original CNF-O. CNF-GS demonstrates a reinforcing role for the mechanical property of epoxy composites, while CNF-N-AP and CNF-I-AP are effective to hinder the deterioration of the tensile strength of CNFs/epoxy composites. The amount of surface silanes on the fillers determines the electrical conductivity of corresponding epoxy composites. The thicker is the silane coating on fillers; the lower is the electrical conductivity of the filler/epoxy composite. In addition, the silanization of nanofillers can facilitate the interfacial heat transport through the improved adhesion between fillers and matrices. Therefore the enhancement of the thermal conductivity of silanized CNFs/epoxy composites is greater than that of the original CNFs/epoxy composites with the exception of CNF-I-AP/epoxy composites. Because the amount of amorphous silanes on CNF-I-AP is much higher than other silanizations (CNF-GS and CNF-N-AP), the phonon scattering by those amorphous functional groups increases the interfacial thermal resistance between fillers and matrices greatly and thus compromises the thermal conductivity of composites. The electrical conductivity of MWCNTs/epoxy composites is also decreased through the surface silanization.

- What are the different effects of CNFs and CNTs on the properties of epoxy composites?

  Due to the smaller diameter and higher graphitization of CNTs, the composites with pristine MWCNTs at the same filler loading have higher electrical conductivity than CNF-O/epoxy composites. But the electrical conductivity decreased more significantly for aminosilanized MWCNTs/epoxy composites than for aminosilanized CNFs/epoxy composites compared to their unmodified counterparts. At 0.5 wt% filler loading, the composite containing silanized MWCNTs showed an AC electrical conductivity 23 times

lower than that with unmodified MWCNTs at the frequency of 1×10^5 Hz; while the same silanized CNFs/epoxy composites indicated only 16 % decrease of electrical conductivity compared to original CNF/epoxy composites. Due to the higher aspect ratio of MWCNTs than CNFs, MWCNTs possess better physical properties. However, the properties of MWCNTs are affected in a larger extent than CNFs by the silanization. It seems that MWCNTs have higher sensitivity to the silanization procedure than CNFs, which also leads to a remarkable difference in the properties of resultant composites.

- What's the relationship between properties and structures of epoxy composites containing CNFs or CNTs?

  The physical property of epoxy composites containing carbon nanofillers such as CNFs or CNTs is alterable through the change of the surface chemistry of the fillers. It is found that the silanization process improves the distribution and dispersion of fillers in the polymer matrices. Meanwhile, the covalent linkage between silanes on the filler surface and polymer matrices ensures the efficient mechanical load transfer from matrices to fillers, which improves the mechanical properties of composites.

  Figure 4.1 demonstrates the possible reactions among glycidoxysilanized CNFs (CNF-GS), the hardener and the epoxy resin. The amine group at one end of the hardener reacts with one oxirane ring from the epoxy resin and the amine moiety at the other end links with the epoxy group on CNF-GS. The resultant secondary amine groups further react with the epoxy rings from the resin. The reaction continues and finally forms a crosslinking network of the epoxy polymer with CNF embedded inside.

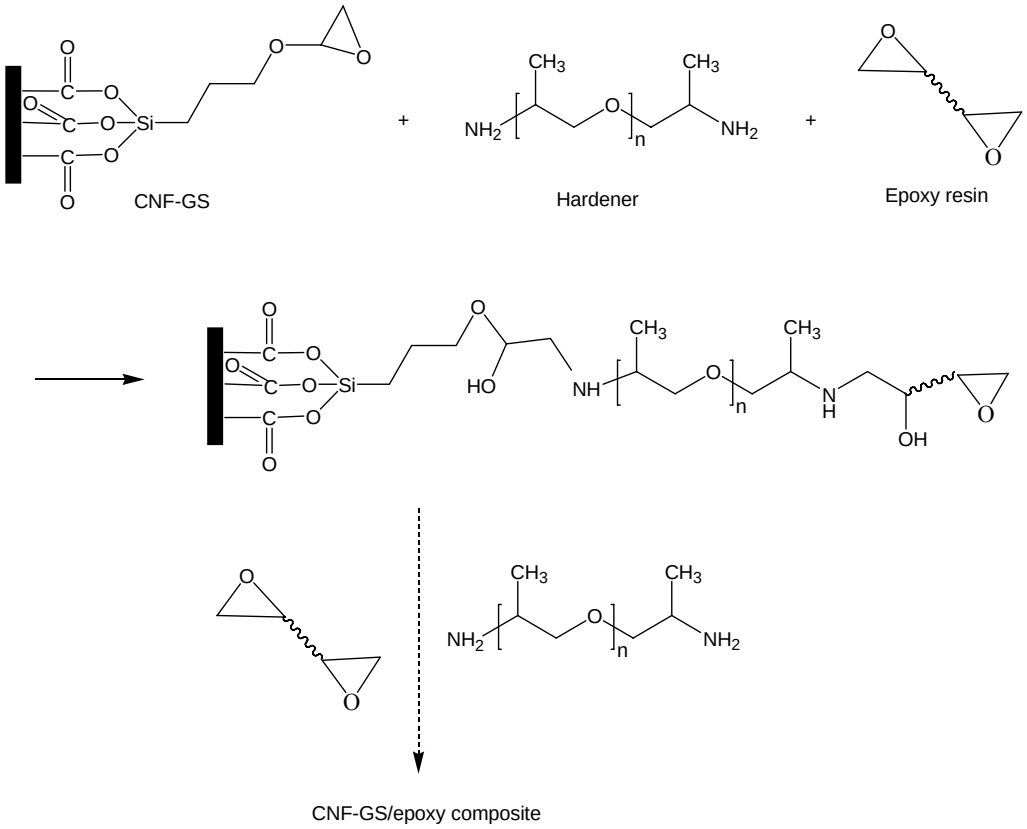

Figure 4.1 Possible reactions among CNF-GS, epoxy resin and hardener.

Figure 4.2 shows the probable reactions among aminosilanized CNFs (CNF-N-AP), the epoxy resin and the hardener. First the primary amine group on CNF-N-AP reacts with the epoxy ring from the resin and the resultant secondary amine continues to bond with the resin until no active hydrogen exists. The hardener also reacts with the epoxy resin, which crosslinks the liquid resin into the solid polymer. Finally a crosslinked network of the epoxy polymer embedded with CNF-N-AP will be constructed. Since CNF-I-AP has a surface terminated with aminosilanes, the possible reactions between CNF-I-AP and the resin will resemble those in the sample CNF-N-AP, which is not repeatedly plotted here.

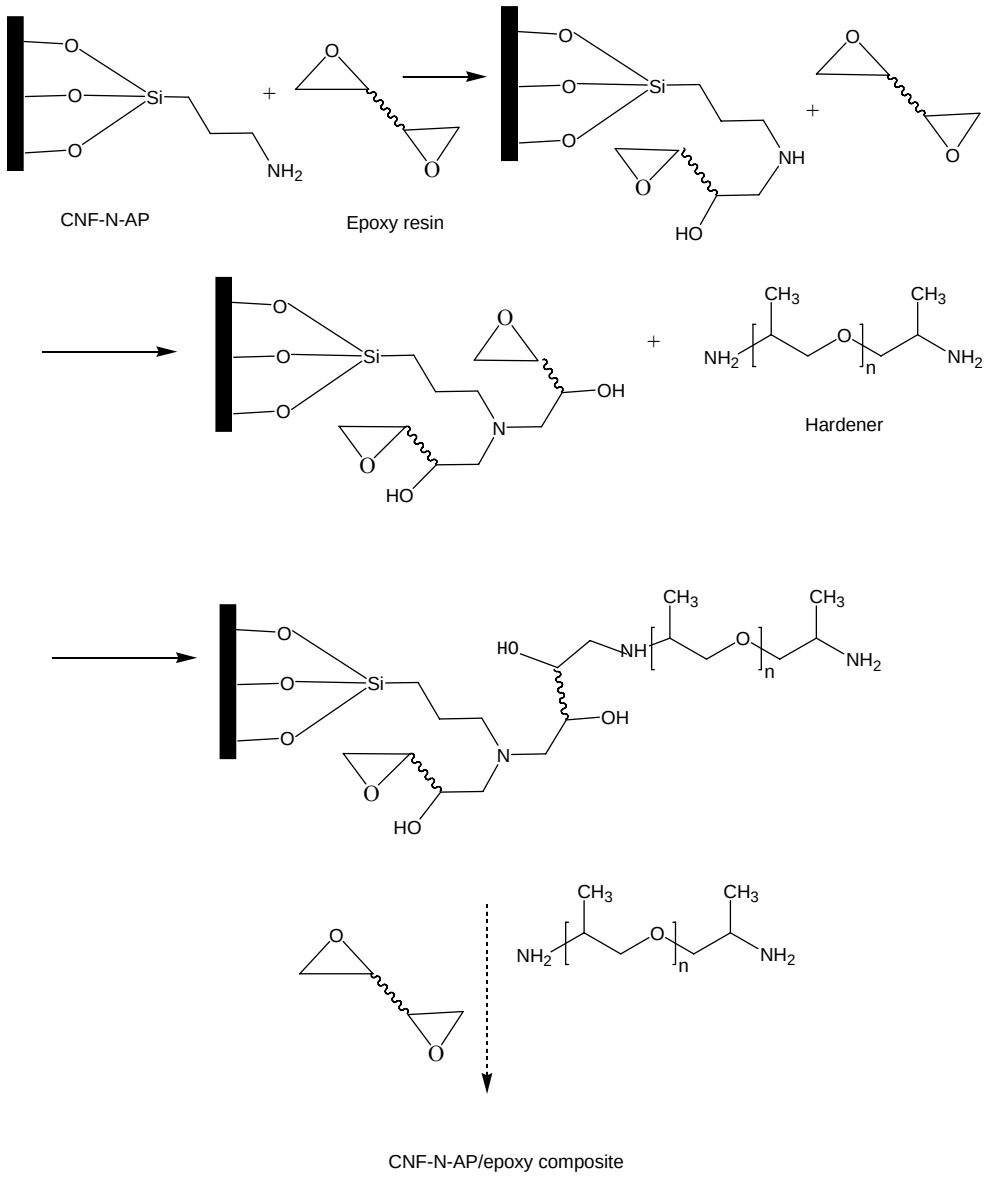

Figure 4.2 Possible reactions among CNF-N-AP, epoxy resin and hardener.

Thermal conductivity of composites is influenced by two competitive elements - the better interfacial heat transport and the more phonon scattering due to silanization. The dominant factor will determine whether the thermal conductivity of composites is improved or deteriorated compared to the unmodified CNFs/epoxy composites. For CNF-GS and CNF-N-AP, the former factor is predominant; while for CNF-I-AP, the latter factor prevails.

The electrical conductivity of composites is diminished because the direct contact of conductive nanofillers is hindered by the silane coating on the surface of fillers. The alignment of MWCNTs in the epoxy composites can also bring anisotropic electrical properties to composites.

In a word, the properties of epoxy composites containing CNFs or CNTs depend on the dispersion and distribution of fillers, the interfacial adhesion between fillers and polymers, and the surface chemistry of fillers. The relationship is shown in Figure 4.3. CNFs or CNTs are silanized in order to change their surface chemistry. The surface silanization of nanofillers facilitates their dispersion and distribution in the polymer, and increases the interfacial adhesion through chemically covalent bonds. As a result, the silanized nanofillers will affect the physical properties of epoxy composites more significantly than their pristine counterparts.

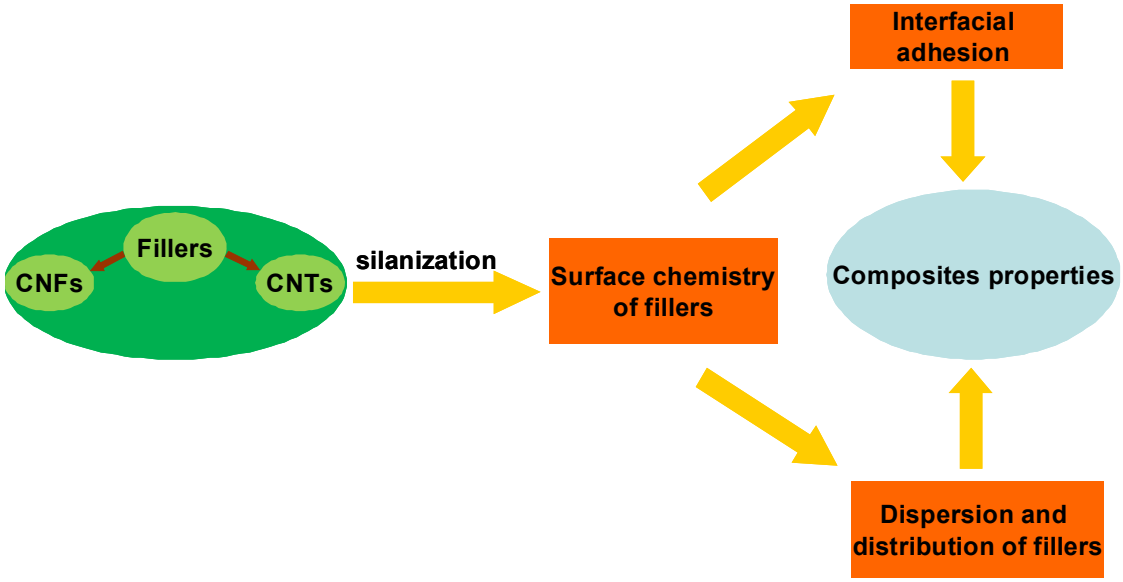

Figure 4.3 The relationship between properties and structures of composites.

5 Outlook

In order to fully use the potential of CNFs and MWCNTs as fillers for improving the properties of polymer matrices desirably, it is necessary to have a homogeneous dispersion and a good distribution of fillers in the matrix. To realize this purpose, surface modifications and suitable physical blendings should be applied.

Physical blending methods such as extruder and chaotic mixing will be tried later in order to disperse carbon nanofillers uniformly in the matrix at higher filler loading.

Efforts will be made to find an optimal reaction condition for the silanization of carbon nanofillers to improve the interfacial interaction but minimize the phonon scattering at the interface.

Mechanical properties and thermal conductivities of polymer composites with aligned MWCNTs will be investigated in more details to understand the anisotropy of composites better.

On one hand, in integrated circuit industries, polymer adhesives with good heat transport but modest electrical conductivity are required for package sealing applications. Except for the surface silanization of carbon nanofillers, the introduction of materials with a superior thermal conductivity but an electrical insulation will be another choice to realize this aim. Aluminum oxide will be introduced by sol-gel method onto carbon nanofillers to see if the alumina coating improves the thermal conductivity of composites better than the silane coating. The three phase system containing boron nitride microparticles, carbon nanofillers and polymers will be also investigated to see if synergetic effects for the higher enhancement of the thermal conductivity exist.

On the other hand, in aerospace industries, polymer materials with strong mechanical properties as well as superior electrical and thermal conductivities are demanded to ensure electromagnetic shielding and avoid overheat of the materials. Therefore the surface modification of carbon nanofillers with metal nanoparticles such as silver and gold to improve both the thermal and electrical conductivity will be done in the future.

6 References

1. M. Endo, Y.A. Kim, T. Hayashi, K. Nishimura, T. Matusita, K. Miyashita, and M.S. Dresselhaus, *Carbon*, **2001**. *39*, 1287.
2. S. Banerjee, T. Hemraj-Benny, and S.S. Wong, *Advanced Materials (Weinheim, Germany)*, **2005**. *17*, 17.
3. R.H. Baughman, A.A. Zakhidov, and W.A. de Heer, *Science*, **2002**. *297*, 787.
4. P. Avouris, *Accounts of Chemical Research*, **2002**. *35*, 1026.
5. N. Tsubokawa, *Polymer Journal*, **2005**. *37*, 637.
6. J. Bai, *Carbon*, **2003**. *41*, 1325.
7. Y. Breton, G. Desarmot, J.P. Salvetat, S. Delpeux, C. Sinturel, F. Beguin, and S. Bonnamy, *Carbon*, **2004**. *42*, 1027.
8. O.S. Carneiro, J.A. Covas, C.A. Bernardo, G. Caldeira, F.W.J. Van Hattum, J.M. Ting, R.L. Alig, and M.L. Lake, *Composites Science and Technology*, **1998**. *58*, 401.
9. Y.K. Choi, K. Sugimoto, S.M. Song, and M. Endo, *Composites Part a-Applied Science and Manufacturing*, **2006**. *37*, 1944.
10. C.A. Martin, J.K.W. Sandler, M.S.P. Shaffer, M.K. Schwarz, W. Bauhofer, K. Schulte, and A.H. Windle, *Composites Science and Technology*, **2004**. *64*, 2309.
11. C.C.M. Ma, C.C. Teng, B.D. Cheng, Y.F. Shih, J.W. Chen, and Y.K. Hsiao, *Composites Part a-Applied Science and Manufacturing*, **2011**. *42*, 928.
12. A. Garg and S.B. Sinnott, *Chemical Physics Letters*, **1998**. *295*, 273.
13. C.W. Padgett and D.W. Brenner, *Nano Letters*, **2004**. *4*, 1051.
14. H. Bubert, S. Haiber, W. Brandl, G. Marginean, M. Heintze, and V. Bruser, *Diamond and Related Materials*, **2003**. *12*, 811.
15. K.L. Ding, B.J. Hu, Y. Xie, G.M. An, R.T. Tao, H.Y. Zhang, and Z.M. Liu, *Journal of Materials Chemistry*, **2009**. *19*, 3725.
16. J.H. Zhu, S.Y. Wei, J. Ryu, M. Budhathoki, G. Liang, and Z.H. Guo, *J. Mater. Chem.*, **2010**. *20*, 4937.
17. Y. Nie and T. Hübert, *Polymer International*, **2011**. *60*, 1574.
18. http://invsee.asu.edu/nmodules/carbonmod/crystalline.html.
19. E.T. Thostenson, Z.F. Ren, and T.W. Chou, *Composites Science and Technology*, **2001**. *61*, 1899.
20. G.G. Tibbetts, M.L. Lake, K.L. Strong, and B.P. Rice, *Composites Science and Technology*, **2007**. *67*, 1709.
21. O. Breuer and U. Sundararaj, *Polymer Composites*, **2004**. *25*, 630.
22. I.C. Finegan and G.G. Tibbetts, *Journal of Materials Research*, **2001**. *16*, 1668.
23. X.L. Xie, Y.W. Mai, and X.P. Zhou, *Materials Science & Engineering R-Reports*, **2005**. *49*, 89.
24. K.I. Winey and R.A. Vaia, *Mrs Bulletin*, **2007**. *32*, 314.
25. P. Kim, L. Shi, A. Majumdar, and P.L. McEuen, *Physical Review Letters*, **2001**. *87*.
26. M.H. Al-Saleh and U. Sundararaj, *Carbon*, **2009**. *47*, 2.
27. R.M. Reilly, *Journal of Nuclear Medicine*, **2007**. *48*, 1039.
28. C.Y. Wei and D. Srivastava, *Applied Physics Letters*, **2004**. *85*, 2208.
29. J.W. Mintmire, B.I. Dunlap, and C.T. White, *Physical Review Letters*, **1992**. *68*, 631.

30. C.T. White, D.H. Robertson, and J.W. Mintmire, *Physical Review B*, **1993**. *47*, 5485.
31. R. Saito, G. Dresselhaus, and M.S. Dresselhaus, *Physical Properties of Carbon Nanotubes* 1998, London: Imperial College Press.
32. Y.H. Hu, O.A. Shenderova, Z. Hu, C.W. Padgett, and D.W. Brenner, *Reports on Progress in Physics*, **2006**. *69*, 1847.
33. L.X. Benedict, V.H. Crespi, S.G. Louie, and M.L. Cohen, *Physical Review B*, **1995**. *52*, 14935.
34. A.D. Bozhko, D.E. Sklovsky, V.A. Nalimova, A.G. Rinzler, R.E. Smalley, and J.E. Fischer, *Applied Physics a-Materials Science & Processing*, **1998**. *67*, 75.
35. J.C. Charlier and J.P. Issi, *Journal of Physics and Chemistry of Solids*, **1996**. *57*, 957.
36. J.E. Fischer, H. Dai, A. Thess, R. Lee, N.M. Hanjani, D.L. Dehaas, and R.E. Smalley, *Physical Review B*, **1997**. *55*, R4921.
37. G.T. Kim, E.S. Choi, D.C. Kim, D.S. Suh, Y.W. Park, K. Liu, G. Duesberg, and S. Roth, *Physical Review B*, **1998**. *58*, 16064.
38. H.J. Dai, E.W. Wong, and C.M. Lieber, *Science*, **1996**. *272*, 523.
39. T.W. Ebbesen, H.J. Lezec, H. Hiura, J.W. Bennett, H.F. Ghaemi, and T. Thio, *Nature*, **1996**. *382*, 54.
40. J.O. Lee, C. Park, J.J. Kim, J. Kim, J.W. Park, and K.H. Yoo, *Journal of Physics D-Applied Physics*, **2000**. *33*, 1953.
41. M.S.P. Shaffer and J.K.W. Sandler, *Carbon Nanotube/Nanofibre Polymer Composites*. PROCESSING AND PROPERTIES OF NANOCOMPOSITES, ed. S.G. Advani. 2006: World Scientific Publishing Co.
42. L. Fourdrinier, H. Le Poche, N. Chevalier, D. Mariolle, and E. Rouviere, *Journal of Applied Physics*, **2008**. *104*, 114305.
43. R. Khare and S. Bose, *Journal of Minerals & Materials Characterization & Engineering*, **2005**. *4*, 31.
44. J. Hone, *Carbon Nanotubes: Thermal Properties*. Dekker Encyclopedia of Nanoscience and Nanotechnology. 2009: Taylor & Francis
45. L.X. Benedict, S.G. Louie, and M.L. Cohen, *Solid State Communications*, **1996**. *100*, 177.
46. J. Hone, *Carbon Nanotubes*, **2001**. *80*, 273.
47. B.T. Kelly, *Physics of Graphite*. 1981, London: Applied Science.
48. K. Perepelkin, *Sov. Mater. Sci.*, **1972**. *8*, 198.
49. A.B. Dalton, S. Collins, E. Munoz, J.M. Razal, V.H. Ebron, J.P. Ferraris, J.N. Coleman, B.G. Kim, and R.H. Baughman, *Nature*, **2003**. *423*, 703.
50. H.W. Zhu, C.L. Xu, D.H. Wu, B.Q. Wei, R. Vajtai, and P.M. Ajayan, *Science*, **2002**. *296*, 884.
51. J.N. Coleman, U. Khan, and Y.K. Gun'ko, *Advanced Materials*, **2006**. *18*, 689.
52. S.S. Xie, W.Z. Li, Z.W. Pan, B.H. Chang, and L.F. Sun, *Journal of Physics and Chemistry of Solids*, **2000**. *61*, 1153.
53. G.G. Tibbetts and J.J. McHugh, *Journal of Materials Research*, **1999**. *14*, 2871.
54. B.O. Lee, W.J. Woo, and M.S. Kim, *Macromolecular Materials and Engineering*, **2001**. *286*, 114.
55. S. Iijima, *Nature*, **1991**. *354*, 56.

56. C. Journet, W.K. Maser, P. Bernier, A. Loiseau, M.L. delaChapelle, S. Lefrant, P. Deniard, R. Lee, and J.E. Fischer, *Nature*, **1997**. *388*, 756.
57. A. Thess, R. Lee, P. Nikolaev, H.J. Dai, P. Petit, J. Robert, C.H. Xu, Y.H. Lee, S.G. Kim, A.G. Rinzler, D.T. Colbert, G.E. Scuseria, D. Tomanek, J.E. Fischer, and R.E. Smalley, *Science*, **1996**. *273*, 483.
58. P.M. Ajayan and T.W. Ebbesen, *Reports on Progress in Physics*, **1997**. *60*, 1025.
59. S.S. Xie, B.H. Chang, W.Z. Li, Z.W. Pan, L.F. Sun, J.M. Mao, X.H. Chen, L.X. Qian, and W.Y. Zhou, *Advanced Materials*, **1999**. *11*, 1135.
60. P. Szroeder, N.G. Tsierkezos, P. Scharff, and U. Ritter, *Carbon*, **2010**. *48*, 4489.
61. C.A. May, *Epoxy Resins: Chemistry and Technology*. 1988: Marcel Dekker.
62. W.J. Blank, Z.A. He, and M. Picci, *Journal of Coatings Technology*, **2002**. *74*, 33.
63. K. Lafdi and M. Matzek. *Carbon nanofibers as a nano-reinforcement for polymeric nanocomposites*. in *48th International SAMPE symposium proceedings*. 2003. Long Beach, USA.
64. L.S. Tan, D.H. Wang, S. Sihn, A.K. Roy, and J.B. Baek, *Eur. Polym. J.*, **2010**. *46*, 1404.
65. S.G. Prolongo, M. Campo, M.R. Gude, R. Chaos-Moran, and A. Urena, *Composites Science and Technology*, **2009**. *69*, 349.
66. Y.K. Choi, K. Sugimoto, S.M. Song, Y. Gotoh, Y. Ohkoshi, and M. Endo, *Carbon*, **2005**. *43*, 2199.
67. D.R. Dean, K.J. Green, U.K. Vaidya, and E. Nyairo, *Composites Part a-Applied Science and Manufacturing*, **2009**. *40*, 1470.
68. Y.X. Zhou, F. Pervin, V.K. Rangari, and S. Jeelani, *Materials Science and Engineering a-Structural Materials Properties Microstructure and Processing*, **2006**. *426*, 221.
69. R.D. Patton, C.U. Pittman, L. Wang, and J.R. Hill, *Composites Part a-Applied Science and Manufacturing*, **1999**. *30*, 1081.
70. K. Lafdi, W. Fox, M. Matzek, and E. Yildiz, *Journal of Nanomaterials*, **2007**, 52729.1.
71. L.H. Sun, Z. Ounaies, X.L. Gao, C.A. Whalen, and Z.G. Yang, *Journal of Nanomaterials*, **2011**, 307589.
72. P.M. Ajayan, O. Stephan, C. Colliex, and D. Trauth, *Science*, **1994**. *265*, 1212.
73. L.S. Schadler, S.C. Giannaris, and P.M. Ajayan, *Applied Physics Letters*, **1998**. *73*, 3842.
74. X.D. Li, H.S. Gao, W.A. Scrivens, D.L. Fei, X.Y. Xu, M.A. Sutton, A.P. Reynolds, and M.L. Myrick, *Nanotechnology*, **2004**. *15*, 1416.
75. M. Weber and M.R. Kamal, *Polymer Composites*, **1997**. *18*, 711.
76. I.C. Finegan and G.G. Tibbetts, *Journal of Materials Research*, **2001**. *16*, 1668.
77. S.A. Gordeyev, F.J. Macedo, J.A. Ferreira, F.W.J. van Hattum, and C.A. Bernardo, *Physica B-Condensed Matter*, **2000**. *279*, 33.
78. M.J. Biercuk, M.C. Llaguno, M. Radosavljevic, J.K. Hyun, A.T. Johnson, and J.E. Fischer, *Applied Physics Letters*, **2002**. *80*, 2767.
79. A. Moisala, Q. Li, I.A. Kinloch, and A.H. Windle, *Composites Science and Technology*, **2006**. *66*, 1285.
80. Z.D. Han and A. Fina, *Progress in Polymer Science*, **2011**. *36*, 914.
81. Y.M. Chen and J.M. Ting, *Carbon*, **2002**. *40*, 359.
82. C. Baudot and C.M. Tan, *Carbon*, **2011**. *49*, 2362.

83. S.T. Huxtable, D.G. Cahill, S. Shenogin, L.P. Xue, R. Ozisik, P. Barone, M. Usrey, M.S. Strano, G. Siddons, M. Shim, and P. Keblinski, *Nature Materials*, **2003**. *2*, 731.
84. C.W. Nan, G. Liu, Y.H. Lin, and M. Li, *Applied Physics Letters*, **2004**. *85*, 3549.
85. D. Tasis, N. Tagmatarchis, A. Bianco, and M. Prato, *Chemical Reviews (Washington, DC, United States)*, **2006**. *106*, 1105.
86. J.B. Baek, C.B. Lyons, and L.S. Tan, *Journal of Materials Chemistry*, **2004**. *14*, 2052.
87. J.B. Baek, C.B. Lyons, and L.S. Tan, *Macromolecules*, **2004**. *37*, 8278.
88. G. Wei, K. Fujiki, H. Saitoh, K. Shirai, and N. Tsubokawa, *Polymer Journal (Tokyo, Japan)*, **2004**. *36*, 316.
89. G. Wei, H. Saitoh, K. Fujiki, T. Yamauchi, and N. Tsubokawa, *Polymer Bulletin (Berlin)*, **2008**. *60*, 219.
90. G. Wei, S. Saitoh, H. Saitoh, K. Fujiki, T. Yamauchi, and N. Tsubokawa, *Polymer*, **2004**. *45*, 8723.
91. C. Velasco-Santos, A.L. Martinez-Hernandez, M. Lozada-Cassou, A. Alvarez-Castillo, and V.M. Castano, *Nanotechnology*, **2002**. *13*, 495.
92. D.S. Bag, R. Dubey, N. Zhang, J. Xie, V.K. Varadan, D. Lal, and G.N. Mathur, *Smart Materials & Structures*, **2004**. *13*, 1263.
93. C. Palencia, F. Rubio, C. Merino, J. Rubio, and J.L. Oteo, *J. Nano Res.*, **2008**. *4*, 33.
94. Z. Zhou, S.F. Wang, L. Lu, Y.X. Zhang, and Y. Zhang, *Composites Science and Technology*, **2008**. *68*, 1727.
95. A. Nistal, C. Palencia, M.A. Mazo, F. Rubio, J. Rubio, and J.L. Oteo, *Carbon*, **2011**. *49*, 1635.
96. P.C. Ma, J.K. Kim, and B.Z. Tang, *Carbon*, **2006**. *44*, 3232.
97. P.C. Ma, J.K. Kim, and B.Z. Tang, *Composites Science and Technology*, **2007**. *67*, 2965.
98. K.Y. Rhee, J.L. Lee, J. H., and S.J. Park, *Composites Part a-Applied Science and Manufacturing*, **2011**. *42*, 478.
99. G. Nikolic, S. Zlatkovic, M. Cakic, S. Cakic, C. Lacnjevac, and Z. Rajic, *Sensors*, **2010**. *10*, 684.
100. Q.H. Zhang, J. Li, X. Zhao, and D.J. Chen, *Polymer International*, **2009**. *58*, 557.
101. K.M.R. Kallury, U.J. Krull, and M. Thompson, *Analytical Chemistry*, **1988**. *60*, 169.
102. J.P. Blitz, R.S.S. Murthy, and D.E. Leyden, *Journal of Colloid and Interface Science*, **1988**. *126*, 387.
103. ISO 15472, Surface chemical analysis - X-ray photoelectron spectrometers calibration of energy scales, **2001**.
104. A.J. Bard and L.R. Faulkner, *Double-layer structure and adsorption*, in *Electrochemical Methods: Fundamentals and Applications*. 2001, John Wiley & Sons, Inc. 534.
105. J.C. Berg, *Electric double layer formation and structure*, in *An introduction to interfaces & colloids: the bridge to nanoscience*. 2010, World Scientific Publishing Co. Pte. Ltd. 466.
106. G. Steinborn and R. Wäsche, *Chemie Ingenieur Technik*, **2007**. *79*, 257.
107. P.E. Bocquet, C.M. Sliepcevich, and D.F. Bohr, *Industrial and Engineering Chemistry*, **1956**. *48*, 197.
108. D. Erickson and D.Q. Li, *Journal of Colloid and Interface Science*, **2001**. *237*, 283.

109. P.V. Lakshminarayanan, H. Toghiani, and C.U. Pittman, *Carbon*, **2004**. *42*, 2433.
110. G.X. Zhang, S.H. Sun, D.Q. Yang, J.P. Dodelet, and E. Sacher, *Carbon*, **2008**. *46*, 196.
111. H. Hu, P. Bhowmik, B. Zhao, M.A. Hamon, M.E. Itkis, and R.C. Haddon, *Chemical Physics Letters*, **2001**. *345*, 25.
112. B.C. Satishkumar, A. Govindaraj, J. Mofokeng, G.N. Subbanna, and C.N.R. Rao, *Journal of Physics B-Atomic Molecular and Optical Physics*, **1996**. *29*, 4925.
113. S.C. Tsang, Y.K. Chen, P.J.F. Harris, and M.L.H. Green, *Nature*, **1994**. *372*, 159.
114. P. Mahanandia and K.K. Nanda, *Nanotechnology*, **2008**. *19*.
115. F. Tuinstra and J.L. Koenig, *Journal of Chemical Physics*, **1970**. *53*, 1126.
116. A.G. Souza, A. Jorio, G.G. Samsonidze, G. Dresselhaus, R. Saito, and M.S. Dresselhaus, *Nanotechnology*, **2003**. *14*, 1130.
117. S.S. Xie, W.Z. Li, Z.W. Pan, B.H. Chang, and L.F. Sun, *European Physical Journal D*, **1999**. *9*, 85.
118. A. Jorio, M.A. Pimenta, A.G. Souza, R. Saito, G. Dresselhaus, and M.S. Dresselhaus, *New Journal of Physics*, **2003**. *5*, 139.1.
119. W.T. Wu, L. Shi, Y.S. Wang, W.M. Pang, and Q.R. Zhu, *Nanotechnology*, **2008**. *19*.
120. G.T. Wu, M.H. Chen, G.M. Zhu, J.K. You, Z.G. Lin, and X.B. Zhang, *Journal of Solid State Electrochemistry*, **2003**. *7*, 129.
121. G.T. Wu, C.S. Wang, X.B. Zhang, H.S. Yang, Z.F. Qi, P.M. He, and W.Z. Li, *Journal of the Electrochemical Society*, **1999**. *146*, 1696.
122. C.S. Wang, G.T. Wu, X.B. Zhang, Z.F. Qi, and W.Z. Li, *Journal of the Electrochemical Society*, **1998**. *145*, 2751.
123. C.S. Wang, G.T. Wu, and W.Z. Li, *Journal of Power Sources*, **1998**. *76*, 1.
124. J.X. Guo, Y.G. Li, S.W. Wu, and W.X. Li, *Nanotechnology*, **2005**. *16*, 2385.
125. J. Peng, X.X. Qu, G.S. Wei, J.Q. Li, and J.L. Qiao, *Carbon*, **2004**. *42*, 2741.
126. H.X. Xu, X.B. Wang, Y.F. Zhang, and S.Y. Liu, *Chemistry of Materials*, **2006**. *18*, 2929.
127. R.J. Nemanich and S.A. Solin, *Physical Review B*, **1979**. *20*, 392.
128. V. Volovsek, I.M. Sapic, L. Bistricic, V. Dananic, and K. Furic, *Spectrochimica Acta Part a-Molecular and Biomolecular Spectroscopy*, **2009**. *72*, 833.
129. S. Roy, B.R. Gupta, and B.R. Maiti, *Journal of Elastomers and Plastics*, **1990**. *22*, 280.
130. S. Rooj, V. Thakur, U. Gohs, U. Wagenknecht, A.K. Bhowmick, and G. Heinrich, *Polymers for Advanced Technologies*, **2011**. *22*, 2257.
131. L. Shechter and J. Wynstra, *Industrial and Engineering Chemistry*, **1956**. *48*, 86.
132. L.S. Schadler, A. Eitan, K.Y. Jiang, D. Dukes, and R. Andrews, *Chemistry of Materials*, **2003**. *15*, 3198.
133. Y.F. Zhu, C. Ma, W. Zhang, R.P. Zhang, N. Koratkar, and J. Liang, *Journal of Applied Physics*, **2009**. *105*, 054319.
134. L.X. Benedict, S.G. Louie, and M.L. Cohen, *Physical Review B*, **1995**. *52*, 8541.
135. C.A. Martin, J.K.W. Sandler, A.H. Windle, M.K. Schwarz, W. Bauhofer, K. Schulte, and M.S.P. Shaffer, *Polymer*, **2005**. *46*, 877.
136. B.M. Vogel, M. DeLongchamp, C.M. Mahoney, L.A. Lucas, D.A. Fischer, and E.K. Lin, *Applied Surface Science*, **2008**. *254*, 1789.

137. K. Saalwachter, M. Krause, and W. Gronski, *Chemistry of Materials*, **2004**. *16*, 4071.
138. G. Altankov, K. Richau, and T. Groth, *Materialwissenschaft Und Werkstofftechnik*, **2003**. *34*, 1120.
139. C. Werner, H. Korber, R. Zimmermann, S. Dukhin, and H.J. Jacobasch, *Journal of Colloid and Interface Science*, **1998**. *208*, 329.
140. E. Jagst, PhD thesis, Berlin, **2011**.
141. EN 1465, Adhesives-Determination of tensile lap-shear strength of bonded assemblies, **2009**.
142. J.F. Shen, W.S. Huang, L.P. Wu, Y.Z. Hu, and M.X. Ye, *Composites Science and Technology*, **2007**. *67*, 3041.
143. E.V. Barrera, J. Zhu, H.Q. Peng, F. Rodriguez-Macias, J.L. Margrave, V.N. Khabashesku, A.M. Imam, and K. Lozano, *Advanced Functional Materials*, **2004**. *14*, 643.
144. C.K. Das, S. Kumar, T. Rath, R.N. Mahaling, C.S. Reddy, K.N. Pandey, R.B. Srivastava, and S.B. Yadaw, *Materials Science and Engineering B-Solid State Materials for Advanced Technology*, **2007**. *141*, 61.
145. W. Bauhofer and J.Z. Kovacs, *Composites Science and Technology*, **2009**. *69*, 1486.
146. O. Hilt, H.B. Brom, and M. Ahlskog, *Physical Review B*, **2000**. *61*, R5129.
147. H. Xu, S.M. Anlage, L. Hu, and G. Gruner, *Applied Physics Letters*, **2007**. *90*, 183119.
148. Y. Agari, A. Ueda, and S. Nagai, *Journal of Applied Polymer Science*, **1991**. *43*, 1117.
149. D.J. Yang, Q. Zhang, G. Chen, S.F. Yoon, J. Ahn, S.G. Wang, Q. Zhou, Q. Wang, and J.Q. Li, *Physical Review B*, **2002**. *66*, 165440.
150. R.J. Kuriger, M.K. Alam, D.P. Anderson, and R.L. Jacobsen, *Composites Part a-Applied Science and Manufacturing*, **2002**. *33*, 53.
151. A.H. Windle, A. Moisala, Q. Li, and I.A. Kinloch, *Composites Science and Technology*, **2006**. *66*, 1285.
152. K. Yang, M.Y. Gu, Y.P. Guo, X.F. Pan, and G.H. Mu, *Carbon*, **2009**. *47*, 1723.
153. A. Lazarenko, L. Vovchenko, D. Matsui, Y. Prylutskyy, L. Matzuy, U. Ritter, and P. Scharff, *Molecular Crystals and Liquid Crystals*, **2008**. *497*, 397.

7 List of Figures

Figure 1.1 Graphite crystallite structures (the balls represent carbon atoms and the sticks represent the bonding) [18]. 6

Figure 1.2 a) Schematic diagram of how the graphene sheet rolling up into SWCNT b) armchair SWCNT c) zig-zag SWCNT [19]. 7

Figure 1.3 Comparison of structures between a) MWCNTs [27] and b) CNFs [28]. 8

Figure 1.4 Scheme of an apparatus for the preparation of Pyrograf III CNFs [20]. 11

Figure 1.5 Chemical formula of the epoxy resin based on diglycidyl ether of bisphenol A (DGEBA) [62]. 13

Figure 1.6 The sketch of the percolation behavior of CNFs [26]. 16

Figure 1.7 Scheme for the distribution and dispersion of CNFs in polymer matrices [26]. 17

Figure 1.8 The enhancement of thermal conductivity of composites compared to that of pure polymer as a function of CNT volume fraction [80]. 18

Figure 1.9 Scheme of the silanization process on CNTs [91]. 21

Figure 1.10 Sketch of CNFs in epoxy resin (a) as-received CNFs, (b) silanized CNFs [16]. 23

Figure 1.11 Scheme of epoxy-amine reactions (formulas 1-3) and the etherification (formula 4) [99]. 23

Figure 2.1 TEM picture of original CNFs. 27

Figure 2.2 TEM picture of pristine MWCNTs. 27

Figure 2.3 Scheme for the different oxidation processes of CNFs. 29

Figure 2.4 Sketch for the silanization process of CNFs with GPTMS. 29

Figure 2.5 Sketch for the silanization process of CNFs with APTMS. 30

Figure 2.6 Sketch for the silanization process of CNFs with IPTES and APTMS. 31

Figure 2.7 Sketch for the silanization process of MWCNTs with APTMS. 31

Figure 2.8 Scheme of the electrical double layer and Zeta potential. 33

Figure 2.9 Apparatus for the measurement of the streaming potential [108]. 34

Figure 2.10 IR spectra of original CNFs (CNF-O) and oxidized CNFs (CNF-AS, CNF-AH, CNF-PMS, CNF-PMH). 35

Figure 2.11 Raman spectra of original CNFs (CNF-O) and oxidized CNFs (CNF-AS, CNF-AH, CNF-PMS, CNF-PMH). 37

Figure 2.12 SEM pictures of original and oxidized CNFs by different methods: a) CNF-O, b) CNF-AS, c) CNF-AH, d) CNF-PMS, e) CNF-PMH. 38

Figure 2.13 FTIR spectra of silanized CNFs (CNF-GS) compared with original CNFs (CNF-O) and oxidized CNFs (CNF-AS). 39

Figure 2.14 XPS Si 2p peak fitting of CNF-GS. 41

Figure 2.15 Scheme of the possible reactions between alkoxysilanes and CNFs. 41

Figure 2.16 SEM of a) original CNFs (CNF-O), b) oxidized CNF (CNF-AS), c) silanized CNFs (CNF-GS); and d) EDX analysis of CNFs. 43

Figure 2.17 TGA measurements of silanized CNFs (CNF-GS) compared with original CNFs (CNF-O) and oxidized CNFs (CNF-AS). 44

Figure 2.18 Raman spectra of CNF-GS compared with the original CNFs (CNF-O) and oxidized CNFs (CNF-AS). 45

Figure 2.19 Optical microscopy of CNF ethanol suspension under AC electric field (6×10^4 $V\cdot m^{-1}$): a) CNF-O, 0 min; b) CNF-O, 30 min; c) CNF-GS, 0 min; d) CNF-GS, 30 min. The magnification is 200×. 46

Figure 2.20 IR spectra of original CNFs and modified CNFs at different steps (CNF-O: original nanofibers; CNF-AS: oxidized CNFs after acid sonication; CNF-N: reduced CNFs by $NaBH_4/I_2$; CNF-N-AP: silanized CNFs with APTMS). 47

Figure 2.21 XPS Si 2p peak fitting of CNF-N-AP. 50

Figure 2.22 TGA measurements of silanized CNFs (CNF-N-AP) compared with original CNFs (CNF-O), oxidized CNFs (CNF-AS) and reduced CNFs (CNF-N). 51

Figure 2.23 Streaming potential of CNFs versus pH after each chemical treatment in the aminosilanization procedure. 52

Figure 2.24 Raman spectra of CNF-N-AP compared with the original CNFs (CNF-O), oxidized CNFs (CNF-AS) and reduced CNFs (CNF-N). 53

Figure 2.25 IR spectra of silanized CNFs (CNF-I, sample after the first silanization; CNF-I-AP, sample after the second silanization) compared with original CNFs (CNF-O) and oxidized CNFs (CNF-AS). 54

Figure 2.26 XPS Si 2p peak fitting of CNF-I. 56

Figure 2.27 XPS Si 2p peak fitting of CNF-I-AP. 56

Figure 2.28 TGA measurements of silanized CNFs (CNF-I and CNF-I-AP) compared with original CNFs (CNF-O) and oxidized CNFs (CNF-AS). 57

Figure 2.29 Streaming potential of CNFs versus pH after each chemical treatment in the two-silanization procedure. 58

Figure 2.30 XRD patterns of CNFs before and after chemical treatments in the two-silanization procedure. 59

Figure 2.31 Raman spectra of silanized CNFs (CNF-I, CNF-I-AP) compared with original CNFs (CNF-O) and oxidized CNFs (CNF-AS). 60

Figure 2.32 IR spectra of pristine MWCNTs (MWCNT) and oxidized MWCNTs (MWCNT-AS, MWCNT-PMH). 61

Figure 2.33 Raman spectra of pristine MWCNTs (MWCNT) and oxidized MWCNTs (MWCNT-AS, MWCNT-PMH). 62

Figure 2.34 IR spectra of pristine MWCNTs and modified MWCNTs (MWCNT: pristine MWCNTs; MWCNT-PMH: oxidized MWCNTs; MWCNT-PMH-N: reduced MWCNTs; MWCNT-PMH-N-AP: silanized MWCNTs with APTMS). 63

Figure 2.35 Scheme for the derivatization of a) MWCNT-PMH-N with TFAA and b) MWCNT-PMH-N-AP with TFBA. 65

Figure 2.36 XPS Si 2p peak fitting of MWCNT-PMH-N-AP. 66

Figure 2.37 Raman spectra of MWCNT-PMH-N-AP compared with pristine MWCNTs (MWCNT), oxidized MWCNTs (MWCNT-PMH) and reduced MWCNTs (MWCNT-PMH-N). 67

Figure 3.1 Scheme for the preparation of CNFs/epoxy nanocomposites. 71

Figure 3.2 Sketch for the alignment of MWCNTs in epoxy resin. 71

Figure 3.3 Picture of the set-up for the preparation of aligned MWCNTs/epoxy composites. 72

Figure 3.4 Scheme for the measurement of the tensile shear strength based on EN 1465. 73

Figure 3.5 SEM pictures of composites a) 1 wt% CNF-O/epoxy b) 3 wt% CNF-O/epoxy and c) 1 wt% CNF-GS/epoxy d) 3 wt% CNF-GS/epoxy e) 10 wt% CNF-GS/epoxy. 74

Figure 3.6 SEM pictures of epoxy composites containing 2 wt% CNFs a) CNF-O/epoxy composite; b) magnified picture from a); c) CNF-N-AP/epoxy composite; d) magnified picture from c). 76

Figure 3.7 SEM pictures of composites a) 2 wt% CNF-O/epoxy b) 2 wt% CNF-I-AP/epoxy.77

Figure 3.8 Dynamic mechanical analysis: a) variation of storage modulus with temperature for epoxy composites filled with CNFs; b) variation of tan δ with temperature for epoxy composites filled with CNFs. 80

Figure 3.9 Dependence of a) tensile strength and b) tensile shear strength on the CNF loading of epoxy composites. 82

Figure 3.10 Dependence of the tensile shear strength on CNF loading for CNF-I-AP/epoxy composites compared with that for CNF-O/epoxy composites. 83

Figure 3.11 a) DC electrical conductivity of epoxy composites versus the weight concentration of CNFs; b) dependence of the AC electrical conductivity on the frequency for CNF-O/epoxy composites; c) dependence of the AC electrical conductivity on the frequency for CNF-GS/epoxy composites. 86

Figure 3.12 Dependence of the AC electrical conductivity on the frequency for a) CNF-O/epoxy composites and b) CNF-N-AP/epoxy composites; c) dependence of the DC electrical conductivity of epoxy composites on the weight concentration of CNFs. 89

Figure 3.13 Dependence of the AC electrical conductivity on the frequency for a) CNF-I-AP/epoxy composites compared with that for b) CNF-O/epoxy composites. 90

Figure 3.14 Dependence of the AC electrical conductivity of pure CNF powders on the frequency. 91

Figure 3.15 Dependence of the thermal conductivity on the weight concentration of CNFs for CNF-GS/epoxy composites compared with that for CNF-O/epoxy composites. 92

Figure 3.16 Enhancement of the thermal conductivity compared to the pure epoxy polymer as a function of CNF loading. The empty circles represent the thermal conductivity enhancement of composites containing original CNFs (CNF-O); the empty squares represent the thermal conductivity enhancement of composites containing silanized CNFs (CNF-GS); straight lines are fitted values based on Agari model. 94

Figure 3.17 Dependence of the thermal conductivity on the weight concentration of CNFs for CNF-N-AP/epoxy composites compared with that for CNF-O/epoxy composites. 95

Figure 3.18 Dependence of the thermal conductivity on the weight concentration of CNFs for CNF-I-AP/epoxy composites compared with that for CNF-O/epoxy composites. 96

Figure 3.19 Dependence of AC electrical conductivity on frequency for MWCNTs/epoxy composites. 97

Figure 4.1 Possible reactions among CNF-GS, epoxy resin and hardener. 108

Figure 4.2 Possible reactions among CNF-N-AP, epoxy resin and hardener. 109

Figure 4.3 The relationship between properties and structures of composites. 110

8 List of Tables

Table 2.1 XPS measurements of CNF surface composition. 36

Table 2.2 Relative percentage of functional groups from the deconvolution of XPS C 1s peak. 36

Table 2.3 XPS measurements of CNF surface composition. 40

Table 2.4 Relative percentage of functional groups from the deconvolution of XPS C 1s peak. 40

Table 2.5 XPS measurements of CNF surface composition. 48

Table 2.6 Relative percentage of functional groups from the deconvolution of XPS C 1s peak. 49

Table 2.7 XPS measurements of CNF surface composition. 55

Table 2.8 Relative percentage of functional groups from the deconvolution of XPS C 1s peak. 55

Table 2.9 Summary of XRD results of CNFs before and after chemical treatments in the two-silanization procedure. 59

Table 2.10 XPS measurements of MWCNT surface composition. 64

Table 2.11 Relative percentage of functional groups from XPS C 1s peak deconvolution. 64

Table 2.12 XPS measurements of MWCNT surface composition after derivatization. 65

Table 3.1 Storage modulus at RT and the glass transition temperature (T_g) of the pure epoxy polymer and epoxy composites. 79

9 List of Publications

Articles

1. **Y. Nie** and T. Hübert, Effect of carbon nanofiber (CNF) silanization on the properties of CNF/epoxy nanocomposites, *Polymer International*, **2011**. *60*, 1574.
2. **Y. Nie** and T. Hübert, Surface modification of carbon nanofibers by glycidoxysilane for altering the conductive and mechanical properties of epoxy composites, submitted to *Composites Part A: Applied Science and Manufacturing*.

Presentation

Y. Nie and T. Hübert, Surface silanization of carbon nanofillers for tailoring the properties of epoxy composites, 9th EUROFILLERS International Conference, **2011**, Dresden, Germany.

Posters

1. **Y. Nie**, T. Hübert and A. Leistner, Surface modification of carbon nanofibers (CNFs) with silanes for tuning the conductive and mechanical properties of CNFs/epoxy composites, 5th Asia-Europe Symposium on Processing and Properties of Reinforced Polymers, **2011**, Dresden, Germany.

2. **Y. Nie** and T. Hübert, Tuning the mechanical and conductive properties of epoxy/CNTs composites by chemical modification of CNTs fillers, E-MRS **2010** spring meeting, Strasburg, France.